Quantifying the Aboveground Biomass Stock Changes Associated with Oil Palm Expansion on Tropical Peatlands using Plot-based Methods and L-band Radar

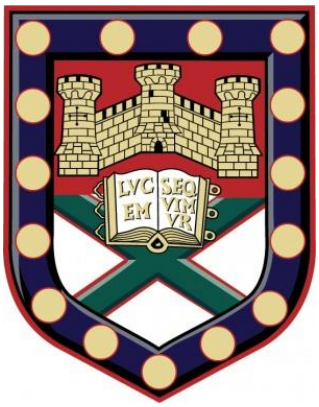

Submitted by Kennedy Lewis to the University of Exeter
as a dissertation for the degree of
Master of Science by Research in Geography
In December 2019

I certify that all material in this dissertation which is not my own work has been identified and that any material that has previously been submitted and approved for the award of a degree by this or any other University has been acknowledged.

Signature……

Abstract

The recent rapid expansion of oil palm (OP, *Elaeis guineensis*) plantations into tropical forest peatlands has resulted in net ecosystem carbon emissions. However, quantifications of the net carbon flux from biomass changes require accurate estimates of the above ground biomass (AGB) accumulation rate of OP on peat in working plantations. Current efforts that aim to reduce the emissions from OP expansion would also benefit from the development of economically viable remote sensing approaches that enable the detection of OP plantation expansion and monitoring of AGB stocks across at a fine spatial and temporal resolution.

Here, destructive harvest and non-destructive plot inventories are conducted across a chronosequence of OP planting blocks (3 to 12 years after planting (YAP)) in plantations on drained peat in Sarawak, Malaysia. The effectiveness of using a timeseries of L-band synthetic aperture radar (SAR) scenes (ALOS PALSAR-1/2) and a novel 'biomass matching' approach to detect, quantify and map the AGB stock changes associated with OP establishment and growth was then assessed.

Peat specific allometric equations for palm (9 palms, $R^2 = 0.92$) and frond biomass are developed and upscaled to estimate AGB at the plantation block-level (902 palms). Aboveground biomass stocks on peat accumulated at ~6.39 ± 1.12 Mg ha^{-1} per year in the first 12 years after planting. However, high inter-palm and inter-block AGB variability was observed in mature classes as a result of variations in palm leaning and mortality. The 'biomass matching' approach detected statistically significant deforestation associated with OP establishment. OP growth was well estimated between 4 and 10 YAP, however sensitivity to increases in AGB was lost at ~ 45 - 60 Mg ha.

Validation of the allometric equations defined and expansion of non-destructive inventories across alternative plantations and age classes on peat would further strengthen our understanding of OP AGB accumulation rates. With further investigation into the relationship between OP structural characteristics and L-band radar cross section (RCS) in the HV and HH polarisations, 'biomass matching' could be a feasible tool for monitoring AGB stock changes to inform carbon emission mitigation strategies.

Table of Contents

List of Figures

Chapter 1

Chapter 2

Chapter 3

Chapter 4

List of Tables

Acknowledgements

Firstly, I would like to thank Dr Tim Hill for introducing me to the study site and integrating me into an amazing research project and team. I would like to give a huge thank you to both my supervisors; Dr Tim Hill and Dr Angela Gallego-Sala for guiding and supporting me throughout the project, sharing their knowledge and enthusiasm and for being so generous with their time. I am very lucky to have worked with you both.

I am extremely grateful to Dr Lip Khoon Kho and Elisa Rumpang at the MPOB Tropical Peat Research Institute (TROPI) for helping me to set up and conduct the fieldwork for this project and for sharing their expertise and their time. I also wish to thank Dr Jon McCalmont for his support and enthusiasm in the field and for his advice throughout the duration of my masters. Thanks, is also due to Steward Saging and Ham Jonathan for their help in the field – it would have been impossible without their support, knowledge and experience. Thanks to Justin Goh and the teams at the Sabaju and Sebungan Estates for to helping collect samples and conduct measurements across the plantations. Thank you, to everyone who welcomed me in Bintulu and made my time at the plantations so enjoyable.

In addition, I would like to thank the Sarawak Oil Palms Berhard (SOP) and plantation managers for their logistical support and permissions to conduct research across the plantations. I am also grateful to the Malaysian Oil Palm Board (MPOB) for their continual support, the generous provision resources and the use of their labs.

I would like to thank Dr Ed Mitchard at the University of Edinburgh for allowing me to access the ALOS PALSAR datasets and for giving me valuable advice when using them. At the University of Exeter, I would also like to thank David Hein-Griggs for his technical support and the geography laboratories, for their support and the loan of equipment.

Finally, I would like to thank my family and friends for their love and support throughout.

Chapter 1: Scientific Context

1.1) Anthropogenic climate change and the carbon cycle

The global atmospheric CO_2 concentration has risen by approximately 20 ppm per decade since 2000, ~10 times faster than any sustained rise in CO_2 during the past 800,000 years (Lüthi *et al.*, 2008; Bereiter *et al*., 2015). Accompanied by rises in emissions of other greenhouse gasses (CH_4 and N_2O) this has resulted in a human-induced climate warming of 1°C (±0.2°C) above pre-industrial levels (period 1850–1900) (IPCC, 2018). This temperature rise has resulted in profound alterations to human and natural systems including increases in the frequency and severity of droughts, floods and other extreme weather events, sea level rise and biodiversity loss (IPCC, 2018, Mysiak *et al.* 2016). To avoid worsening impacts on global populations and ecosystems the United Nations Framework Convention on Climate Change (UNFCCC) Paris Agreement encourages governments to "pursue efforts to limit the temperature increase to 1.5°C above pre-industrial levels" (UNFCCC, 2015).

Fossil fuel combustion is the largest source of global CO_2 emissions, these emissions are absorbed by the Earth's atmosphere, oceans and the terrestrial land carbon sink (Pan *et al.* 2011, IPCC, 2013). Despite significant carbon storage and uptake by terrestrial vegetation and soils, land use changes (LUC) whereby intact or secondary vegetation is converted to alternative land cover types is increasingly resulting in carbon emissions (Le Quéré *et al.* 2018). Recently tropical ecosystems have been the global epicentre of land use change (Mitchard *et al.* 2018).

1.2) Tropical land use change and the terrestrial carbon store

Tropical forest trees store between 200 - 300 Pg of carbon (Mitchard et al, 2018). Living biomass stocks; all living biomass above the soil (aboveground biomass, AGB) and root biomass below the soil (below ground biomass, BGB) made up a large proportion of the overall tropical carbon stocks (FAO, 2007, Pan *et al.* 2011). Soil organic matter (SOM); all organic matter in mineral and organic soils, also makes a large contribution to the tropical land carbon sink (FAO, 2007, Pan *et al*. 2011) Especially when deep, carbon dense tropical peatlands are considered (Page *et al*. 2011a, Dargie *et al*. 2017, Draper *et al*. 2014).

Recent studies suggest that intact and re-growing tropical forests have been a net carbon sink of ~2 Pg C per year between 1900 and 2009 owing to increases in net primary production (NPP) as a result of CO_2 fertilisation (Pan *et al.* 2011, Sitch *et al.* 2015, Schimel *et al.* 2015). However, this is subject to high inter-annual variability with intact tropical forests switching to net carbon sources in high temperature or low precipitation

years, typically associated with El Niño events (Liu *et al.* 2017, Wang *et al.* 2013, Petra *et al.* 2017). Observations from long term monitoring plots also suggest the historical increases in NPP appear to be levelling off, coupled with increases in mortality, thus the strength of these carbon sinks may have reduced in recent years (Brienen *et al*. 2015). Despite variation, increases in NPP observed across intact and re-growing tropical forest ecosystems appear to have offset emissions from tropical land use change (LUC), leaving the system approximately carbon neutral over this period (Mitchard *et al.* 2018). However, this is likely to change if the current trajectory of tropical deforestation and degradation continues, especially when coupled with uncertain tropical forest responses to climate change (IPCC, 2013). As a result of this dynamism, the tropical land carbon sink is still the most uncertain major component of the global carbon cycle (LeQuéré *et al*. 2018).

Globally deforestation reduced tropical forest area by ~ 2.3 million km^2 between 2000 and 2012 (Hansen *et al.* 2013). Deforestation is broadly defined as the long-term reduction of tree canopy cover to below 10-30% and is usually associated with conversion of forest to other types of land use, such as cropland or pasture (van der Werf *et al.* 2009). However, deforestation can be succeeded by the establishment of monoculture woody plantations resembling forests (Houghton, 2005). In addition to deforestation, forest degradation, where the ecological processes that underlie forest dynamics are diminished or severely constrained, but canopy cover remains high enough to be classified as forest (more than 10-30% canopy cover), also results in net carbon emissions (Ghazoul *et al.* 2015, van der Wef *et al.* 2009). Estimates of annual emissions from tropical deforestation and degradation range between 0.5 and 3.5 Pg C yr^{-1} (Mitchard *et al.* 2018). This wide range is attributed to differing definitions, differences in methodologies, including what processes are accounted for, and large uncertainties in the resultant quantifications of individual studies (Mitchard *et al.* 2018).

1.3) Tropical peatlands: carbon sinks and carbon sources

Tropical peat swamps cover an area of ~ 577,000 km^2 globally with recent discoveries of tropical peatlands in the Congo and Amazonian basins raising tropical peatland carbon stock estimates to ~ 104.7 Pg C (min 69.6 to max 129.8 Pg C) (Page *et al.* 2011, Dargie *et al.* 2017, Draper *et al.* 2014). Despite their obvious importance as carbon stores this estimate remains highly uncertain as the true extent and carbon content of peatlands in the tropics is unknown (Lawson *et al*. 2015, Gumbricht *et al*. 2017, Leifeld & L. Menichetti, 2018). Global estimates of peatland area are often the result of modelling attempts based on abiotic and environmental parameters (Gumbricht *et al*. 2017). Tropical peatlands are heterogeneous and often remote, hence, accurately sampling tropical peatland area,

depth, bulk density and carbon content is both challenging, time consuming and expensive (Lawson *et al*. 2015, Leifeld & L. Menichetti, 2018).

These organic rich deposits form due to the build-up of partially decomposed organic debris in waterlogged, anoxic conditions contained within low topographic relief zones (Page *et al.* 2004, Page *et al*. 2010). Contemporary Southeast Asian (SEA) peat deposits were initiated ~26,000 cal. yr BP accumulating most rapidly in the early Holocene to thicknesses of between 5 and 7m (Page *et al.* 2004, Page *et al.* 2011). Lowland tropical peatlands in South East Asia consist of slightly or partially decomposed woody debris containing well preserved tree trunks, branches, twigs and coarse roots within a matrix of humified amorphous organic material (Page *et al.* 2006). Across inland peat domes vegetation is dominated by trees and mirrors the species composition of Southeast Asian lowland Dipterocarp forests, although Dipterocarp trees are typically lower in stature than when found on mineral soils (Whitmore. 1984). Distinct forest subzones are formed across the peat domes coinciding with changes in peat thickness and hydrology (Whitmore, 1984, Page *et al.* 1999). This vegetation cover then provides the organic matter input for further peatland accumulation (~1.5 ± 0.5 mm y^{-1}) (Page *et al.* 2004, Murdiyarso *et al*. 2010).

In Southeast Asia, tropical peatlands are increasingly being subjected to extensive degradation and land cover change, largely due to the expansion of industrial plantation and smallholder agriculture (Miettinen *et al.* 2016, 2017). Prior to the establishment of industrial plantations or any other agricultural land use, established peat swamp forest aboveground biomass is cleared and the peat soils are then drained and compacted, halting peat accumulation processes (Miettinen *et al.* 2017, Page *et al.* 2011b). This drainage, when combined with changes in vegetation cover and the addition of fertilisers results in the oxidation of the upper peat profile and the release of CO_2 to the atmosphere (Couwenberg *et al*. 2010, Hoojer *et al.* 2012, Hergoualc'h and Verchot, 2011). In addition to this, peatland drainage also leads to an increased flux of fluvial dissolved organic carbon, CH_4 and NO_2 (Cook *et al.* 2018, Jauhiainen and Silvennoinen, 2012). Undisturbed, primary peat swamp forests are naturally fire resilient as a result of their moist microclimate and the low-flammability of pristine wet peat soils (Turetsky *et al.* 2014). Clearance and drainage significantly diminishes this resilience and drained tropical peat soils can burn to depths of 50cm, particularly in El Niño years resulting in large CO_2 emissions (Page *et al.* 2002, Ballhorn *et al.* 2009).

1.4) *Oil palm growth, usage and harvest*

Oil palm (*Elaeis guineensis*, OP) is a tropical palm species native to West and Central Africa (Sheil *et al*. 2009). Since its domestication oil palm has been cultivated as a

perennial crop throughout the humid tropics (Sheil *et al*. 2009, Corley and Tinker, 2016). Commercial planting for palm oil production was initiated in SEA in 1917 (Corley and Tinker, 2016). Palm oil is used largely in food products (71 %), with smaller fractions used in cosmetics (24 %) and as an energy source (5 %) (Byerlee *et al.* 2017). Oil can be acquired from the kernel and mesocarp of individual OP fruits, in fruit bunches which develop in the axil of each frond (Corely *et al.* 1976, Figure 1.1). During harvesting rounds fruit bunches are removed by hand, fronds are also progressively pruned before being piled on the plantation floor (Corely *et al.* 1976, Corley and Tinker, 2016).

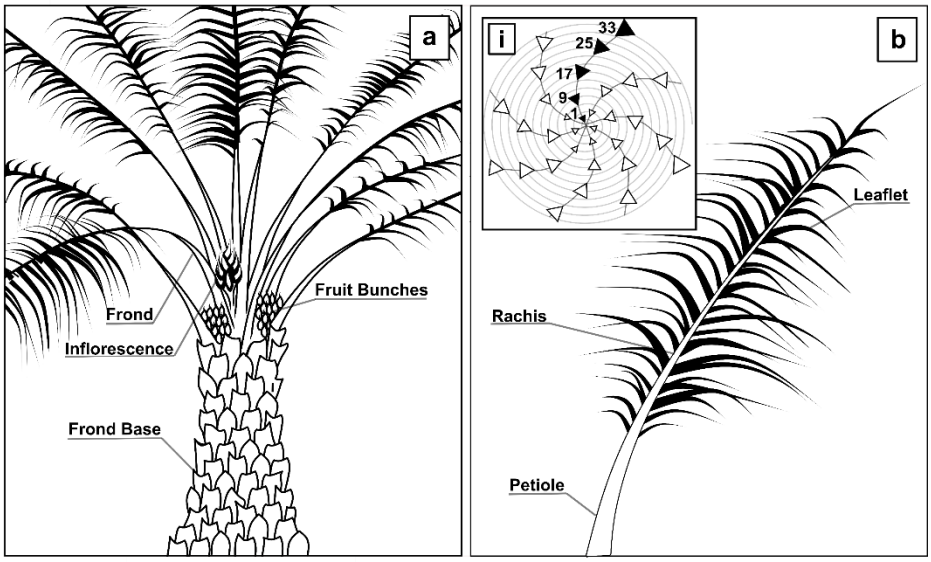

Figure 1.1: Oil palm AGB components. *Panel A: An upright Young Mature oil palm with OP fruit bunches and other AGB components indicated. Panel B: Labelled frond diagram, i) indicates frond rank numbering and crown phyllotaxis (after Aholoukpè et al. 2013).*

1.5) Contemporary oil palm expansion

Oil crop production has increased rapidly in recent decades and has shifted towards tropical areas. Global demand for palm oil has risen. The land area supporting oil palm plantations has increased to ~25 Mha globally; making oil palm the 12th largest edible crop by land area (FAO, 2019). Indonesia and Malaysia are the largest producers of palm-oil in the global market; between 1990 and 2017 their combined land area supporting oil palm (OP, *Elaeis guineensis*) plantations increased by almost 600 % to cover ~14.4 Mha (FAO, 2019). The majority of this increase has been attributed to the expansion of industrial oil palm plantations (IOPPs) with smallholders (land areas up to ~5 ha) making a much smaller contribution (Sayer *et al.* 2012). Expansion of both industrial and smallholder plantations have been linked to economic growth and development, particularly in poor rural areas (Sayer *et al.* 2012, Gatto *et al*. 2017, Rist *et al.* 2010). Oil palm plantations in the tropics can produce 4 tonnes of oil per hectare annually, approximately 4 times the yield of other oil crops in temperate regions

(rapeseed, sunflowers, or soybeans) (Rochmyaningsih, 2019). Taking into account the high productivity of oil palms and their carbon accumulation over the cropping cycle some studies conclude that the plantations are a reasonable use of already degraded land on mineral soils (Sayer *et al.* 2012, de Vries *et al.* 2010).

However, in addition to the replacement of logged and degraded forests with oil palm plantations, a large proportion of expansion has occurred at the expense of old growth, primary forests in lowland areas (Gaveau *et al.* 2016, Vijay *et al.* 2016). Malaysia, Sumatra and Kalimantan are dominated by tall dense lowland Dipterocarp forest species on mineral soils (Koh *et al.* 2015). Aboveground biomass stocks of undisturbed forests are therefore high (503.8 ± 35.0 Mg ha^{-1}) and often remain high subsequent to selective logging relative to other forest cover types (258.2 ± 20.6 Mg ha^{-1}) (Koh *et al*. 2015, Silk *et al.* 2010). The rapid expansion of oil palm plantations across lowland Dipterocarp forests in Malaysia and Indonesia has therefore resulted in large scale carbon emissions in addition to biodiversity losses (Koh and Wilcove, 2008, Koh *et al*. 2015, Gaveau et al. 2016, Carlson *et al.* 2012, Carlson *et al*. 2013).

1.6) Contemporary oil palm expansion on tropical peats and quantification of emissions

The demand for oil palm has led to the expansion of this crop onto tropical peatlands, with approximately 3.1 Mha of oil palm (OP) plantations now situated on managed peat soils (Miettinen *et al.* 2016). In 2015, industrial plantations covered ~27% of the total peatland area in Insular Southeast Asia, the vast majority of which are oil palm plantations (72.5 %) with the remainder mostly pulp wood plantations (26%, *Acacia and Eucalyptus*) (Miettinen *et al.* 2016). Despite the considerable carbon losses from biomass replacement and land clearance, large and sustained CO_2 emissions from peat oxidation make up the most significant part of the emissions from this land use change (Page *et al.* 2011b).

Miettinen *et al* (2017) estimate an annual emission of 64.3 Mt C from peat oxidation in drained industrial OP plantations across Malaysia, Sumatra and Kalimantan; based on peat OP land cover areas and IPCC peat oxidation emissions factors (IPCC, 2014). An additional 49.2 Mt C has been calculated to be emitted from smallholder areas (Miettinen *et al.* 2017). However, the IPCC emissions factors for peat oxidation following the drainage of industrial plantations (15 Mg C ha^{-1} yr^{-1}, [95% CI, 10 to 21]) do not take into account the variation in emissions across the lifecycle of a plantation (IPCC, 2014, Miettinen *et al.* 2017). Peat surface emissions are much higher immediately following conversion and drainage; hence these estimates are likely conservative (Hooijer *et al.* 2012, Page and Hooijer, 2014). Net carbon loss is related to water table depth (WTD), which also fluctuates across the planting cycle (Hooijer et al. 2012, Carlson et al. 2015).

When calculating these emissions, only those from peat oxidation are accounted for with no consideration of CO_2 loss or uptake from changes in aboveground biomass (Miettinen *et al.* 2017). Few studies comprehensively consider CO_2 emissions across a full planting cycle for oil palm on peat (Page *et al.* 2011b).

In addition to the uncertainties associated with peat oxidation emissions, the rate and magnitude of peat OP aboveground biomass accumulation is also unclear, and therefore the limited extent to which the plantation growth may offset peat oxidation emissions remains unknown (Page *et al.* 2011b, Murdiyarso *et al.* 2010, Germer and Sauerborn, 2008, Koh and Jepsen, 2015). Few studies directly compare the aboveground biomass stocks of oil palm plantations to that of their prior land covers, especially for oil palm situated on peatlands (Koh *et al.* 2011, Carlson *et al.* 2013, Murdiyarso *et al.* 2010).

Drainage associated with agricultural practice causes subsidence; the irreversible lowering of the surface as a consequence of peat oxidation, mechanical compaction and shrinkage (Hoojier *et al.* 2012). When combined with the poor anchorage of palms in the low bulk density peat soils, this often results in palm leaning, root exposure and desiccation and eventual mortality of oil palms on peat soils (Lim *et al*. 2012). This has become a major limiting factor for peat OP performance and planting cycles are typically limited to ~20 years, shorter than on mineral soils (~25 years) (Lim *et al*. 2012, Othman *et al*. 2012). In response to higher rates of OP failure on peat soils, higher planting densities are adopted for OP on peat compared to OP planted on mineral soils (Woittiez *et al*. 2017). As a result, peat OP AGB accumulation rates are likely different to those reported for OP on mineral soils. Hence, peat OP AGB stocks at various points in the planting cycle need to be accurately quantified in order to realistically evaluate peat OP emissions and greenhouse gas lifecycle assessments for OP on peat (Kho and Jepsen, 2015, Page *et al.* 2011b).

A large proportion of peat OP plantations are approaching the end of their first planting cycle, the AGB stocks of these plantations are soon to be redundant (Miettinen *et al.* 2012). Given the vast area of peat OP plantations across Insular Southeast Asia it is important to quantify the potential carbon emission from first generation peat OP plantation AGB clearance (Miettinen *et al.* 2012, Miettinen *et al.* 2017, Carlson *et al.* 2012). Optimally utilizing oil palm biomass residues may offset some of these emissions. Multiple studies highlight their potential as inputs either for bioenergy production or for the production of biochar for fertiliser or solid fuel applications (Liew *et al*. 2018, Hamzah *et al*. 2019, Abnisa *et al*. 2013). Developing methodologies that allow the accurate measurement of OP biomass residues and stocks through the planting cycle are therefore important.

1.7) Efforts to reduce emissions from peat oil palm expansion

Improving our current understanding of the carbon fluxes associated with oil palm expansion into tropical peat swamp forests across the lifecycle of a plantation would inform current and future efforts to reduce emissions from peat oil palm expansion (Miettinen *et al.* 2017).

The carbon-based mechanism REDD+ (reducing emissions from forest degradation) provides financial compensation from developed to developing nations who agree to decrease their deforestation and forest degradation rates by forgoing other land uses (den Besten, 2014). However, in Southeast Asian lowland forests, the high profitability of forest logging and converting land to high yield oil palm plantation agriculture often outweighs the potential revenues from conserving forests under REDD+ and other voluntary carbon credit schemes (Fisher *et al.* 2011, Butler *et al.* 2009, Abram *et al.* 2016). Despite this, the recent inclusion of peatland soil organic carbon in REDD+ schemes will hopefully improve the available incentives for landowners (Murdiyarso *et al.* 2010, Murdiyarso *et al.* 2019, Joosten *et al.* 2016). Effective implementation of REDD+ is however reliant on the accurate quantification of potential emissions from land use changes combined with effective land cover and carbon stock monitoring (Angelsen et a, 2009, Gibbs *et al.* 2007, Birdsey *et al.* 2013, Murdiyarso *et al.* 2019).

In Indonesia a moratorium on new oil palm concessions in primary forests and peatlands was issued in 2011 and enforced in 2018 in an attempt to limit deforestation, but so far has had limited success so far (Murdiyarso *et al.* 2011, Austin *et al.* 2017, Busch *et al.* 2015, PRI, 2018). In addition to interventions from governments, increasing pressures from consumers and commodity markets has led to an increase in palm oil certification; third-party audits that ensure producers follow a set of social and environmental practices to improve the 'sustainability' of oil palm production (Milder *et al.* 2015). The Roundtable on Sustainable Palm Oil (RSPO) certified ~2,246,763 ha of oil palm plantations across Indonesia and Malaysia in 2014 (Garrett *et al.* 2016). Certified growers agree to comply with the RSPO Principles and Criteria standards, which, amongst other criteria, limit the land covers that can be developed for oil palm (RSPO, 2018). Whilst certification has effectively reduced deforestation when compared to non-certified plantations, deforestation rates in these certified plantations still remained high, including primary and peat swamp forest clearance (Carlson *et al.* 2018). Commencing in 2018, the new standard aims to prevent new planting on peat soils regardless of peat depth in existing and new development areas (RSPO, 2018). However, a large proportion of palm oil production currently remains un-certified (80%) (Garrett *et al.* 2016).

1.8) Monitoring oil palm expansion using remote sensing techniques

Remote sensing techniques allow the mapping and monitoring of OP expansion. These maps, when produced at fine spatial and temporal resolutions assist in enforcing OP certification efforts and minoring the success of attempts to reduce deforestation (Carlson *et al.* 2018, Angelsen *et al*. 2009, Gibbs *et al.* 2007).

Land cover classifications of different vegetation types across a timeseries of satellite images have been used to track the establishment of industrial oil palm plantations (IOPP) at regional scales (Gaveau *et al.* 2016, Gaveau *et al.* 2014, Miettinen *et al.* 2011). The establishment of OP plantations on tropical peatlands has been monitored by combining IOPP maps with existing maps of tropical peatland extent (Koh *et al.* 2011, Miettinen *et al.* 2016). In addition to industry and government records of expansion the distinctive geometric planting associated with the establishment of plantations make them easily identifiable in optical remotely sensed datasets at high resolutions (Wicke *et al.* 2011, Gaveau *et al.* 2016, Nomura and Mitchard, 2018). Optical imagers from passive sensors record reflected and emitted electromagnetic radiation from the earth's surface and overlying atmosphere in the visible to thermal infrared spectrum (λ = 380 nm – 8000 nm). Vegetation characteristics can be discriminated by their optical spectral signatures, however, in the tropics, dataset availability is often hindered by cloud (Gibbs *et al*. 2007). In addition to using spectral datasets, information about vegetation structural characteristics can been inferred using active remote sensing techniques (Xie *et al*. 2008). L-band synthetic aperture radar (SAR) datasets have frequently been used in combination with spectral data to monitor oil palm plantation extent and establishment, in many instances producing a more reliable classification when compared to methodologies using only optical products (Cheng *et al.* 2018, Cheng *et al.* 2016, Morel *et al.* 2012, Miettinen *et al.* 2012, Gaveau *et al.* 2016). The changes in AGB stocks that accompany forest clearance and OP plantation establishment can then estimated by upscaling forest AGB estimates and OP AGB accumulation models to match land cover maps at provincial and regional scales (Carlson *et al.* 2013).

Multiple studies have mapped oil palm extent and expansion over time, however, few attempt to directly quantify the *in-situ* carbon stock changes associated with this land use change. Several well cited maps of woody aboveground biomass density (AGBD) at coarse spatial resolutions (0.5 – 1 km) are available across the tropics (Saatchi *et al.* 2011, Baccini *et al.* 2012, Avitabile *et al.* 2016). These could potentially be used as benchmarks from which to calculate in-situ emissions from conversion to OP if they pre-date plantation establishment. However, the accuracy of these maps have been widely criticised (Mitchard *et al.* 2013, Hill *et al.* 2013, Hansen *et al.* 2019). Several studies have attempted to produce continuous maps of AGBD which include both forest and IOPP

land covers using airborne LiDAR and SAR datasets (Nunes *et al.* 2017, Morel *et al.* 2011). Airborne LiDAR point cloud data (0.4m footprint) produced good estimates of aboveground biomass density for oil palm of various ages (8 and 14 years after planting) on mineral soils across 27 1-ha plots (Nunes *et al.* 2017). Despite positive results, airborne LiDAR datasets are expensive to produce and time consuming to process, the frequent re-visitation of sites to monitor OP AGB accumulation across the scale required is not currently feasible. Morel et al (2011) attempted to directly quantify the AGB stocks of intact and degraded forests and OP plantations of various ages in Sabah, Malaysia, using L-band SAR. Despite reliably classifying forest and OP land covers (97.0% accuracy), the AGB stocks of OP plantations were not reliably predicted as the AGB/RCS relationship derived solely from forest plots did not accurately estimate the AGB stocks of OP palm plantations (Morel *et al.* 2011).

1.9) Synthetic aperture radar sensors for vegetation monitoring

Synthetic aperture radars (SAR) are active sensors which transmit microwave signals and measure the backscattered portion of this signal returned to the sensor, the radar cross section (RCS), in order to analyse features on the earth surface.

SAR Acquisition and polarisation

Imaging radar is an active remote sensing system, a sensor transmits a radar signal in a side looking direction towards the Earth's surface. The return signal received by the sensor is reflected from within the ground swath footprint at the earth's surface (Figure 1.2a). SAR sensors mounted on moving objects use the motion of the radar antenna over a target region to provide a finer azimuth resolution product than conventional beam-scanning radars with a similar antenna size (Woodhouse, 2006, JAXA, 2019a, Figure 1.2a).

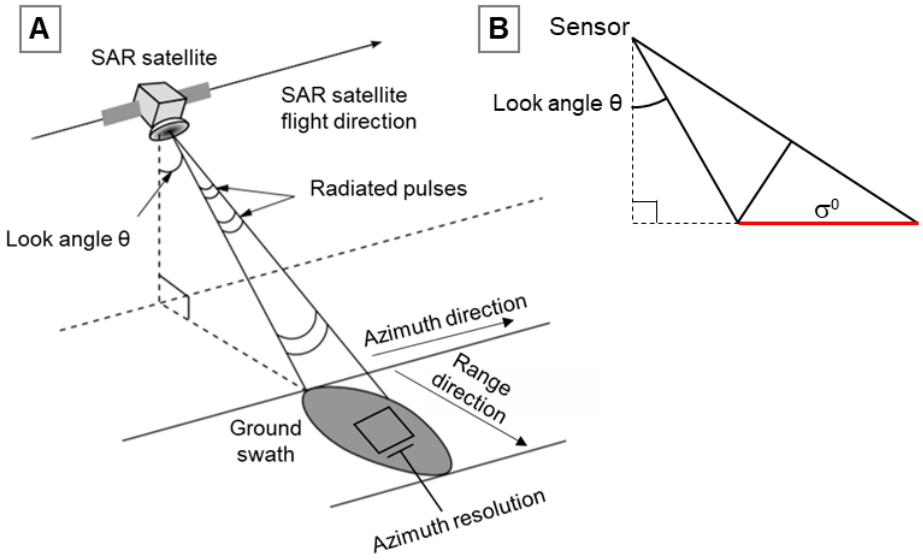

Figure 1.2: Geometry of Synthetic Aperture Radar systems. *Panel A: Simplified geometry of a SAR system (Adapted from Lauknes (2010)), Panel B: Geometry of RCS in the Sigma Nought (σ^0) plane (Adapted from ASF, 2019).*

The polarisation of SAR sensors can also be specified. Polarization refers to the orientation of the electric field of an electromagnetic wave transmitted or measured by the sensor (ESA, 2009, Figure 1.3). Reflectivity and scattering of microwaves from an object depends on the relationship between the polarization state and the geometric structure of the object (ESA, 2009, Woodhouse, 2006). Common notation refers to radar co-polarization: HH (horizontal transmit, horizontal receive) and VV and cross-polarisation: HV and HV (Woodhouse, 2006, CEOS, 2018).

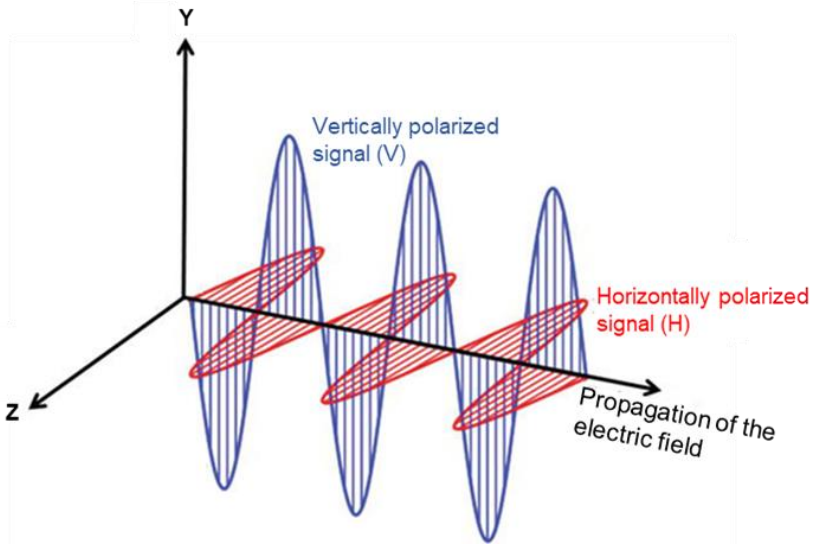

Figure 1.3: SAR Polarisation. *Horizontal (red) and vertical (blue) orientation of the electric field of an electromagnetic wave along the direction of propagation (Adapted from JAXA, 1997 and Dabboor and Brisco, 2018).*

Radiometric calibration and terrain correction

Upon acquisition SAR images are typically provided in digital number (DN) format (ASF, 2019, JAXA, 2009). Radiometric calibration coefficients specific to SAR sensors and acquisition modes are then applied to the DN to produce a radiometrically calibrated power image. Sigma Nought (σ^0), is the conventional measure of the radar cross section. Often expressed in in decibels (σ^0dB), the RCS is a is a normalized dimensionless number, which compares the strength of backscatter observed to that expected from an area of one square metre (m^2/m^2) (ESA, 2009, ASF, 2019, Ryan et al, 2012). Sigma Nought RCS is defined with respect to the nominally horizontal plane and therefore has significant variation with incidence angle, wavelength and polarization (ESA, 2009, Woodhouse, 2006, Figure 1.2b).

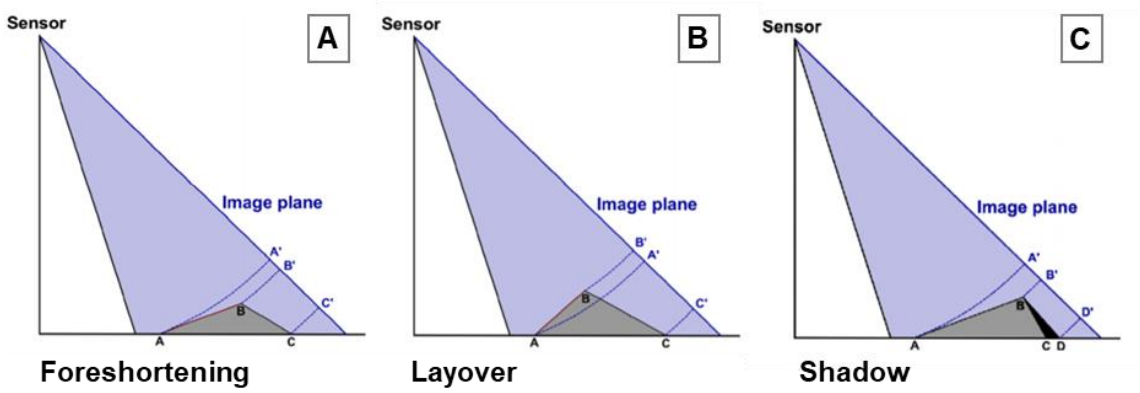

Figure 1.4: Geometric distortions in SAR imagery. *Panel A: Foreshortening, Panel B: Layover and Panel C: Shadow. (Adapted from ASF, 2013). Letters A – D in black represent feature position and relative distances between features on the ground, letters A' – D' in blue represent the position and relative distances between features in the image plane.*

As SAR images are acquired in a side looking geometry, this can lead to multiple distortions in the imagery, particularly in sloped areas. In figure 1.4a foreshortening occurs when the time difference of two signals backscattered at the bottom and the top of a steep slope (B'-A', Figure 1.4a) is shorter than from the top to the back-side flat area (C'–B', Figure 1.4a). The first two points are mapped with a shorter difference between them in the image plane, compressing the backscattered signal coming from the foreshortened areas (Figure 1.4a). Image layover occurs when the signal received from the peak of a slope is received earlier than the signal from the slopes base (Figure 1.4b). Pixel information from various location is superimposed. The shadow effect in radar imagery occurs when no information is received from the back of a slope (Figure 1.4c).

Terrain corrections, successfully applied, can remove geometry induced distortions in SAR images by making use of height information derived from digital elevation models (DEM) (ASF, 2019, ESA, 2009).

Radar scattering biomass estimation

SAR images represent an estimate of the radar backscatter for the corresponding area at the surface. Darker areas represent surfaces with low backscattering characteristics while brighter areas represent high backscatter backscattering characteristics.

Backscatter for a target area at a particular radar wavelength varies depending on conditions such as the physical size of the scatterers in the target area their dielectric properties (Woodhouse, 2006). Therefore, radar sensors are sensitive to changes in moisture with wetter objects appearing brighter (with the exception of flat water bodies, which appear dark) (Woodhouse, 2006).

Radar Frequency Band (IEEE standard)	Frequency (GHz)	Wavelength (cm)
P-band	0.2 to 0.5	65
L-band	1 to 2	23
C-band	4 to 8	5
X-band	8 to 12	3

Table 1.1: Radar Frequency Bands according to the IEEE standard and corresponding wavelengths.

SAR wavelength and polarisation will also effect affect backscatter. Table 1.1 presents the IEEE standard frequency bands for radar sensors. Incident microwaves are scattered by structures that correspond to their wavelength (ESA, 2009). When monitoring vegetation, P-band and L-band SAR sensors are most sensitive to woody vegetation characteristics (tree trunks and branches) (ESA, 2009). While C-band and X-band sensors are sensitive to leafy vegetation surface characteristics, like leaves and grasses and cannot penetrate the canopy of woody vegetation (ESA, 2009).

For low frequency SAR systems (L and P-band), the observed RCS of SAR images integrates multiple scattering mechanisms (Figure 1.5, Brolly and Woodhouse, 2012, Brolly and Woodhouse, 2014). Diffuse scattering occurs from rough surfaces (relative to the radar wavelength), results in the signal being scattered in different directions, the rougher the surface the higher the co-polarisation (HH or VV) backscatter (Figure 1.5a, CEOS, 2018). Direct backscatter occurs when the transmitted signal is reflected directly back to the sensor by a single reflection, usually by a surface oriented perpendicular to the radar illumination direction (Figure 1.5b and c). This results in a strong co-polarisation reflection and appears bright in the SAR image. Double bounce scattering occurs when

vegetation/ground structures act as corner reflectors, as waves remain coherent double bounce scattering only occurs at co-polarisation (Figure 1.5d, CEOS, 2018). Volume scattering occurs when the radar signal is subject to multiple reflections within 3-dimensional matter. Since the orientation of scatterers in the canopy is typically random, return signal polarisation is also random, backscatter is therefore equal in co- or cross-polarisation (Figure 1.5e, CEOS, 2018).

L-band spaceborne sensors are frequently used for woody vegetation and forest monitoring as increases in RCS have been correlated increases in woody AGB up until a saturation point (Yu and Saatchi, 2016). The mechanisms that determine RCS sensitivity to woody biomass and saturation are poorly understood however, it is likely due to transitions between scattering mechanisms (Figure 1.5, Woodhouse, 2006, ESA, 2009, Brolly and Woodhouse, 2012, Brolly and Woodhouse, 2014). When using L-band radar the strength of the correlation between AGB and RCS is frequently found to be stronger when using the HV polarisation when compared to the co-polarised sensors (HH) (Yu and Saatchi, 2016, Morel et al, 2011, Ryan et al, 2012). This is likely because HV signals are more relatively dominated by radar volume scattering within the forest canopy when compared to the HH (CEOS, 2018).

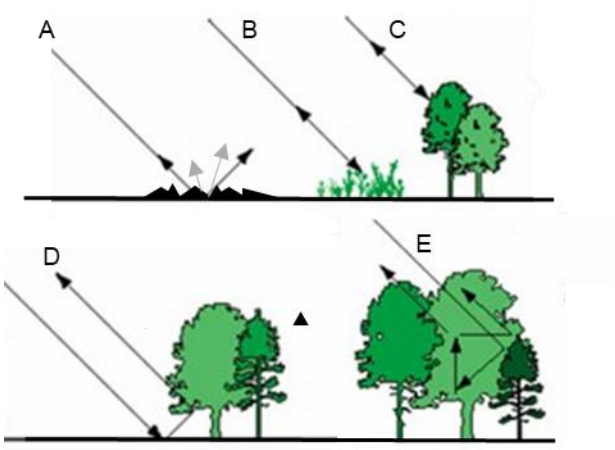

Figure 1.5: Scattering mechanisms for SAR interactions with surface vegetation. *A: Diffuse scattering from the ground, B: Direct scattering from grass, C: Direct scattering from the canopy (high frequency radar), D: Double bounce scattering from the ground-vegetation, E: Volume scattering from within the forest canopy (low frequency radar). (Adapted from Piwowar (1997)).*

Multiple studies have used the relationship between RCS and forest structural characteristics to estimate and map biomass stocks (Supplementary Table S4.1). Some produce timeseries maps of AGBD with enough sensitivity to directly monitor deforestation, degradation and growth (Ryan *et al.* 2012, Joshi *et al.* 2015, Mitchard *et al.* 2011). In order to achieve this, SAR radar cross section is typically calibrated to co-

located field inventory plots where AGB stocks have been measured using a regression model (Supplementary Table S4.1). The coefficients of these regression models are then used to estimate AGB stocks using the RCS over a wider area (Ryan *et al.* 2012, Mitchard *et al.* 2011, Morel *et al.* 2011).

1.10) SAR vegetation monitoring – challenges and uncertainties

Radar backscatter is not a direct measure of forest biomass (Woodhouse et al. 2012). The sensitivity of L-band SAR sensors to AGB saturates at between 80 to 250 Mg C ha^{-1} depending on forest structure and surface characteristics (Yu and Saatchi, 2016). SAR radar cross section is also influenced by topography; effective terrain correction of SAR scenes is therefore important as topographic artefacts can result in inaccuracies, particularly in mountainous areas or areas of variable slope (Figure 1.4, Atwood et al. 2014). The speckle observable in synthetic aperture radar due to the coherent interference of waves reflected by scatterers also complicates image interpretation and both reduces the accuracy of image classification and the legitimacy of detected changes between sequential SAR observations (Lee et al. 1999, Joshi et al. 2015). In addition, radar sensors are sensitive to changes in soil, canopy and vegetation moisture, characteristics that frequently change over time (Balenzano, et al. 2010, Morel et al. 2011). This noise in L-band SAR datasets is problematic particularly when attempting to detect forest disturbance or growth (Joshi et al. 2015).

Despite this, L-band radar datasets such as ALOS PALSAR-1/2 feature multiple observations of the same area over time, some products having multiple scenes per year (JAXA, 2019a). Time-series analysis allows the same RCS pixel to be observed multiple times across the duration of a LUC allowing more confidence in determining the condition of the vegetation and AGB stocks at the pixel location (Joshi et al. 2015). Despite this, inter-scene variability in the surface characteristics that influence radar scattering mean that the relationship between AGB and RCS must ideally be calibrated independently for each SAR scene acquired (Ryan et al. 2012). Successful timeseries analysis would therefore typically require a large number of calibration plots monitored frequently across the timeseries, a time consuming and potentially limiting process (Supplementary Table S4.1, Picard et al. 2012, Chave et al. 2005).

New methodologies have however been developed which reduce the need for *in-situ* calibration plots when using L-band SAR for AGB mapping (Hill *et al*. in prep). The iterative 'Biomass Matching' algorithm identifies areas where no perceived AGB change has occurred across a timeseries of SAR scenes to derive the scene specific calibration coefficients needed to map gains and losses in AGB stocks (Hill *et al.* in prep). This requires an initial relationship between AGB and *in-situ* RCS to be defined by the user

for a single SAR scene (Hill *et al*. in prep). These recent methodological developments may allow the utilization of publicly accessible L-band radar datasets (like the ALOS PALSAR-1/2 global mosaic product) to accurately estimate peat OP AGB accumulation over time, without the need for extensive inventory plots over multiple years. Firstly though, the relationship between peat OP AGB and in-situ RCS must be defined (Hill *et al*. in prep, Ryan *et al.* 2012, Morel *et al.* 2011).

*1.11) **Project Rationale***

The rapid contemporary expansion of OP across tropical peatlands has resulted in net ecosystem emissions (Miettinen *et al.* 2017, Couwenberg *et al*. 2010, Hoojer *et al*. 2012, Hergoualc'h and Verchot, 2011). In order to address key uncertainties, there is an ongoing effort to quantify the emissions from peat oxidation in drained OP plantations over time (Miettinen *et al.* 2017). OP plantations on peat are typically cleared ~20 years after planting (Lim *et al*. 2012, Corley &Tinker, 2016). Despite this, the rapidly growing oil palms are a temporary carbon sink, potentially offsetting a small proportion of these emissions. There is a scarcity of studies measuring AGB stocks and accumulation of working OP plantations on peat, potentially due to the comparatively recent expansion of OP across peatlands compared to mineral soils (Koh & Jepsen, 2015, Carlson *et al.* Murdiyarso *et al.* 2010, Page *et al.* 2011b). Even fewer studies consider the OP plantation AGB accumulation within the context the AGB stocks of the previous land cover (Koh & Jepsen, 2015).

Direct monitoring of peat OP AGB stocks which assess the variation of stocks over time and within age classes is needed and could potentially inform GHG lifecycle assessments for oil palm on peat. Most peat OP plantations are currently in the middle of or approaching the end of their first planting cycle (Lim *et al*. 2012, Kho *et al*. 2011, Miettinen *et al*. 2016). Given the time scale over with we must act if we wish to ensure global temperature increases are limited to 1.5°C above pre-industrial levels, and the extent of this land cover type, increasing our understanding of this temporary carbon store is important to inform decisions concerning the next planting cycle and land management over the next 20 years (IPCC, 2013, IPCC, 2018, Kho *et al*. 2011).

Remote sensing approaches that enable the detection of OP plantation expansion and AGB stock monitoring across a broad scale may be an economically viable monitoring tool. Despite efforts to map OP plantation expansion (Wicke *et al.* 2011, Gaveau *et al.* 2016), studies are yet to attempt to directly quantify the *in-situ* carbon stock changes associated with this land use change using remote sensing techniques. Course resolution maps of AGBD across the tropics are available (Saatchi *et al.* 2011, Baccini *et al.* 2012, Avitabile *et al.* 2016), however the accuracy and reliability of these maps has been challenged (Mitchard *et al.* 2013, Hill *et al.* 2013).

L-band SAR sensors have frequently been used to estimate and map vegetation AGB stocks and are in some instances used to detect AGB accumulation and degradation (Ryan *et al.* 2012 Joshi *et al.* 2015 Mitchard *et al*. 2011). However, saturation of the AGB/RCS relationship at high AGBs across many vegetation types is a significant challenge (Yu and Saatchi, 2016, Joshi *et al.* 2017).

The large number of calibration plots required to be monitored across the timeseries is also potentially limiting when mapping changes in AGB using SAR over time (Supplementary Table S4.1, Picard et al. 2012, Chave et al. 2005). Using the novel 'Biomass Matching' technique, which reduces the need for calibration plots, may make using L-band SAR to monitor small scale changes in peat OP AGB stocks more feasible. For this technique to be viable, some plot based AGB stock assessments for working industrial oil palm plantations on peat are required.

This study aims to address the lack of available plot based estimated of AGB and AGB accumulation for oil palm on drained tropical peats. By using the a timeseries of L-band SAR images and the 'Biomass Matching' technique, this study aims to map changes in AGB across a peat OP plantation over time from initial establishment to 12 years after planting.

1.12) Research Aims

Chapter 3: 'An assessment of oil palm plantation aboveground biomass stocks on tropical peat using destructive and non-destructive methods'

- Develop allometric relationships for assessing oil palm and frond biomass specifically for oil palm plantations on drained tropical peat.

- Evaluate how AGB is distributed within various parts of the oil palms when grown on peat.

- Use developed allometric relationships to quantify per hectare AGB stocks for oil palm on drained tropical peat at various points in the planting cycle.

- Quantify AGB stock variation within age classes and AGB accumulation with plantation age for an industrial OP plantation on peat.

Chapter 4: 'Monitoring the aboveground biomass accumulation of oil palm on peat using L-band radar'

- Define the relationship between the radar cross section and AGB stocks of oil palm on peat at varying stages in the oil palm planting cycle.

- Use the 'biomass matching' approach to detect changes in AGB across a timeseries of L-band SAR scenes and map the AGB losses and gains accompanying OP establishment.

- Assess the sensitivity of OP biomass stock estimation using this approach by validating oil palm AGB maps against plot inventories and an oil palm AGB accumulation model *(Chapter 3).*

- Identify the potential point of saturation of L-band SAR sensitivity to increases in AGB.

- Compare the resulting biomass maps with existing maps of aboveground biomass density.

Chapter 2: Study site

2.1) Location, soil and climate

The Sebungan Estate and Sabaju Estate Complex were established and converted to oil palm in Sarawak, Malaysian Borneo between 2007 and 2016 and are currently in their first planting cycle (3.19˚N 113.43˚E) (Figure 2.1). In 2018, the plantations had an area of ~10,200 ha. The Estates are surrounded by oil palm plantations on both peat and mineral soils (Figure 2.1).

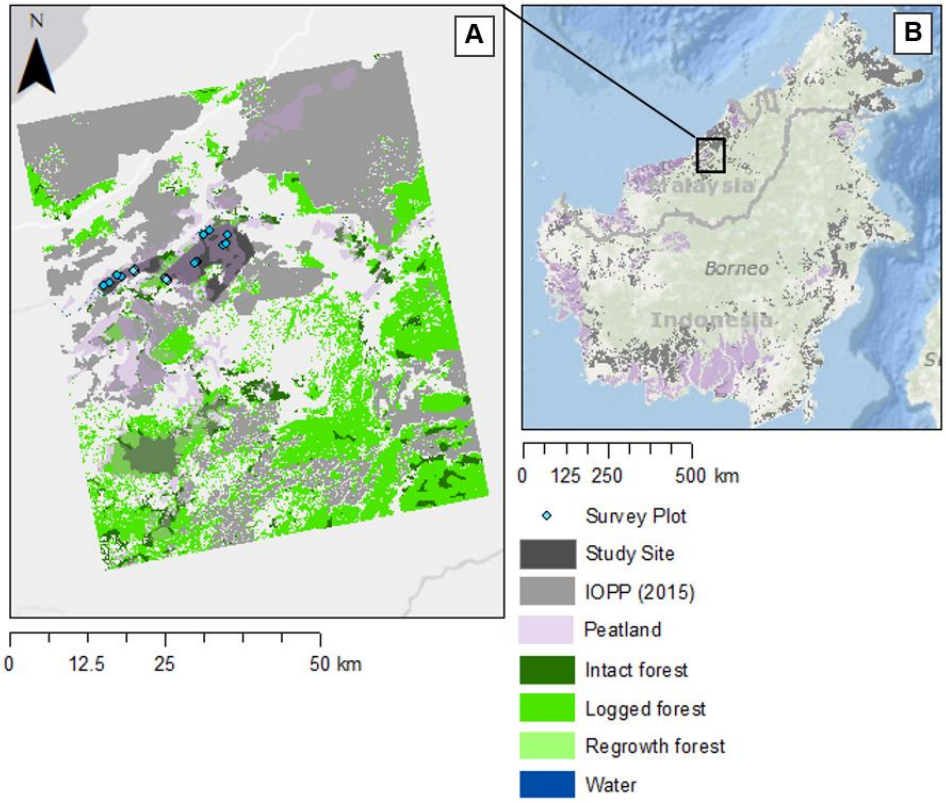

Figure 2.1: The Sebungan Estate and Sabaju Estate Complex *(Panel A), located in Sarawak, Malaysian Borneo (Panel B). Survey plots (blue circles) are indicated across the plantations (dark grey). Industrial oil palm plantations (IOPPs) as outlined by Gaveau et al. 2016 are indicated (light grey), peatland extent across Borneo is also indicated (light purple) (GFW, 2019a, GFW, 2019b). Land cover types in Panel A are taken from Gaveau et al. 2016 and indicate land covers in 2015.*

The plantation is low lying (~23.0 ± 7.6 m above sea level), with soil surveys indicating a majority composition of lowland organic deposits with an underlying marine clay mineral layer (84.8%). Very deep peat (> 3m thick) covers the majority of the plantation; 42.2% has highly decomposed sapric surface (0 – 0.5 m) and subsurface (0.5 – 1.5 m) tiers. A further 42.6% is comprised of a partially decomposed sapric surface tier (0 – 0.6 m) and hemic subsurface tier (0.5 – 1 m). Both deposit types contain partially decomposed wood

between 0.5 – 1m (Supplementary Figure S2.1, Environmental Impact Assessment, 2006). The Sebungan Estate plantation is situated on a peat dome between two rivers, the Sebungan estate consists of 4 plantations on an irregular peat dome with patches of mineral soils and hills (Cook *et al.* 2018, Supplementary Figure S2.1).

The site receives ~ 3075 mm rainfall per year (typically ranging from 3000 to 3200 mm, Cook et al, 2018) with an average annual temperature of 27.2 °C. Annual rainfall patterns are dominated by two monsoons; October-January and May-August, with the former contributing most to the annual precipitation at the site.

2.2) Conversion, OP plantation establishment and management

Prior to conversion, large trees at the study site were selectively logged. During conversion, drainage ditches were dug, and water tables have since been maintained at an optimal depth of ~0.4 – 0.6 m from the peat surface to allow cultivation (Cook *et al.* 2018, Lim *et al.* 2012, Othman *et al.* 2010). Woody debris at various stages of decomposition were removed from the peat and piled up on the land surface, often parallel to drains. Burning was not used for land cover clearance at the site, vegetation was felled and debris was piled up on the land surface and left to decompose, oxidizing to CO_2 over time as is typical for peat OP plantations. After clearance, the peat was compacted using heavy machinery to increase bulk density (Lim *et al.* 2012).

Planting bocks were established gradually, the Sebungan Estate (West, Figure 2.1) was converted and planted between 2007 and 2008 and the Sabaju Estate Complex (East, Figure 2.1) between 2007 and 2016. Blocking maps can be observed in Appendices 1 (Supplementary Figures S2.2 and S2.3). Oil palm seedlings were then planted at a density of 160 palms per hectare (Figure 2.2).

The estates appear managed, in 2017 at the Sebungan Estate water tables were kept at a mean depth of 0.54 ± 0.14 m (WTD measured at 30-minute intervals at single location in the Sebungan Estate, McCalmont, 2020, pers. comm, 04 Apr). In the same year fresh fruit bunch (FFB) harvest was 26.6 Mg FFB ha^{-1} in the Sebungan Estate (Koh 2020, pers. comm, 04 Apr). Yields appear high when compared to available yield data from other mature OP plantations on peat and the Malaysian (19.9 Mg FFB ha^{-1} yr^{-1}) and Indonesian (17.1 Mg FFB ha^{-1} yr^{-1}) average FFB yields for the same year (FAOSTAT, 2019, Woittiez *et al*. 2017, Veloo *et al.* 2015, MPOB, 2013, Latif et al. 2002). However, yield data should be interpreted with some caution. Leaning and fallen palms as a result of poor palm anchorage and peat subsidence are present within mature plantation plots. However, the severity and frequency of palm leaning and mortality varies across the various plantations making up the Estates. Leaning is most common in mature plots in Sabaju

Plantations 1 and 3 and on patches of peat in Sabaju Plantation 2 (Supplementary Figure S2.3). Severe leaning and palm failure is rare across the Sebungan plantations.

The Sebungan Estate and Sabaju Estate Complex have been the subject of multiple environmental surveys and carbon balance studies. These include high resolution ecosystem scale measurements of land-atmosphere fluxes of CO_2 (McCalmont *et al*. in prep), monthly soil, root, stem and frond pile respiration (Manning *et al.* 2019), drain dissolved organic carbon content (Cook *et al.* 2018) and young palm root biomass (Rumpang *et al.* unpublished). Studies have yet to address the AGB stocks across a range of OP ages at the site, quantification of these stocks would improve GHG life cycle assessments and carbon balance estimates at the sites.

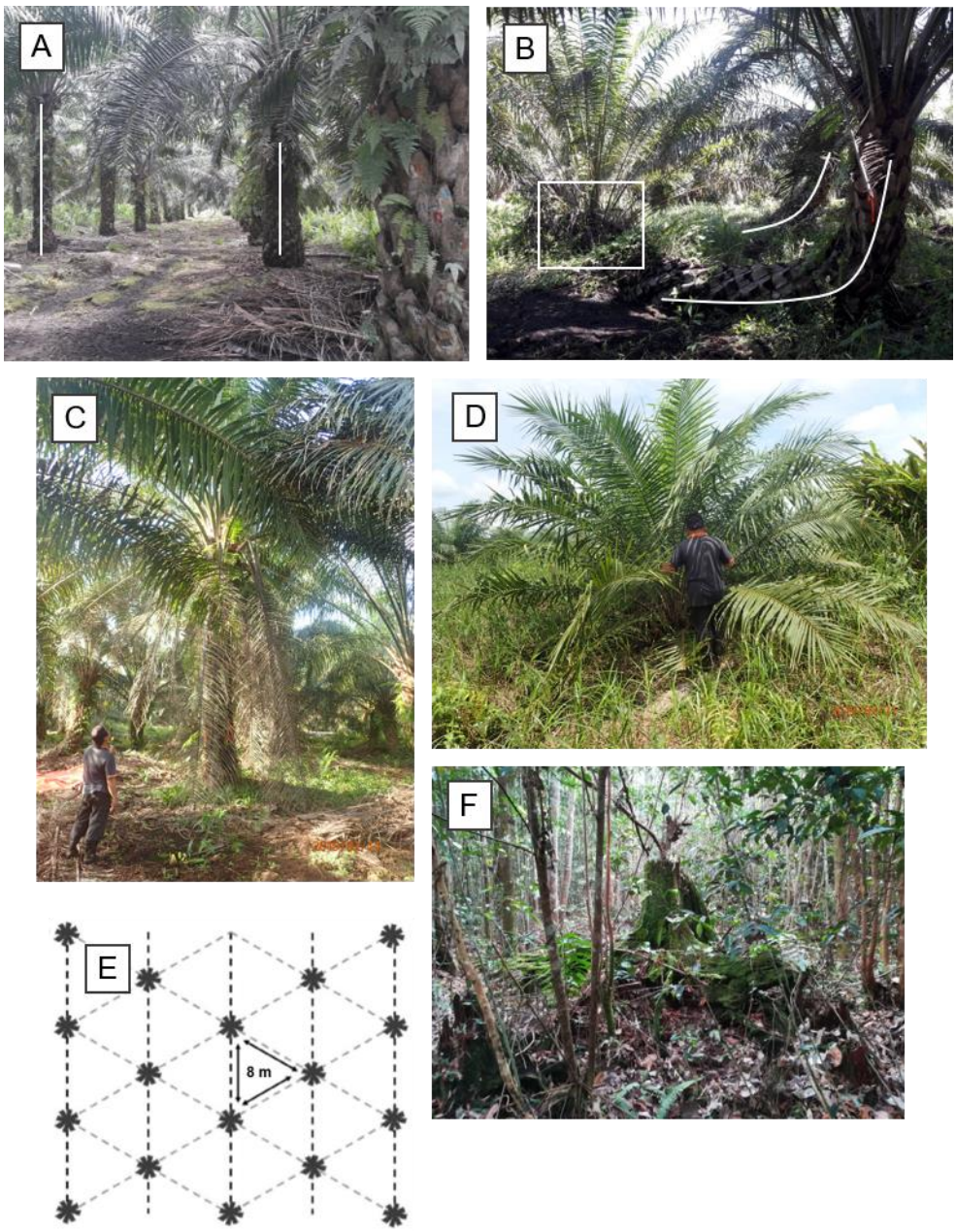

Figure 2.2: Vegetation and planting at the Sebungan Estate and Sabaju Estate Complex.

- *A) Upright oil palms on peat (Sebungan, 11 years after planting (YAP)) – trunks highlighted using white lines.*
- *B) Leaning oil palms (while lines) and replanted palms (white box) on peat (Sabaju, 10 YAP)*
- *C) Oil palm, 12 years after planting (Sebungan)*
- *D) Oil palm 3 years after planting (Sabaju)*
- *E) Industrial oil palm plantation planting pattern (peat soils, planting density of 160 m). Adapted from* Chong *et al.* 2017.
- *F) Peat swamp forest fragment on the Sabaju Estate, some large trees removed (Source: McCalmont, 2019).*

Chapter 3: 'An assessment of oil palm plantation aboveground biomass stocks on tropical peat using destructive and non-destructive methods'

Kennedy Lewis*[1], Elisa Rumpang[2], Lip Khoon Kho[2], Jon McCalmont[1], Yit Arn Teh[3], Angela Gallego-Sala[1], Timothy Charles Hill[1]

[1] College of Life and Environmental Science, University of Exeter, Streatham Campus, Rennes Drive. Exeter, EX4 4RJ. UK

[2] Tropical Peat Research Institute, Biological Research Division, Malaysian Palm Oil Board, 6, Persiaran Institusi, Bandar Baru Bangi, 43000 Kajang, Selangor, Malaysia

[3] School of Natural and Environmental Science, Newcastle University, Drummond Building, Newcastle-upon-Tyne, NE1 7RU UK

Author contribution: K.L. wrote this manuscript, designed the experiment and completed the data processing and analysis with input from all authors (see Section 3.6).

Citation: Lewis, K., Rumpang, E., Khoon, K.L., McCalmont, J., Arn, T.Y., Gallego-Sala, A. and Hill, T.C. 2020. An assessment of oil palm plantation aboveground biomass stocks on tropical peat using destructive and non-destructive methods. *Scientific Reports,* 10: 2230.

3.1) Abstract

The recent expansion of oil palm (OP, *Elaeis guineensis*) plantations into tropical forest peatlands has resulted in ecosystem carbon emissions. However, estimates of net carbon flux from biomass changes require accurate estimates of the above ground biomass (AGB) accumulation rate of OP on peat.

We quantify the AGB stocks of an OP plantation on drained peat in Malaysia from 3 to 12 years after planting using destructive harvests supported by non-destructive surveys of a further 902 palms. Peat specific allometric equations for palm (R^2 = 0.92) and frond biomass are developed and contrasted to existing allometries for OP on mineral soils. Allometries are used to upscale AGB estimates to the plantation block-level.

Aboveground biomass stocks on peat accumulated at ~6.39 ± 1.12 Mg ha^{-1} per year in the first 12 years after planting, increasing to ~7.99 ± 0.95 Mg ha^{-1} yr^{-1} when a 'perfect' plantation was modelled. High inter-palm and inter-block AGB variability was observed in mature classes as a result of variations in palm leaning and mortality. Validation of the allometries defined and expansion of non-destructive inventories across alternative plantations and age classes on peat would further strengthen our understanding of peat OP AGB accumulation rates.

*3.2) **Introduction***

Global demand for palm oil has risen such that the land area supporting oil palm (OP, *Elaeis guineensis*) plantations has increased to ~25 Mha globally; making OP the 12th largest edible crop by land area [1]. The rapid expansion of OP in Insular Southeast Asia during the last quarter decade has resulted in the conversion of 3.1 Mha of tropical peatlands [2]. The carbon emissions from the oxidation of soil organic matter following the conversion of peat swamp forest to OP are relatively well known, yet the net carbon emission of peat swamp forest conversion to OP across the life of a plantation remains poorly constrained [3-6]. In part, uncertainty is attributed to a scarcity of literature which addresses the rate at which OP on peat accumulates carbon in biomass over time [6-10]. The majority of OP standing biomass is stored as aboveground biomass (AGB) constituting 84% of biomass stocks, with the reminder (16%) stored as belowground biomass (BGB); consequently, efforts here focus primarily on AGB quantification [11-13].

Recent efforts to quantify the AGB stocks of forests and plantations have increasingly used remote sensing techniques [14,15]. However, remote sensing estimates ultimately rely on direct ground-based measurement of AGB stocks either for calibration or validation [15,16]. Forest and plantation vegetation is destructively harvested to obtain the vegetation dry-weight (DW) and infer biomass carbon stocks (~47.4% of dry biomass) [17,18]. These destructive measurements are essential but are costly in terms both of time and resources; allometric equations which relate AGB stocks to non-destructive or semi-destructive measurements of vegetation structural characteristics are therefore invaluable [18,19]. Destructive and non-destructive AGB stock estimates are common for OP on mineral soils but are almost entirely absent for OP on peat [6,8]. Furthermore, much of the literature and allometries are contained within '*grey*' literature. The lack of published direct ground-based estimates of AGB for OP on peat is also a major limitation for remotely sensed estimates of OP AGB and in carbon bookkeeping models [6,21,22].

OPs are typically managed for a planting cycle of ~25 years after which profitability reduces and the next cropping rotation is initiated [23]. However, during each growing cycle only a proportion of the biomass produced is retained by the palm to augment its existing biomass, the remainder is lost as a result of the natural and managed turnover of fruit, inflorescences, fronds and frond bases (Figure 3.1a) [10,23,24]. Fruit bunches develop in the axil of each frond and are harvested cyclically. Fronds emerge at a rate of 20-25 fronds per year and are progressively pruned before being piled on the plantation floor during harvesting rounds [23,25]. Frond bases; which are left adhering to the trunk subsequent to pruning accumulate during the early to middle years of the planting cycle and are typically shed ~12 years after planting [23]. The single growing apex of OPs, absence of secondary stem thickening once mature and regular phyllotaxis of

fronds within the palm crown mean they are well suited to dry weight quantification and allometric development (Figure 3.1b, 3.1c) [26,27]. On mineral soils allometric equations have been produced to monitor each palm AGB component in order to accurately equate biomass stocks and turnover spatially and over time (Table 3.1). However, many OP AGB assessments state biomass values without information pertaining to planting density and local environment and are subject to uncertainties associated with a lack of standardised methods (Supplementary Table S3.1) [8,9]. Models of OP biomass stock accumulation on mineral soils have also been developed and have been incorporated into large scale LUC carbon flux and bookkeeping models [8,21,28,29,30].

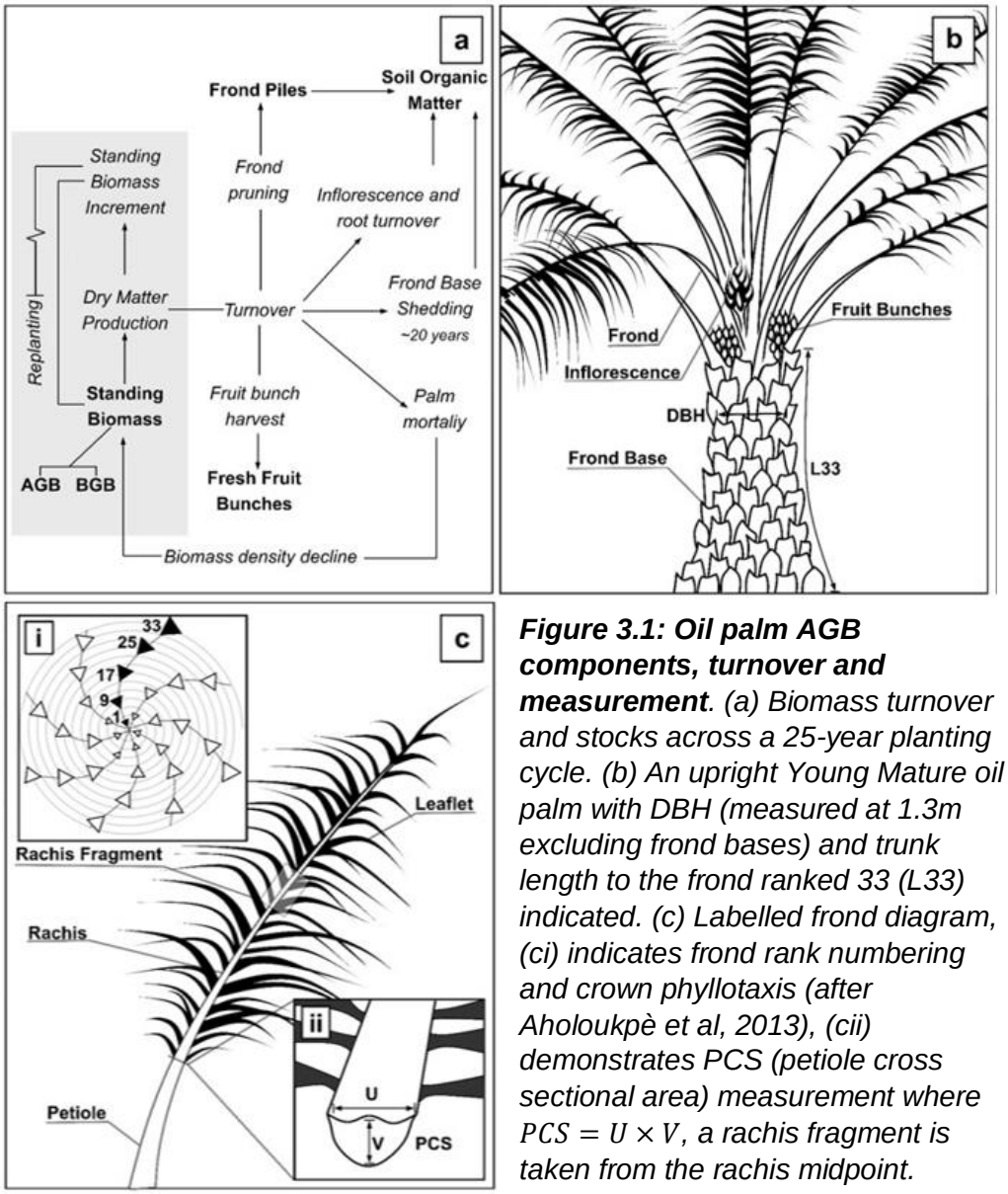

Figure 3.1: Oil palm AGB components, turnover and measurement*. (a) Biomass turnover and stocks across a 25-year planting cycle. (b) An upright Young Mature oil palm with DBH (measured at 1.3m excluding frond bases) and trunk length to the frond ranked 33 (L33) indicated. (c) Labelled frond diagram, (ci) indicates frond rank numbering and crown phyllotaxis (after Aholoukpè et al, 2013), (cii) demonstrates PCS (petiole cross sectional area) measurement where* $PCS = U \times V$*, a rachis fragment is taken from the rachis midpoint.*

OP plantations on peat are markedly different to those on mineral soils with potential impacts on AGB stock estimations. Following the clearance of forest biomass, peatlands are drained to an optimum water table depth 0.4 – 0.6 m from the peat surface to allow cultivation [31-33]. Peat bulk density is increased to ~ 0.20 g cm^{-1} by mechanical compaction using heavy machinery, often including the compaction of residual forest material into the peat [31,34,35]. This increases the load-bearing capacity of peat soils and improves the anchorage of OPs which allocate a relatively small proportion of total biomass to belowground root systems [11,32,33,34]. Following this initial compaction further peat subsidence occurs as a result of peat shrinkage, consolidation and decomposition following drainage [36]. This subsidence, when combined with poor root anchorage, frequently results in individual palms leaning at an angle to the ground. As leaning becomes more severe roots become exposed and vulnerable to desiccation and breakage which can result in the palms falling over entirely, the likelihood of this increases as palms mature with associated gains in trunk and crown biomass [32]. This has become a serious limiting factor for OP performance on peat and will likely have detrimental effects on AGB stocks as plant density per area is reduced due to palm mortality (Figure 3.1a) [10,32,33]. Initial palm planting densities are optimised for maximum fresh fruit bunch (FFB) yield across the life of the plantation; higher densities are therefore adopted for less favourable soils [24]. In contrast to OP on mineral soils, optimal planting densities on peat range from 160 to 200 palms per hectare (110 – 148 palms per hectare on mineral soils) [10,24,33].

In this study, we quantify the AGB (dry-weight) of OPs on deep peat in Sarawak, Malaysia. Destructive harvests of nine palms split amongst three age classes (IM: immature, YM: young-mature and M: mature) are supported with non-destructive measurements and surveys of a further 902 palms. Harvest data is used to develop new allometric equations for palm and component AGB. Non-destructive measurements are then used to upscale the destructive harvests to the plantation block level. We develop models of AGB accumulation rates on peat to inform existing OP AGB growth and carbon balance models. Finally, a meta-analysis of existing OP allometries for palms on both peat and mineral soils is performed and the results contrasted with data and allometries developed as part of this study.

No	Component	Equation	Source	Note
Allometries Tested				
3.1	Frond DW	$DW_{Frond} = 0.102 \times PCS + 0.21$	Corley et al, 1971	-
3.2	Frond DW	$DW_{Frond} = \alpha + \beta \times PCS$ $\alpha = -0.0076 + 0.0394 \times YAP$ $\beta = 0.0284 + 0.0101 \times YAP$	Henson (1993): in Henson and Dolmat 2003	Palms YAP ≤ 6
3.3	Rachis DW Frond DW	$DW_{Rachis} = 1.133 \times \frac{DW_{Frag}}{L_{Frag}} \times L_{Rachis}$ $DW_{Frond} = 1.147 + 2.135 \times DW_{Rachis}$	Aholoukpè et al, 2013	-
3.4	Trunk DW Trunk Density	$DW_{Trunk} = T_{Vol} \times \rho = \rho(\pi r^2 \times L_{Trunk})$ $\rho = 0.0076 \times YAP + 0.083$	Corley et al, 1971	Trunk biomass without frond bases
Biomass Accumulation Models				
M1	Standing Biomass (Mg ha^{-1})	$SB = -0.00020823 \times YAP^4 \times 0.000153744 \times YAP^3 - 0.011636 \times YAP^2 + 7.3219 \times YAP - 6.3934$	Henson, 2003	Standing biomass, adjusted to AGB (Morel et al, 2011).
M2	Aboveground Biomass (Mg ha^{-1})	$AGB = 18.95 \times YAP^{0.5}$	Germer and Sauerborn, 2006	-
M3	Aboveground Biomass (Mg ha^{-1})	$AGB = 1.526(5.97 \times YAP^{0.62})$	Carlson et al, 2012	Model adjusted from carbon to AGB

Table 3.1: Existing allometric equations for the estimation of OP component dry weight (kg) and OP AGB accumulation models for OP on mineral soils. *Where DW_{Frond} is frond dry weight (kg), PCS is the petiole cross sectional area (cm), DW_{Rachis} is rachis dry weight (kg), DW_{Frag} is rachis fragment dry weight (kg), L_{Frag} is rachis fragment length (m), L_{Rachis} is rachis length (m), DW_{Trunk} is trunk dry weight, T_{Height} is trunk height (m) , DW_{Palm} is palm dry weight (kg), T_{Vol} is trunk volume (m^3), DBH is the diameter at breast height (m) and YAP is years after planting.*

3.3) Results

3.3.1) OP biomass distribution in immature, young-mature and mature palms

Of the palms destructively harvested, one mature palm was mildly leaning (Supplementary Table S3.2). As expected, the palm trunk makes the largest contribution (33 to 46 %) to the total palm dry weight (DW_{palm}), particularly in the YM and M classes (Figure 3.2). Frond base biomass also constitutes a large proportion of the overall biomass (13 to 32 %), again particularly in the older age classes (Figure 3.2, Table 3.2). Palm trunks retained all frond bases in all palms harvested. In immature palms, fronds make up a larger proportion of overall biomass.

Contrasting palm trunk and total frond dry weight for each age class to those on mineral soils revealed no differences (Figure 3.3). However, accessible data was scarce on both mineral and peat soils.

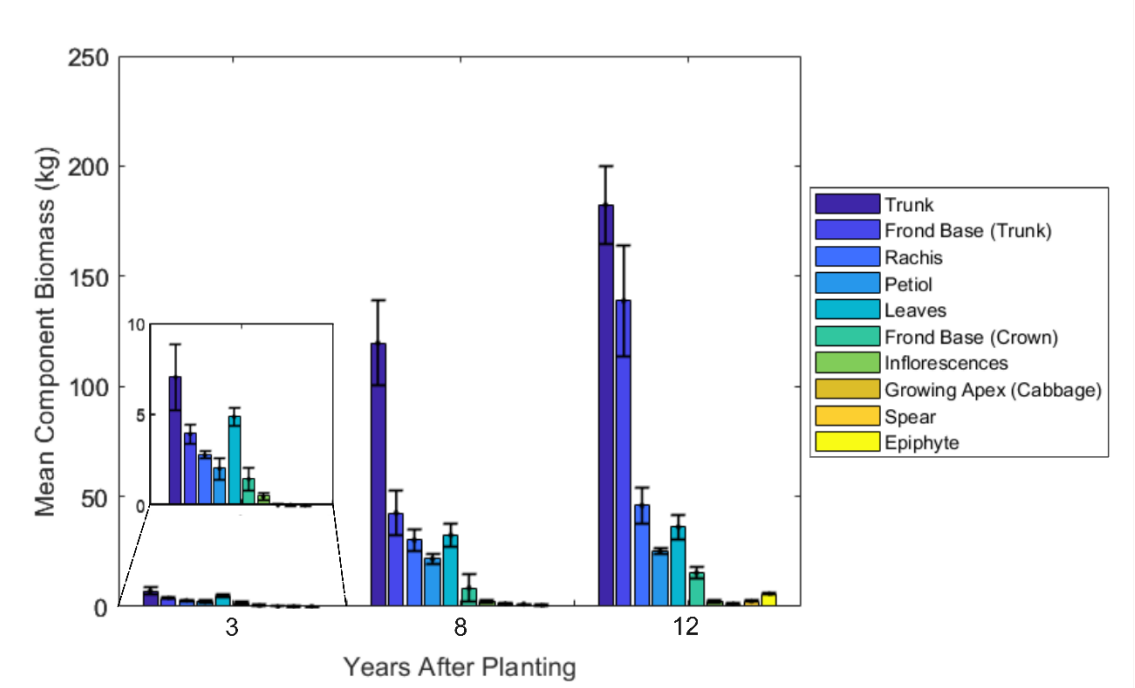

Figure 3.2: Mean AGB component dry weights (kg) for immature, young mature and mature OPs. *Error bars indicate standard error. Frond Base (Crown) is the remaining frond base left in the crown subsequent to live frond removal (see methods).*

YAP	Stem			Frond				Spear	Cabbage	Total (All)
	Trunk	Frond Base	Total	Rachis	Petiole	Leaflet	Total			
3	7.0 ± 1.8	3.9 ± 0.5	11.0	2.8 ± 0.2	2.0 ± 0.9	4.9 ± 0.5	9.7	0.3 ± 0.1	0.3 ± 0.1	21.3 ± 5.9
8	111.8 ± 19.3	42.5 ± 10.2	154.3	30.2 ± 4.9	21.3 ± 2.6	32.3 ± 5.1	83.8	1.2 ± 0.1	1.3 ± 0.6	240.6 ± 15.3
12	182.4 ± 17.6	138.8 ± 25.2	321.2	45.7 ± 8.1	25.0 ± 1.4	36.1 ± 5.7	106.9	2.4 ± 0.4	1.3 ± 0.5	431.8 ± 90.1

Table 3.2: Mean AGB component dry weights (kg) for immature, young mature and mature OPs *(standard error indicated).*

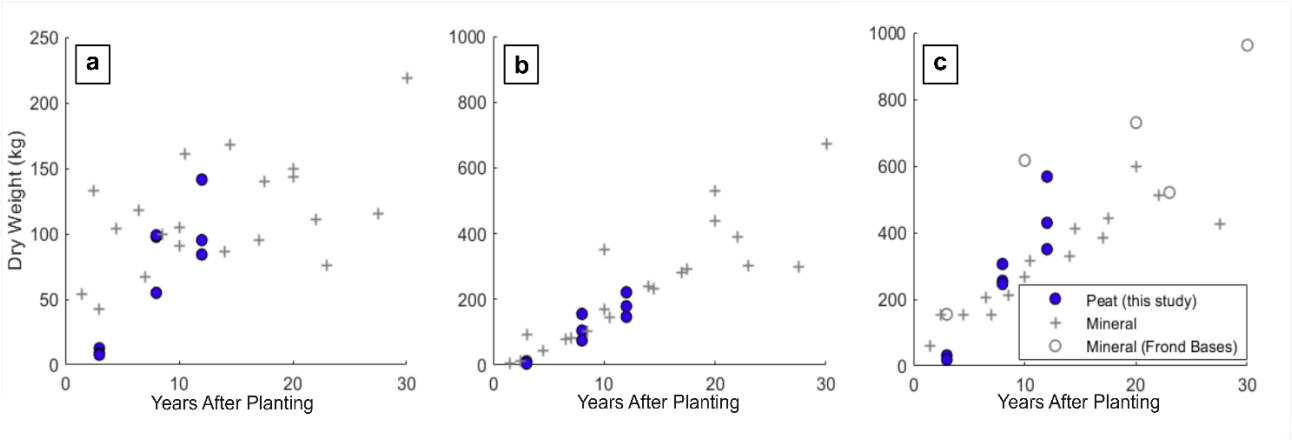

Figure 3.3: Dry weights of OP components (kg). *Dry weights where quantified using destructive harvests including total frond biomass per palm (a), palm trunk biomass (b) and palm biomass (excluding fruit and epiphytes) (c). Per palm DWs of OP AGB components on mineral soils are taken from Corley et al (1971), Khalid et al, (1999), Rees and Tinker (1963) and Syahrinudin (2005). Frond base biomass is included in palm (total) where reported ((c) - grey open circle).*

3.3.2) Allometric estimation of palm and frond component biomass

Harvest data was used to validate existing allometric equations and develop equations for Malaysian OP on deep peat (Table 3.1, Table 3.3).

3.3.2.1) Frond DW Estimation

Existing allometric equations estimating frond dry weight (DW_{frond}) using the petiole cross sectional area (PCS) (Equation (3.1) and (3.2)) and rachis linear density (RLD) (Equation (3.3)) were tested. The petiole cross sectional area is the sectional area at the junction of the petiole and rachis (at the point of insertion of the lowest leaflet) (Figure 3.1 c). The rachis linear density is derived from the dry weight of a rachis fragment and is used to predict rachis dry weight (DW_{Rachis}) and infer DW_{Frond}.

All existing allometric equations tested overestimated frond dry weight (Supplementary Figure S3.1). Frond DW estimation using the petiole cross sectional area (Equation (3.1)) overestimated DW_{frond} by ~56% for young mature and mature palms and ~119% for immature palms. However, using Equation 3.2 to estimate DW_{frond} from the PCS for palms < 6 years after planting improved estimation in the immature age class, overestimating frond dry weight by only 21%. Estimation using rachis linear density (Equation (3.3)) resulted in an overestimation of ~61% for young mature and mature palms and ~300% for immature palms. Rachis dry weight was however well predicted from rachis linear density (Equation (3.3), Supplementary Figure S3.2). Further allometries referred to in Corley and Tinker (2016) both over and underestimated DW_{Frond} (Supplementary Figure S3.3).

Allometric relationships for DW_{frond} estimation on deep peat were then defined. Frond dry weight in each age class was lower than reported for palms on mineral soils but was more consistent with those sampled by Henson and Dolmat (2003) from OPs on peat (Supplementary Figure S3.4). Leaflets in immature palms made a larger contribution to overall frond dry weight when compared to the mature age classes (Supplementary Figure S3.5), equations were adjusted to include all palm ages sampled. Rachis linear density was a marginally better predictor of DW_{Frond} (R^2 = 0.83), when compared to the petiole cross section (R^2 = 0.76) once adjusted to harvested fronds (Figure 3.4). However, estimation of DW_{Frond} using the petiole cross sectional area was considered more practical in the field. Rachis length was also used to predict DW_{Frond} to a similar degree of accuracy (R^2 = 0.81).

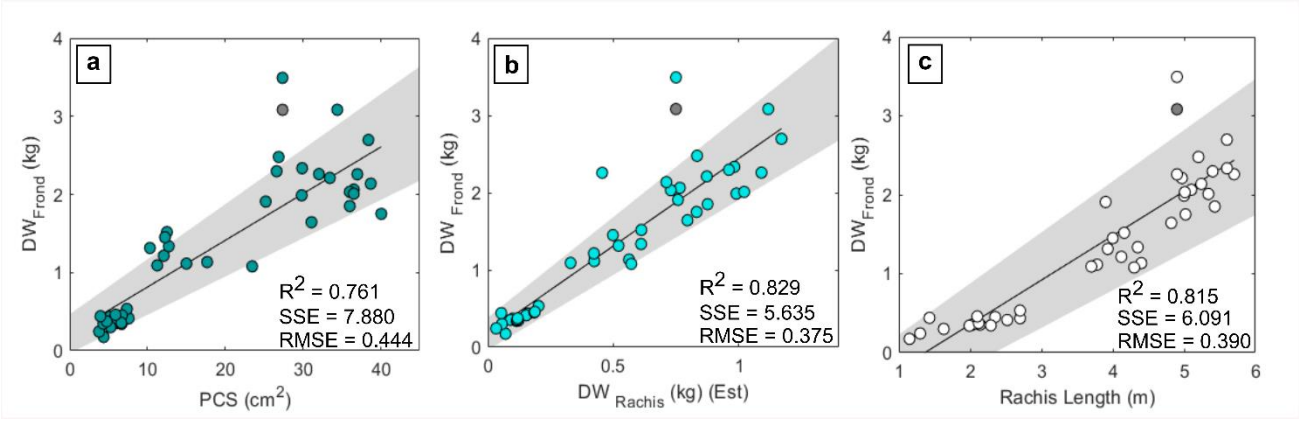

Figure 3.4: Linear relationship between frond structural characteristics and Frond DW (DW_{Frond}). *DW_{Frond} is compared to the petiole cross sectional area (PCS) ((a) - equation (3.5)), rachis dry weight (DW_{Rachis}) derived from rachis linear density ((b) – equation (3.6)) and rachis length ((c) – equation (3.7)). A total of 45 fronds were sampled, fronds ranked 1, 9, 17, 25 and 33 were sampled for each of the nine destructively harvested palms. 95% confidence interval of fit indicated in grey; consistent outliers indicated as a black closed circle.*

No	Component	Equation	Note
Derived Allometries			
3.5	Frond DW	$DW_{Frond} = 0.060 \times PCS + 0.217$	Frond DW estimation using the petiole cross sectional area of a pruned frond.
3.6	Rachis DW Frond DW	$DW_{Rachis} = 1.126 \times \frac{DW_{Frag}}{L_{Frag}} \times L_{Rachis}$ $DW_{Frond} = 0.176 + 2.267 \times DW_{Rachis}$	Frond DW estimation using the DW of a rachis fragment taken from a pruned frond.
3.7	Frond DW	$DW_{Frond} = 0.562 \times L_{Rachis} - 0.767$	Frond DW estimation using rachis length.
3.8	Palm DW	$DW_{Palm} = 12.87 + 560.8 \times T_{Vol}$ $T_{Vol} = (\pi \times 0.5 \times DBH)^2 \times L_{Trunk}$	Palm DW estimation derived from non-destructive trunk volume measurement. DBH measured excluding frond bases
Derived Biomass Accumulation Models			
P1	Aboveground Biomass (Mg ha^{-1})	$AGB = 6.389 \times YAP - 17.59$	AGB accumulation on peat – observed plantation biomass.
P2	Aboveground Biomass (Mg ha^{-1})	$AGB = 7.992 \times YAP - 26.29$	AGB accumulation on peat - 'perfect plantation' model. All palms are modelled as live and standing.

Table 3.3: Allometric equations for the estimation of OP component dry weight (kg) and OP AGB accumulation models for OP on peat soils. Allometric equations are derived from destructive harvest data at the study site. Where DW_{Frond} is frond dry weight (kg), PCS is the petiole cross sectional area (cm), DW_{Rachis} is rachis dry weight (kg), DW_{Frag} is rachis fragment dry weight (kg), L_{Frag} is rachis fragment length (m), L_{Rachis} is rachis length (m), DW_{Trunk} is trunk dry weight, FIT_{Height} is trunk height (m), DW_{Palm} is palm dry weight (kg), T_{Vol} is trunk volume (m^3), DBH is the diameter at breast height (m) and YAP is years after planting.

3.3.2.2) Palm DW Estimation

The palm trunk makes the greatest proportional contribution to overall palm biomass (Figure 3.2). Equation (3.4) underestimated trunk dry weight by 32% in YM and M palms (frond bases not included). Total palm DW (DW_{palm}) is estimated using trunk height (height to frond 33) in existing allometries (Supplementary Table S3.3). Whilst trunk length was found to be a good estimator of DW_{palm} (R^2 = 0.88), the use of trunk volume was marginally more effective for the palms sampled (R^2 = 0.92) (Equation (3.8)) (Figure 3.5). A model was developed to predict DW_{palm} excluding frond bases to simulate frond

base shedding, however R^2 = 0.52, potentially due to a small sample size (n = 6) and the highly variable contribution of frond bases to the overall DW_{palm} of palms sampled.

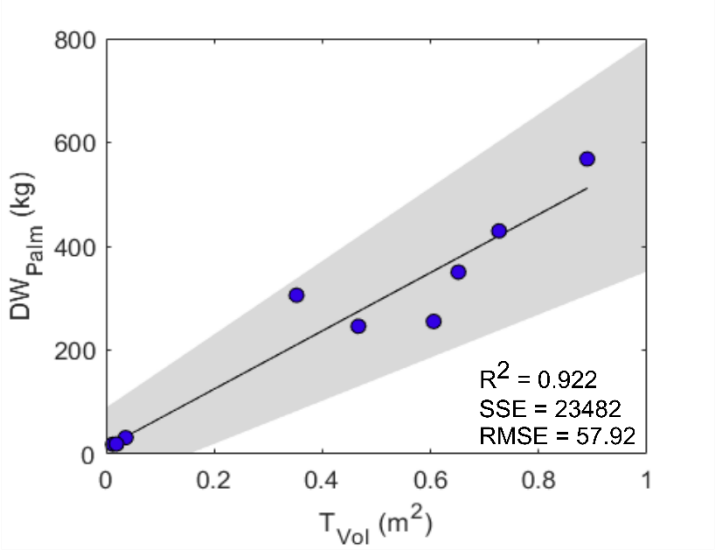

Figure 3.5: Linear relationship between palm trunk volume (T_{Vol}) and palm dry weight (DW_{Palm}) for the nine destructively sampled OPs. *95% confidence interval of fit indicated in grey (Table 2, equation (3.8)).*

3.3.3) Upscaling biomass to the plantation block scale

Non-destructive measurements were combined with the allometric equations defined for OP on peat to assess biomass stocks at the plantation block level. Equation (3.8) was used to estimate the biomass stock of live palms in 22 0.25 ha plots in plantation blocks at various stages of maturity (Figure 3.6). This confirmed a large variation in biomass stocks in the more mature plots with a mean AGB of 65.9 ± 8.7 Mg ha^{-1} 11 years after planting and 56.04 ± 12.0 Mg ha^{-1} after 12 years at the study site (Figure 3.6). A 'perfect' plantation on peat was then modelled, this included only healthy upright palms, upscaled to a planting density of 160 palms per hectare, simulating a plantation where there was no occurrence of palm leaning or mortality. Once all fallen, missing and re-planted palms (which represented 13% of palms in plots > 8 YAP in this study) had been disregarded aboveground biomass stocks accumulated at ~7.99 ± 0.95 Mg ha^{-1} yr^{-1} in the first 12 years after planting. However, this is reduced to ~6.39 ± 1.12 Mg ha^{-1} per year considering all 22 assessed plantation blocks when palm mortality and replacement is taken into account. Mild (Leaning at < 45° from the vertical) and severely leaning palms (Leaning at > 45° from the vertical) made up 17% of live palms in plots > 8 YAP, however, inter-plot variation within age classes across the plantation was high.

Aboveground biomass stocks at the study site were compared to assessments of OP AGB on mineral soils in addition to comparison with AGB accumulation models (Figure

3.6). Only 3 accessible assessments of OP AGB stocks on peat soils were available (Figure 3.6). At the time of survey there were no planting blocks aged > 12 YAP at the study site. Henson (2003), Model M1, assumes an AGB reduction ~18 years after planting due to frond base shedding. In contrast, Models M2 and M3 do not indicate this reduction (Figure 3.7). Peat OP AGB at the Sabaju and Sebungan Estates appears consistent with OP on mineral soils. However, in mature blocks where palm falling and missing palms were common AGB stocks were notably lower than modelled OP growth (Figure 3.6, Figure 3.7).

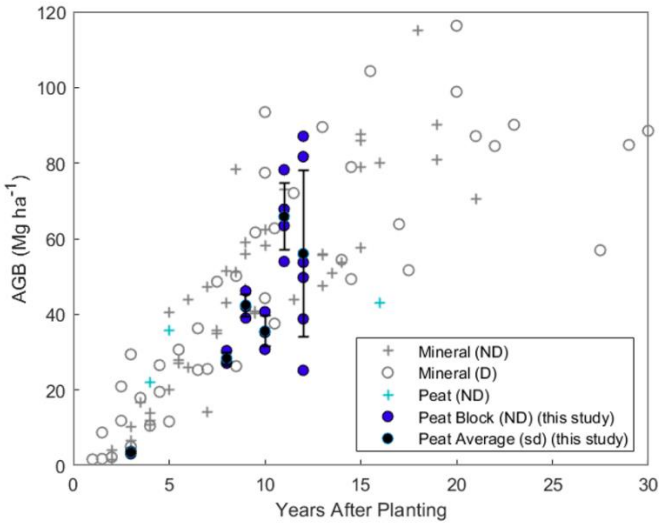

Figure 3.6: Oil palm block-level cumulative AGB stock (Mg ha^{-1}) for peat (blue markers) and mineral soils (grey markers). *OP aboveground biomass stocks on mineral soils (Table S3.1) were obtained using destructive (D) and non-destructive (ND) methods and are presented in addition to existing values for OP on peat. Existing data for non-destructive mineral estimates (+) and destructive mineral ( ) and non-destructive peat (+). Block AGB stocks at the study site are included ( ) and the plantation mean for each YAP plotted ( ), standard deviation indicated (Black error bars).*

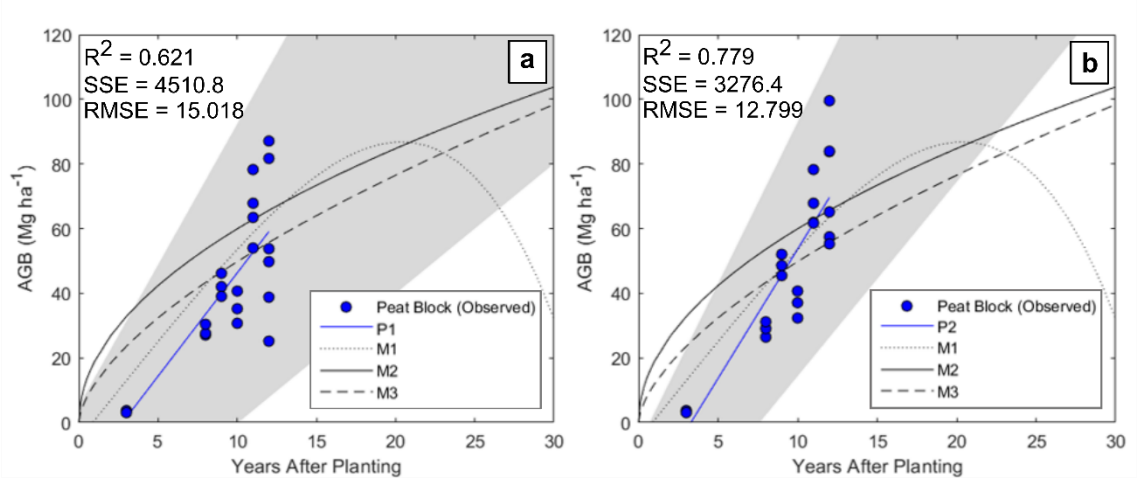

Figure 3.7: AGB accumulation models (Mg ha^{-1}) for oil palm on deep peat from 3 to 12 YAP. *(a)models observed OP accumulation at the Sabaju and Sebungan OP estate complex (Model P1). (b) models a 'perfect' plantation on peat modelling all palms as live, present and standing (Model P2). 95% confidence intervals of both fits indicated in grey. Existing AGB accumulation models for OP on mineral soils (YAP 0 – 30) are plotted (Models 1, 2 and 3, Table 1).*

3.4) Discussion

3.4.1) Dry weight distribution of OP on peat

The dry weight of OPs in three age classes was quantified using destructive harvests. As palms transitioned from youth to maturity trunk length and dry weight increased; this was also accompanied by an increase in frond base biomass relative to the total palm dry weight. Studies that destructively harvest frond bases to quantify biomass are few when compared with other AGB components [12,30,37,38]. This is likely due to the practical difficulties associated with frond base removal [37]. It is often also unclear whether non-destructive OP biomass assessments that quantify plantation biomass stocks using allometries have included the dry weight contribution of adhering frond bases [8,9]. Henson et al (2012) found total frond base dry biomass per palm to be 10.8, 62.8 and 56.0 kg, 3, 10 and 13 years after planting in Papua New Guinea (with 94.6% of frond bases adhering to the trunk 13 YAP). Frond bases made an even greater contribution to overall palm biomass in this study, particularly in mature palms (Table 3.2). A review of studies quantifying frond base biomass highlights the high variation in palm frond base dry weight when compared to both palm age and trunk biomass [37]. Despite this variation, frond bases make a large contribution to the overall AGB of OP plantations in the young mature and mature age classes (~17.5 and 32.1% of total AGB respectively). This will become a large carbon source following shedding before the end of the plantation planting cycle as frond base litter decomposes [37,39].

The biomass of a single mature frond grown on peat was consistently lower than on mineral soils in all age classes when compared to pooled frond DWs for palms on mineral

soils (Supplementary Figure S3.4) [40]. Studies have also found the rate of frond emergence reduces significantly as planting density is increased [10,42]. Taking into account the higher planting density of OP on peat, it is therefore surprising that there was no observable difference between total per palm frond biomass on mineral and peat soils (Figure 3.3a). The acidity, low nutrient content and poor fertiliser retention of managed tropical peat soils is likely to result in reduced vegetative dry matter production and biomass accumulation when compared to OP on mineral soils [42]. In addition to this, palms at higher densities are subjected to increased competition for light thus reducing the dry matter production per palm [23]. Despite these expectations, our study revealed no notable differences in palm, trunk or frond biomass between mineral and peatland plantations. However, the lack of available literature which documents DW_{Palm}, DW_{Trunk} and the total frond biomass for individual palms on mineral soils and the small sample (n = 9) of palms on peat in this study makes it difficult to identify significant differences in palm and component biomass. Differences may however be detectable with a larger sample size. To confound this, palms on mineral soils have been sampled using non-standardized methodologies and are influenced by differences in genotype, eco-region and plantation management [8, 11,12,26,30].

3.4.2) Allometric equations for OP component DW on peat

This study defined allometric relationships for OP and OP component dry biomass on drained tropical peats. Allometries produced here for the estimation of frond dry weight incorporate fronds of various ranks from multiple age classes. Here, the frond rachis linear density and petiole cross sectional area were both effective predictors of DW_{Frond} (R^2 = 0.82, R^2 = 0.76). In contrast to Corley and Tinker (1971) (Equation (3.1)), Aholoukpè et al (2013) found frond biomass to be poorly predicted using the PCS in YM and M palms (R^2 = 0.22) but found rachis linear density to be a better predictor (R^2 = 0.62). However, the increased effort required to measure rachis linear density from the dry weight of a rachis fragment in the field is perhaps not justified by the marginally stronger relationship between rachis linear density and DW_{Frond} when compared to using the petiole cross sectional area in this study. An allometry was defined relating trunk volume to the total palm biomass (Equation (3.8)). To take into account the structural variation of OP on peat T_{Vol} was modelled as a cylinder the length of the trunk to F33, measuring along the inner curve of the trunk for leaning palms [32].

3.4.3) Application of existing allometries to peat OP

Frond biomass for palms on peat was overestimated by the majority of existing allometric equations tested (derived using palms on mineral soils), most notably in the immature age class. This overestimation of young palm DW_{Frond} is also acknowledged by Henson

(1993) and a large improvement was observed when applying Equation (3.2), which is adjusted for use on young palm fronds. Equation (3.3) has yet to be validated for young palm fronds and whilst DW_{rachis} was well estimated for all age classes, adjustment is needed before it can be used for young palm DW_{Frond} prediction on peatlands [43].

In the mature age classes, trunk biomass was underestimated by ~32% when using Equation (3.4), much greater than the underestimation of ~10% acknowledged by Morel et al (2011) when using this allometry. Corley et al (1971) model the trunk (without frond bases) as a cylinder with a constant diameter with wood density estimated according to palm age. Aholoukpè et al (2018) attempted reduce the uncertainty introduced though these assumptions by modelling the true inverted cone shape of the stem and incorporating the changes in trunk wood density as a function of trunk height. However, this assumes an upright palm and hence is often not applicable to OP on peat due to high incidence of palm leaning [32].

Here palm dry weight was best predicted using trunk volume. Thenkabail et al (2004) relate DW_{Palm} to trunk height in Benin; the resulting allometry greatly underestimated DW_{Palm} in mature and young mature palms in this study resulting in a mean underestimation of 72%. However, no palms with a trunk height > 1.95m were incorporated into the initial model. Dewi et al (2009) produced a similar allometry for OP on mineral soils in Indonesia which can be used more successfully with a mean underestimation of only 16% when applied here to OP on peat (Supplementary Table S3.3).

3.4.4) Plantation block-level AGB

The allometries developed using destructive sampling were combined with non-destructive palm structural measurements and frond pruning to upscale biomass stock estimates to the plantation block level. Trunk DBH remained consistent across the age classes (YAP > 8) whilst trunk length increased with age in standing palms (Supplementary Figure S3.6). In 'successful' blocks, per hectare AGB was similar to that observed on mineral soils (Figure 3.6). Vegetative dry matter production and standing biomass per hectare increases with planting density as observed in studies on both peat and mineral soils, disregarding fruit bunch biomass [10,48]. The higher planting density of palms on unfavourable peat soils likely contributes to the high per hectare AGB stocks in plots where leaning is infrequent or mild with relatively few fallen palms [24,33]. However, there is a large variation in plot per hectare AGB within age classes and in plots with a high incidence of leaning and fallen palms AGB was greatly reduced. Here, mild and severely leaning palms made up 17% of live palms in plots > 8 YAP with an additional 13% of OPs fallen, missing or replaced. However, inter-plot variation within age classes

across the plantation was high (Figure 3.6). Census of the incidence of palm leaning were carried out at 6-month intervals in an experimental OP block on deep peat in Sarawak [49]. After 12 years 50.3% of palms were mildly leaning and 2.8% had fallen or were severely leaning, this worsened to 55.5 and 6.9% in uncompacted plots [49]. Dolmat et al (1995) found leaning incidences of 44.2 % (compacted) and 71.9% (uncompacted) in Perak.

As a result of the recent rise in OP expansion across tropical peats combined with efforts to increase peat OP sustainability, research increasingly focuses on the optimisation of peat OP growth and fruit bunch yields [23,32,33]. Prior to conversion, site and soil surveys are of high importance as the position on the peat dome, peat composition, maturity and depth have all been found to have an impact on conversion success, palm growth and yield potential [20,35]. Peat compaction to increase bulk density prior to conversion and the thorough removal of woody debris from forest clearance is important to improve palm anchorage, whilst maintenance of a consistent water table increases palm rooting depth potential [32,33,35,50,51]. Maintenance of drainage systems once installed will aid in prevention of flooding, an additional prerequisite to peat oil palm failure [32]. Once palms have reached maturity and leaning has commenced regular pruning to reduce canopy biomass and prevent toppling in addition to soil mounding of roots after exposure both aid in reducing palm falling and limit AGB and yield reductions [52].

3.4.5) Limitations and further work

In addition to the limitations highlighted, further uncertainties arise from the focus of this study on a single plantation. We observed a high variation in palm structural characteristics and plot biomass stocks within mature age classes in a single well managed industrial OP estate. Therefore, the actual variation of monoculture OP plantation AGB stocks on peat across Sarawak, Malaysia and Insular Southeast Asia is likely to be greater considering differences in plantation management and leaning, peat properties and ecoregions.

The sample size of destructively harvested palms is small (n = 9), with few mature palms and no palms > 12 YAP harvested. Similar studies which destructively harvest palms on mineral soils to quantify DW_{Palm} include between 3 to 10 palms sampled for each palm age and span from 1.5 to 33 years after planting (Supplementary Table S3.3) [11,12,26,30,46]. Small sample sizes are common in destructive biomass assessments due to costly sampling procedures (particularly in older, larger palms) and results are therefore vulnerable to the influence of variation between individual palms [9]. We acknowledge the need to extend the temporal scope of the chronosequence here to include mature palms > 12 YAP as AGB stocks after this point are uncertain. This could inform growth models

for OP on peat beyond ~18 YAP where existing models of OP AGB accumulation vary (Figure 3.7) [3,21,28,53]. Continuing the chronosequence would also permit the averaging of biomass stocks across the life of a plantation on peat, aiding in the comparison of biomass stocks with alternative land cover types for LUC flux modelling and carbon accounting [6,54]. Here all palm mortality and replacement has been attributed to palm leaning in the plots considered, however the spread of pests (particularly termites on peat soils) and diseases such as *G. boninense* basal stem or trunk rot are also frequently the cause of palm failure and replanting [55,56]. Despite this, the plantation studied here is in its first planting cycle and with no instances of *Ganoderma boninense* observed [23].

Finally, all allometric relationships defined here would benefit from validation to test their success on OP on drained peats, including mature palms as well as their possible application in alternative ecoregions and at different planting densities [17].

3.5) Conclusion

The recent rapid expansion of OP plantations across managed tropical peatlands is known to result in net carbon emissions. However, the emissions associated with this land use change across the life of a plantation remain poorly constrained as aboveground biomass accumulation rates on peat are uncertain due to a lack of both destructive and non-destructive AGB quantifications.

Here, we produce peat OP specific allometries for the estimation of both palm and frond dry weight and use these allometries to upscale AGB estimates to the plantation block level. This revealed a high variability in aboveground biomass stocks across a plantation in the mature age classes. Increasing non-destructive inventories on peat will not only improve AGB accumulation models but could also inform remote sensing efforts which aim to quantify AGB stocks over a wider spatial scale. Validating the allometries produced by expanding destructive harvests across different plantations on peat in addition to including older palms in harvests and plot inventories would further strengthen our understanding of peat OP AGB stock changes over time.

3.6) Methodology

3.6.1) Study site

Measurements were carried out at the Sebungan and Sabaju Oil Palm Estate Complex, Sarawak, Malaysia (3.19˚N 113.43˚E). The industrial OP plantation has an area of ~10,200 ha. The site receives ~ 3075 mm rainfall per year with an average temperature of 27.2 °C. Meteorology was recorded at 1-minute intervals on a Sutron XLite 9210B datalogger (Sterling, Virginia, US). Air Temperature was measured at 1 m using a

Vaisala HMP155 (Vaisala, Helsinki, Finland). Precipitation was measured at 6 m, i.e. above the canopy, using a Texas Electronics TR525M (Dallas, Texas, US).

The plantation is low lying, soil surveys indicate a majority composition of lowland organic deposits with an underlying marine clay mineral layer (84.8%). Very deep peat (> 3m thick) covers the majority of the plantation; 42.2% has highly decomposed sapric surface (0 – 0.5 m) and subsurface (0.5 – 1.5 m) tiers. A further 42.6% is comprised of a partially decomposed sapric surface tier (0 – 0.6 m) and hemic subsurface tier (0.5 – 1 m). Both deposit types contain partially decomposed wood between 0.5 – 1m.

Prior to conversion the site was covered in logged mixed peat swamp forest (PSF). Land preparation included the removal of remaining large trees and vegetation, the establishment of a drainage system and peat compaction using heavy machinery[31]. OPs are planted at a density of 160 palms per hectare and at the time of measurement ranged from 3 to 12 years after planting (YAP).

3.6.2) Destructive harvests

Palm selection and sampling

Three palms were destructively harvested from each age class: 3 (Immature – I), 8 (Young Mature – YM) and 12 (Mature - M) years after planting. Palms were selected at random at least 50 m from the block edge, all were selected in different planting blocks, GPS coordinates were recorded (Supplementary Table S3.5). Severely leaning or recovered palms were not considered for destructive harvests. Prior to felling, non-destructive measurements of palm structural characteristics were taken.

Destructive measurements

All fresh weights (FW) (kg) were measured and recorded at the felling site as close to the time of felling as possible, with particular attention paid to leaflets. Samples were promptly transferred to the lab oven to avoid capturing decomposition in DW measurements.

Fronds

Fronds were removed from the palm crown as close as possible to the base of the frond using a harvesting sickle (Figure 3.1c). Fronds were counted and any petiole remaining in the crown subsequent to frond removal was harvested and classified as ‘crown frond base’.

Using the frond rankings of Thomas et al (1969), fronds 1, 9, 17, 25 and 33 were subsampled for allometric validation and development (Figure 3.1ci). The petiole cross sectional area, rachis length and the fresh weights of the frond rachis, petiole and leaflets

were recorded (Figure 3.1c). Petiole cross sectional area was measured using callipers at the junction of rachis and petiole (the point of insertion of the lowest leaflet) and was modelled as a rectangle ($PCS = U \times V$, Figure 3.1cii)[11]. A 0.15 m fragment was removed from the midpoint of the rachis and petiole, a subsample of leaflets was also removed. All remaining fronds were split into components (rachis, petiole and leaflets) and their total fresh weight recorded.

Trunk and frond bases

All epiphytes were removed from the palm trunk, the FW of epiphytes was recorded, and a subsample taken. All frond bases were removed from the palm trunk and a disk ~0.2m thick was removed from the trunk midpoint. This disk was weighed, and two perpendicular disk diameters recorded, a sector (~1/8th of the disk) was removed and the fresh weight recorded, and the sector returned to the labs for DW analysis. The palm trunk (without frond bases) was then weighed using suspended scales at the felling site or at the plantation weighbridge. Subsequent to removal, the total FW of all frond bases was recorded, a subsample of 3 frond bases was then returned to the labs.

Inflorescences, fruit, spear and cabbage

The total FW of all inflorescences and fruit bunches and the palm spear and cabbage (growing apex) was recorded at the felling site before removing 3 subsamples per component for DW analysis. Fruit bunch fresh and dry weights where not included in any further analysis due to variation in palm harvesting cycles.

Laboratory analysis

Palm component subsamples were dried at 105°c until a constant, non-changing mass was reached, component moisture contents were then calculated for each sample.

3.6.3) Non-destructive surveys and frond pruning

Plot selection and sampling

Non-destructive survey plots were selected at random across the plantation complex (with a minimum of 3 plots selected for each age class). 22 plots with an area of 0.25 ha were surveyed. Plots were 3, 8, 9, 10, 11 and 12 YAP and were in independent planting blocks, GPS coordinates were recorded at plot corners. The YAP of each plot was checked against planting blocking maps, plots were established away from block edges (Supplementary Table S3.5).

Leaning categorisation

The condition of each palm with the 0.25 ha plot was recorded. Palms were categorised as upright, mildly leaning, severely leaning, recovered, fallen (dead/alive), missing or replanted (see Supplementary Table S3.4). The direction of lean was also recorded.

Non-destructive measurement and pruning

Each 0.25 ha plot contained approximately 40 palms, palms were numbered, and structural measurements taken for 10 randomly selected palms. The canopy height was recorded. Trunk length was measured along the trunk to frond 33 or the most mature frond, for leaning palms the trunk length was measured along the trunk inner curve (Figure 3.1b, Supplementary Figure S3.7). Trunk diameter at breast height (DBH, 1.3m) was measured using callipers so as not to include frond bases, for palms < 1.3m in height the diameter was taken at the trunk midpoint. Frond 33 was pruned from the canopy of the corresponding palm; rachis length was recorded, and petiole cross sectional area was measured using callipers.

3.6.4) Meta-analysis and allometry validation

OP Biomass stock estimates

All accessible literature publishing per hectare standing biomass (SB) and AGB stocks for OP on both peat and mineral soils using destructive and non-destructive methods was collected. Values were adjusted to AGB (Mg ha^{-1}), carbon contents were assumed to be 47.4% of dry biomass[18]. Where SB was reported AGB was assumed to be 84% of total SB based on assessments of belowground biomass (BGB) on mineral soils conducted by Corley and Tinker, 1971 and Khalid et al, 1999[12,13](Root biomass = 16.1 +/- 5.3 % of overall SB in palms 1.5- 27.5 YAP).

Allometric equations

Allometries for estimating palm component biomass derived using the destructive harvest of OP on mineral soils were collected and validated. Existing equations in the main section of the text (Table 3.1) are defined in peer reviewed literature, additional allometries are listed in the supplementary material.

3.5) Acknowledgements

The authors would like to thank the Director-General of the Malaysian Palm Oil Board for permission to publish these results. This study was carried out as part of a wider tropical peat research collaboration between MPOB, University of Exeter and University of Aberdeen and we would like to thank the MPOB staff and the Sarawak Oil Palm Berhard for help and support during the project. Specifically, from the Sarawak Oil Palm Berhard we would like to thank: Mr. Paul (group CEO), Mr. Chua Kian Hong (group plantation manager), Mr. Phang Seng Nam (regional plantation controller) and Mr.

Sammy (Sabaju plantation manager) for being kind enough to allow this research to be carried out within their plantation and for the provision of logistical support. From MPOB we would like to thank the dedicated field technicians, Steward Saging and Ham Jonathon for their invaluable support.

3.6) Author Contributions

K.L. wrote the paper with contributions from E.R., L.K.K., J.M., Y.A.T, A.G.S. and T.C.H. The experimental design for this project was led by K.L. with input from all authors. The fieldwork was led by K.L. and E.R. with support in field from J.M. and L.K.K. The data processing and analysis was led by K.L. with input from T.C.H., and contributions from all authors. This study forms part of a project which was conceived jointly by L.K.K, T.C.H and Y.A.T.

*3.7) **References***

1) FAO. *FAOSTAT* http://www.fao.org/faostat/en/#home (2019).

2) Miettinen, J., Shi, C., & Liew, S., C. Land cover distribution in the peatlands of Peninsular Malaysia, Sumatra and Borneo in 2015 with changes since 1990. *Glob Ecol Conserv.* **6**, 67–78 (2016).

3) Hergoualc'h, K., Hendry, D.T., Murdiyarso, D. & Verchot, L.V. Total and heterotrophic soil respiration in a swamp forest and oil palm plantations on peat in Central Kalimantan, Indonesia. *Biogeochemistry*. **135**, 203-220 (2017).

4) Tonks, A.J. et al. Impacts of conversion of tropical peat swamp forest to oil palm plantation on peat organic chemistry, physical properties and carbon stocks. *Geoderma*. **289**, 36-45 (2017).

5) Melling, L., Hatano, R. and Goh, K. Soil CO2 flux from three ecosystems in tropical peatland of Sarawak, Malaysia. *Tellus B*, **57**, 1-11 (2005).

6) Murdiyarso, D., Hergoualc'h, K. and Verchot, L.V. Opportunities for reducing greenhouse gas emissions in tropical peatlands. *PNAS*. **107**, 19655-19660. (2010).

7) Page, S. E. et al. *Review of peat surface greenhouse gas emissions from oil palm plantations in Southeast Asia.* (The International Council on Clean Transport, 2011).

8) Germer, J. and Sauerborn, J. Estimation of the impact of oil palm plantation establishment on greenhouse gas balance. *Environ. Dev. Sustain.*, **10**, 697-716 (2008).

9) Kho, L.K. and Jepsen, M.R. Carbon stock of oil palm plantations and tropical forests in Malaysia: A review. *SJTG,* **36**, 249-266 (2015).

10) Henson, I.E. & Dolmat, M.T. Physiological analysis of an oil palm density trial on a peat soil. *J Oil Palm Res.*, ***15***, 1-27 (2003).

11) Corley, R.H.V., Gray,B.S. & Ng, S. K. Productivity of the oil palm (Elaeis guineensis Jacq.) in Malaysia. *Exp. Agric.*, **7**, 129-136 (1971).

12) Khalid, H., Zin, Z.Z. & Anderson, J.M. Quantification of oil palm biomass and nutrient value in a mature plantation. I. Above-ground biomass. *J. Oil Palm Res*. **11**, 23-32 (1999).

13) Khalid, H., Zin, Z.Z. & Anderson, J.M. Quantification of oil palm biomass and nutrient value in a mature plantation. II. Below-ground biomass. *J. Oil Palm Res.* **11**, 63-71 (1999).

14) Kumar, L. & Mutanga, O. Remote sensing of above-ground biomass. *Remote Sens.* ***9,*** 935 (2017).

15) Mitchard, E.T. The tropical forest carbon cycle and climate change. Nature, **559**, 527-534 (2018).

16) Gibbs, H.K., Brown, S., Niles, J.O. & Foley, J.A. Monitoring and estimating tropical forest carbon stocks: making REDD a reality. *Environ. Res. Lett.* **2** 045023 (2007).

17) Picard, N., Saint-André, L., Henry, M. *Manual for building tree volume and biomass allometric equations: from field measurement to prediction.* (Food and Agricultural Organization of the United Nations, 2012).

18) Martin, A.R. & Thomas, S.C. A reassessment of carbon content in tropical trees. *PLoS ONE* **6**, 23533 (2011).

19) Chave, J. et al Tree allometry and improved estimation of carbon stocks and balance in tropical forests. *Oecologia*, **145**, 87-99 (2005).

20) Melling, L., Goh, K.J., Uyo, L.J., Sayok, A. & Hatano, O. Biophysical characteristics of tropical peatland. In: Proc. Conf. Peat and other soil factors in crop production (Ed. by J. Hamdan et al.) Malaysian Society of Soil Science, Serdang, Selangor 110-119, (2007).

21) Carlson, K.M. et al. Committed carbon emissions, deforestation, and community land conversion from oil palm plantation expansion in West Kalimantan, Indonesia. *PNAS*, **109**,7559-7564 (2012).

22) Carlson, K.M. et al. Carbon emissions from forest conversion by Kalimantan oil palm plantations. *Nat. Clim. Change.* **3**, 283 (2013).

23) Corley, R.H.V. & Tinker, P.B. *The oil palm.* (John Wiley & Sons, 2016).

24) Woittiez, L.S., van Wijk, M.T., Slingerland, M., van Noordwijk, M. & Giller, K.E., 2017. Yield gaps in oil palm: A quantitative review of contributing factors. *Eur. J. Agron.* **83**, 57-77, (2017).

25) Corley R.H.V. & Gray B.S. Yield and yield components in *Oil palm research* (ed. R.H.V. Corley, R.H.V, Hardon, J.J. & Wood, B.J.), pp. 77-86, (Elsevier, 1976).

26) Rees, A.R. and Tinker, P.B.H. Dry-matter production and nutrient content of plantation oil palms in Nigeria. *Plant Soil*. **19**, 19-32 (1963).

27) Thomas, R.L., Chan, K.W. & Easau, P.T. Phyllotaxis in the oil palm: arrangement of fronds on the trunk of mature palms. *Ann. Bot.***33**, 1001-1008 (1969).

28) Henson, I.E. The Malaysian national average oil palm: concept and evaluation. *Oil Palm B*, **46**, 15-27 (2003).

29) Henson, I.E. OPRODSIM, a versatile, mechanistic simulation model of oil palm dry matter production and yield. In: Proc. Conf. PIPOC 2005 International Palm Oil Congress, Agriculture, Biotechnology and Sustainability Conference (801-832). Malaysian Palm Oil Board Kuala Lumpur (2005).

30) Syahrinudin, S. *The potential of oil palm and forest plantations for carbon sequestration on degraded land in Indonesia.* (ed. P. L. G. Vlek, M. Denich, C. Martius, C. Rodgers and N.V.D. Giesen) (Ecology and Development Series, Cuvillier Verlag, Göttingen, 2005).

31) Cook, S. et al. 2018. Fluvial organic carbon fluxes from oil palm plantations on tropical peatland. *Biogeosciences*, **15**, 7435-7450 (2018).

32) Lim, K.H., Lim, S.S, Parish. F. and Suharto, R. RSPO Manual on Best Management Practices (BMPs) for Existing Oil Palm Cultivation on Peat. (Roundtable on Sustainable Palm Oil, 2012).

33) Othman, H., Mohammed, A. T., Harun, M. H., Darus, F. M., & Mos, H. Best management practises for oil palm planting on peat: optimum groundwater table*, MPOB Information Series*, **528**, 1–7, (2010).

34) Melling, L. and Henson, I.E. Greenhouse gas exchange of tropical peatlands–a review. *J. Oil Palm Res.* **23**, 1087-1095, (2011).

35) Veloo, R., Van Ranst, E. & Selliah, P., 2015. Peat characteristics and its impact on oil palm yield. *NJAS.* **72**, 33-40 (2015).

36) Hooijer, A. et al. Current and future CO2 emissions from drained peatlands in Southeast Asia." *Biogeosciences.* **7**, 1505–1514 (2010).

37) Henson, I.E., Betitis, T., Tomda, Y. & Chase, L.D., 2012. The estimation of frond base biomass (FBB) of oil palm. J *Oil Palm Res*. **24**, 1473-1479.

38) Caliman, J.P., Carcasses, R., Girardin, P., Pujianto, D.B. and Liwang, T. 'Development of agrienvironmental indicators for sustainable management of oil palm growing: general concept and the example of nitrogen.' *PIPOC 2005 International Palm Oil Congress: Agriculture, Biotechnology and Sustainability*. Kuala Lumpur, Malaysia, (2005)

39) Khalid, H., Zin, Z.Z. & Anderson, J.M. Decomposition processes and nutrient release patterns of oil palm residues. J *Oil Palm Res*. **12**, 46-63 (2000).

40) Henson, I.E. Modelling vegetative dry matter production of oil palm. *Oil Palm Bulletin*, **52**, 25-47 (2006).

41) Kwan, B. K. W. *The effect of planting density on the first fifteen years of growth and yield of oil palm in Sabah* (Sabah Department of Agriculture, 1994).

42) Dolmat M., Hamdan A.B., Zulkifli H. & Ahmad Tarmizi M. Fertiliser requirement of oil palm on peat – an update. In: Proc. Conf.1996 PORIM International Palm Oil Congress: Competitiveness for the 21st century (eds. Ariffin et al.), Palm Oil Research Institute of Malaysia, Kuala Lumpur, 131-142, (1996)

43) Aholoukpé, H.N.S. et al. Estimating aboveground biomass of oil palm: allometric equations for estimating frond biomass. *Forest. Ecol. Manag.* **292**, 122-129 (2013).

44) Morel, A.C. et al. Estimating aboveground biomass in forest and oil palm plantation in Sabah, Malaysian Borneo using ALOS PALSAR data. *Forest Ecol. Manag*. **262**, 1786-1798 (2011).

45) Aholoukpè, H.N.S. et al. Allometric equations for estimating oil palm stem biomass in the ecological context of Benin, West Africa. *Trees*, **32,** 1669-1680 (2018).

46) Thenkabail P.S. et al. Biomass estimations and carbon stock calculations in the oil palm plantations of African derived savannas using IKONOS data. *Int. J. Remote Sens.* **25**, 1-27 (2004).

47) Dewi, S., Khasanah, N., Rahayu, S., Ekadinata A., & van Noordwijk, M. *Carbon Footprint of Indonesian Palm Oil Production: a Pilot Study*. (World Agroforestry Centre, 2009).

48) Corley R.H.V. Effects of plant density on growth and yield of oil palm. *Exp. Agric.* **9**, 169-180 (1973).

49) Hasnol, O., Darus, F. M. and Mohammed, A. T. Experiences in Peat Devalopment of Oil Palm Planting in the MPOB Research Station at Sessang, Sarawak. *Oil Palm Bulletin*. **58,** 1-13 (2009).

50) Dolmat M., Hamdan A.B. & Zulkifli H. Novel agronomic innovations in the exploitation of peat for oil palm. In: Proc. 1993 PORIM International Palm Oil Congress: Agriculture (Ed. by B.S. Jalani et al.), Palm Oil Research Institute of Malaysia, Kuala Lumpur, 360-372, (1995).

51) Tie, Y. L. Long-term drainability of and water management in peat soil areas. *Planter*. **80**, 423-439 (2004).

52) Lim, K.H. & Herry, W. 'Management of leaning and fallen palms planted on tropical peat.' *IOPRI International Oil Palm Conference 2010.* Yogyakarta, Indonesia (2010).

53) Henson, I.E. A Review of Models for Assessing Carbon Stocks and Carbon Sequestration in Oil Palm Plantations. *J. Oil Palm Res*. **29**, 1-10 (2017).

54) Agus, F. et al. *Review of emission factors for assessment of CO2 emission from land use change to oil palm in Southeast Asia.* (Roundtable for Sustainable Palm Oil (RSPO), 2013).

55) Cheng S., Kirton L.G. & Gurmit S. Termite attack on oil palm grown on peat soil: identification of pest species and factors contributing to the problem. *Planter*, **84**, 659-670 (2008).

56) Ariffin D., Gurmit S. & Lim T.K. 'Ganoderma in Malaysia – current status and research strategy' *1989 International Palm Oil Development Conference, (*eds. Jalani B.S. et al.) Kuala Lumpur, Malaysia (1990).

Chapter 4: Monitoring the aboveground biomass accumulation of oil palm on peat using L-band radar

4.1) Introduction

The United Nations Framework Convention on Climate Change (UNFCCC) Paris Agreement encourages governments to "pursue efforts to limit the temperature increase to 1.5°C above pre-industrial levels" (UNFCCC, 2015). Land-based climate mitigation strategies rely on increases in biomass energy production with carbon capture and storage (BECCS) balanced with avoided deforestation and reforestation efforts whilst meeting the growing food demand of an increasing population (Harper *et al.* 2018, Griscom *et al.* 2017). Despite this, tropical deforestation and land use change (LUC) currently result in emissions of between 0.5 and 3.5 Pg C yr^{-1} (Mitchard, 2018). Increased efforts to reduce emissions from deforestation and degradation (REDD+) and find nature-based climate solutions (NBS) have resulted in an enhanced focus on accurately quantifying the carbon stocks of forest and agricultural systems and the carbon fluxes associated with land use changes (Baccini *et al.* 2018, Angelsen *et al.* 2009).

The current understanding of the global land carbon sink is limited by a lack of spatially explicit observations of changes in carbon stocks in vegetation biomass and soils (Le Quere *et al.* 2018, Arneth *et al.* 2017). As a result, remote sensing techniques are increasingly being employed to quantify changes in aboveground biomass (AGB) stocks over time (Gibbs *et al.* 2007, Mitchard *et al.* 2018). The spatial extent and rate of deforestation can be quantified using a timeseries of optical satellite data (Hansen *et al.* 2010, Hansen and Loveland, 2012). Changes in AGB stocks can then be estimated by upscaling standardized AGB density estimates specific to ecoregions or land cover types (Angelsen *et al.* 2009, Hill *et al.* 2013).

Continuous benchmark maps of AGB density (AGBD) inferred by upscaling plot inventory measurements of AGB using active and optical remote sensing techniques are increasingly available at pantropical scales (Table 4.1). Similar methodologies are followed for each map; plot-based inventory measurement of vegetation AGB stocks and canopy height are geolocated within the 70-meter footprint of the ICESat GLAS LiDAR sensor (Saatchi *et al.* 2011, Baccini *et al,* 2012). GLAS is a spaceborne waveform LiDAR sensor, vegetation characteristics are calibrated to *in-situ* waveforms derived from measurements of returned energy intensity (Baccini *et al,* 2012). This relationship allows the estimation of forest AGB in the remaining GLAS LiDAR footprints without in-situ plot data (Saatchi et al. 2011, Baccini et al, 2012). Vegetation indices derived from spectral remote sensing approaches; the normalized difference vegetation index (NDVI) and leaf area index (LAI) are then used to produce continuous maps of AGBD from GLAS LiDAR

samples of estimated AGB at a coarse resolution (Saatchi et al. 2011, Baccini et al, 2012, Table 4.1). Recent studies have combined these continuous maps of AGB density with *in-situ* deforestation area estimates to quantify emissions from deforestation (Hansen *et al.* 2013, Tyukayina *et al.* 2015, Baccini *et al.* 2017). However, the spatiotemporal mismatch of source datasets can give rise to biased estimates of carbon pools at regional and national scales (Hill *et al.* 2013, Mitchard *et al.* 2014, Hansen *et al.* 2019). The subtler changes in AGB stocks associated with forest degradation or growth are more challenging to quantify due to the coarse spatial and temporal resolutions of many of these satellite products (Mitchard *et al.* 2018).

Table 4.1: Continuous Pantropical aboveground biomass density maps

Source	Product	Validation	Extent	Resolution	Period
Benchmark Maps					
Saatchi *et al.* 2011	Field Plot Inventories, ICESat GLAS LiDAR, MODIS (NDVI, LAI), QSCAT HH backscatter	Comparison to Amazon AGBD map – Saatchi *et al.* 2007	Tropical Regions	~1 km (0.00833 degrees)	Early 2000s
Baccini *et al.* 2012	Field Plot Inventories, ICESat GLAS LiDAR, MODIS NBAR	GLAS LiDAR derived biomass estimates – testing data Multiple AGB maps	23.4378°N -23.4378°S	463 m	~ 2007-08
Avitabile *et al.* 2016	Saachi *et al.* 2011, Baccini *et al.* 2012, Field Plot Inventories, High resolution local or national AGB maps	Field Plot Inventories, High resolution local or national AGB maps – testing data	23.4378°N -23.4378°S	~1 km (0.00833 degrees)	~ 2000-2010
Timeseries Maps					
Baccini *et al.* 2017	Baccini *et al.* 2012, MODIS NBAR	Comparison to other AGBD maps (national and regional scale)	23.4378°N -23.4378°S (Excluding Australia)	463 m	Annual Scenes : 2003 - 2014

Multiple studies map the large-scale plantation expansion of OP plantations over time across both mineral and peat soils (Wicke *et al.* 2011, Gaveau *et al.* 2016, Koh et al. 2011, Miettinen et al. 2016). However, studies are yet to attempt to directly quantify the *in-situ* carbon stock changes associated with this land use change using remote sensing techniques across a broad scale for OP on peat or mineral soils.

As discussed in Sections 1.9 and 1.10 L-band synthetic aperture radar sensors are increasingly being used to quantify and map woody vegetation biomass stocks (Supplementary table 4.1). However, in order to reliably monitor changes in AGB stocks over time using L-band SAR a large number of in-situ AGB inventory plots monitored over an extended period are required (Ryan et al, 2012). Using the novel 'Biomass Matching' technique, which reduces the need for calibration plots, may make using L-band SAR to monitor small scale changes in peat OP AGB stocks more feasible (Hill *et al.* in prep).

In order to address the aims outlined in Chapter 1 we ask the following research questions:

- How effective is the 'biomass matching' approach for detecting and mapping the losses and gains in AGB that accompany OP establishment on peat across a timeseries of SAR scenes?
- When validated using plot inventories and an oil palm AGB accumulation model *(developed in chapter 3),* how successful is this approach when attempting to accurately quantify AGB stock accumulation?
- In this study, when does the relationship between increasing AGB and increasing RCS saturate?
- How accurate are existing maps of aboveground biomass density at the study sites and how do these maps compare to each other?

4.2) Methods

4.2.1) ALOS PALSAR-1/2 scene selection and JAXA Global Mosaic Product pre-processing

The ALOS PALSAR-1/2 Global mosaic product (GMP) was chosen for this analysis as it is a freely available multi-temporal dual polarisation L-band product with scenes temporally matching plantation establishment and growth at the study sites.

All SAR scenes were acquired from the PALSAR-1/2 sensor onboard the ALOS-1/2 satellites (JAXA, 2019b, Acquired Jan 2018). PALSAR-1 and PALSAR-2 are L-band SAR sensors, ALOS-1 was operational between 2007-2011 whilst ALOS-2 has been operational since 2014, coinciding with forest clearance and plantation establishment at the study sites (See Section 2.2). The JAXA Global 25m Resolution PALSAR-2/PALSAR Mosaic product (GMP) is produced using SAR scenes observed in the sensor's fine beam dual (FBD) mode in ascending pass, tiles are orthorectified with terrain corrections applied on acquisition. Pixels are multilocked to a resolution 25 m upon acquisition (16 looks) (JAXA, 2017). All available scenes that covered the study site extent were acquired in the horizontal transmit/vertical receive (HV) polarisation stored as digital number. The HV polarisation was chosen for this analysis as the relationship between the AGB and RCS is frequently observed to be strongest in this polarisation and hence is usually used for biomass stock estimations (Supplementary Table S4.2, Morel *et al.* 2011, Yu and Saatchi, 2016). The corresponding ALOS PALSAR-1/2 GMP scenes in the horizontal transmit/horizontal receive (HH) polarisation were also acquired, to confirm whether this was the case at the study sites, see Appendixes 3.2.

Following JAXA specifications ALOS PALSAR-1/2 GMP scenes were obtained in DN format and converted to sigma naught (σ^0) radar cross section using *Equation 4.1b*, derived from Shimada *et al.* 2009 (*Equation 4.1a*):

Equation 4.1a: $$\sigma^0 = 10 \log_{10}\langle DN^2 \rangle - CF$$

Taken from Shimada et al. 2009 where CF is the calibration factor (-83.0 for the ALOS PALSAR-1/2 GMP (JAXA, 2017).

Equation 4.1b: $$\sigma^0 = 0.0000000050119 * DN^2$$

Tiles were merged to produce a continual SAR scene, the continual mosaic was then clipped to a final SAR scene extent. This extent was informed by image observation tracks (Figure 1.2a) to ensure the entirety of each scene was observed within a single observation day and reduce intra-scene variance in environmental conditions (Figure 4.1). SAR scenes were aggregated to a resolution of 100m (Esri, 2019). Seven scenes were produced spanning the ten-year study period (2007 – 2017).

4.2.2) DEM acquisition and slope masking

The Shuttle Radar Topography Mission (STRM) digital elevation model was used to calculate the topographic slope across the scene extent using the planar method (USGS, 2019, Burrough, 1998, Figure 4.2). The topography within the SAR scene is largely flat; 72.7% has a slope < 10˚ and 94.8% has a slope < 20˚. Within the plantation boundaries topography is extremely flat (98.1% has a slope < 10˚), as expected for a lowland tropical peatland (Page *et al.* 2006). The SAR scenes were then clipped to remove all areas with a slope > 20˚ in an attempt to reduce the potential influence of shadowing, foreshortening and layover in the calibrated SAR scenes (Atwood *et al.* 2014, Supplementary Figure S4.1).

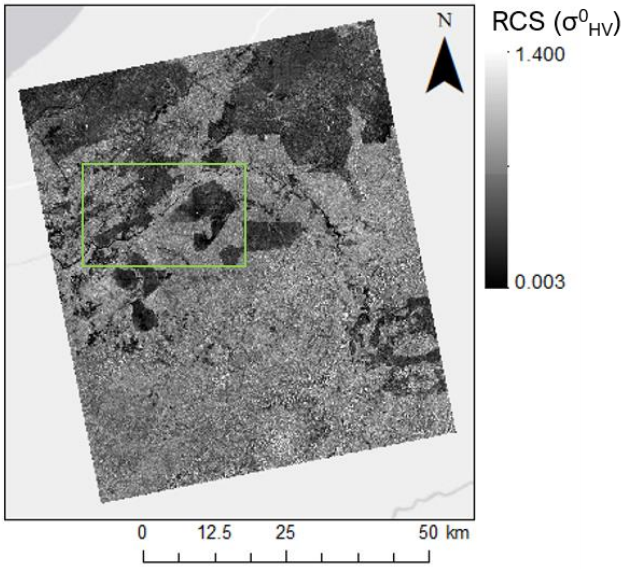

Figure 4.1: Example of SAR radar cross section scene *(σ^0_{HV}, 15-Aug-2010), Sebungan and Sabaju oil palm plantations are located within the green rectangle.*

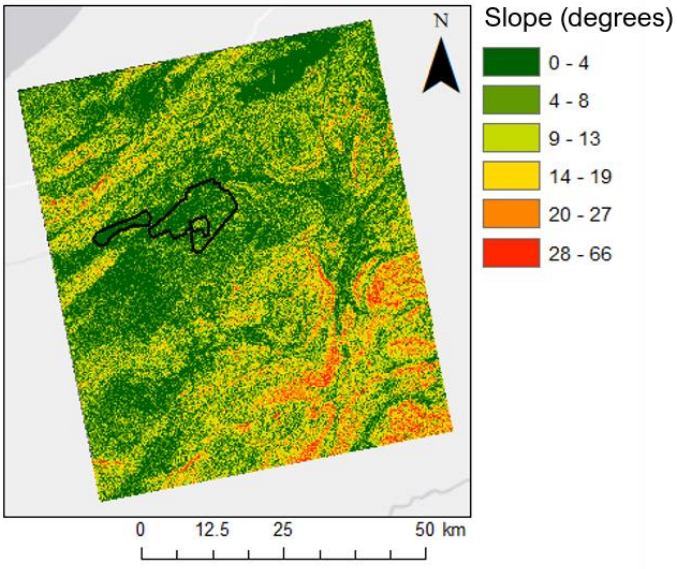

Figure 4.2: Topographic slopes (degrees) across the scene extent, *derived from the SRTM digital elevation model (resolution: 30m), Sebungan and Sabaju oil palm plantation limits shown in black.*

4.2.3) Oil palm blocking map digitisation

Oil palm planting blocking maps were digitised and the date of conversion recorded. A total of 171 planting blocks were digitised, block size was fairly consistent with mean area of 20.1 ± 6.2 ha (containing approximately 20 SAR pixels at 100m resolution). In order to inform block digitisation, planting blocking maps and semi-detailed soil maps were visually compared to Landsat 5 Thematic Mapper (TM) images, plantation blocks and establishment are clearly visible in cloud free scenes (Supplementary Figures S2.1,

S2.2 and S2.2, Supplementary Table 4.3). Blocks were not digitised in Sabaju 2, Sabaju Estate Complex, due to a higher coverage of mineral soils when compared to the rest of the plantations (See Supplementary Figures S2.1).

4.2.4) AGB mapping using 'biomass matching'

The 'biomass matching' approach reduces the need for *in-situ* calibration plots by identifying areas where no statistically significant AGB change has occurred across the timeseries of SAR scenes to derive the scene specific calibration coefficients needed to map AGB (Hill *et al.* in prep).

This approach uses a linear regression between AGB (mg ha^{-1}) and RCS (σ^0_{HV}) defining gain (g) and offset (o) regression coefficients for each scene (Equation 4.2, Ryan et al, 2012).

Equation 4.2: $$AGB = g\sigma^0_{HV} + o$$

The initialisation of the 'Biomass Matching' approach requires the fixing of these regression coefficients for a single SAR scene (S_1) (see section 4.4.5). Here, regression coefficients are fixed for the most recent scene in the timeseries (S_1 = 07-Sep-2017) *(step 2)*. An iterative loop then identifies areas (pixels) where no statistically significant change has occurred across the timeseries. Using the assumption of unchanging AGB within these areas, the regression coefficients of the remaining scenes can then be optimised.

Step 1: Pre-process and input scenes (see section 4.2.1 - 4.2.2)

Step 2: Fix the regression coefficients of one initial scene

The gain and offset for an initial scene (S_1) is fixed (see section 4.2.5).

Step 3: Initialise remaining scenes' regressions coefficients

The regression coefficients for the remaining scenes are then initialised. For the initial 'biomass matching' iteration the gain and offset derived for the fixed scene (S_1) are applied to the remaining scenes (S_2 to S_7) to predict the biomass of each pixel in each scene (Figure 4.3, Table 4.2).

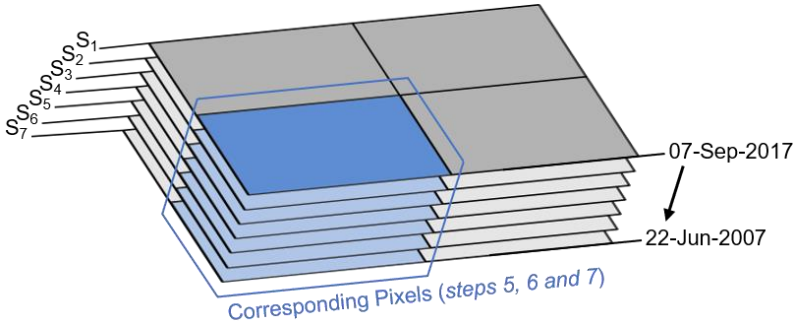

Figure 4.3: Diagram illustrating the timeseries of SAR scenes *including just 4 RCS pixels, corresponding pixels have the same geographic extent within each scene.*

Scene	Observation Date
S_1	07-Sep-2017
S_2	28-Jan-2016
S_3	10-Sep-2015
S_4	15-Aug-2010
S_5	27-Jun-2009
S_6	09-May-2008
S_7	22-Jun-2007

Table 4.2: 'Biomass matching' scene ID across the timeseries of SAR scenes*, the regression coefficients of scene S1 (the initial scene) are fixed throughout the biomass matching routine whilst the coefficients for scenes S2 to S7 are free to be optimised. Observation dates for each scene are indicated, a total of 7 scenes are used in this study, t =7.*

Step 4: Optimise the regression coefficients of the remaining scenes

The predicted pixel biomass for each of the scenes is then sorted into ascending pixel AGB. The optimisation routine then estimates the gain and offset for the unfixed scenes (S_2 to S_7) by simultaneously minimizing the sum of the square differences between the biomass predictions for all possible radar scene pair combinations (c, Eg. 2.3) (Hill *et al.* in prep). In this study, the number of possible scene pair combinations is 21 (Equation 4.3).

Equation 4.3:

$$c = \frac{t(t-1)}{2}$$

Where c is the total number of unique radar scene pair combinations and t is the total number of radar scenes.

Step 5: Calculate pixel precision

The accuracy of the AGB estimates cannot be determined as the true AGB for the area is not known (Hill *et al.* 2013). The pixel precision is therefore evaluated as a function of mean pixel AGB.

For each individual pixel the mean corresponding pixel AGB across all scenes (S_1 to S_7) is calculated, the deviation of each pixel from this mean is then calculated (Figure 4.3). These deviations are sorted into 1 Mg ha^{-1} bins according to the pixels' mean AGB. The pixel precision can be added/subtracted from the pixel AGB value to estimate the upper and lower AGB confidence limits for the pixel.

Step 6: Identify pixels with statistically significant AGB change

Significant biomass loss is defined when the lower AGB confidence limit of a pixel is greater than the upper AGB confidence limit of the same pixel at a later observation date. Similarly, significant biomass gain is defined when the upper AGB confidence limit of a

pixel is lower than the lower AGB confidence limit of the same pixel at a later time. Pixels that do not meet either of these two criteria are considered to remain with no statistically significant change in AGB.

(See Hill et al. in prep)

Step 7: Pixel masking of statistically significant change

Biomass Matching optimisation (step 4) assumes that the AGB of all pixels remains the same between scenes. All corresponding pixels that have been shown to gain or lose biomass at any point in the timeseries in step 6 are therefore masked out and are ignored in the next optimisation iteration. Aside from the first iteration this masking is performed in all subsequent loops.

Step 8: Iterative convergence

Steps 4 to 7 are repeated until convergence is achieved. Here, convergence is reached when the fraction of pixels with a change status (loss, gain, no change) differs from the previous iteration by < 0.02%.

Step 9: Save output and exit Biomass Matching iterative loop

The 'Biomass Matching' approach relies on the assumption that the AGBD of some pixels remains the same throughout the SAR timeseries in order to optimise the regression coefficients of the relationship between RCS and AGB for each SAR scene (Equation 4.2). The true AGB of these pixels is not known. However, despite the likely absence of intensive degradation or high growth rates in these areas, their AGB stocks will not truly be constant thought the timeseries. Some AGB accumulation and turnover across all vegetated areas will occur.

It must be acknowledged that properties aside from vegetation structure (and by extension AGB) affect SAR backscatter (Section 1.9 and 1.10).

The determination of areas where no statistically significant AGB change has occurred across the timeseries requires confidence limits to be set to set (upper and lower quantiles), these thresholds ultimately determine the definition of AGB change and the 'Biomass Matching' performance.

4.4.5) Calibration of the initial RCS/AGB relationship

Despite the reduced need for *in-situ* calibration plots when using the 'Biomass Matching' approach the calibration coefficients for a single initial scene must still be defined. Half of the digitised oil palm planting blocks were randomly selected to be used for calibration whilst the other half were used for result validation. Following the methodology of Ryan *et al.* 2012, the mean block RCS for each 'calibration block' was extracted from each

SAR scene. Where the blocks had been converted for > 3 years at the time of scene observation, the mean RCS was plotted against the estimated block AGB.

Block aboveground biomass was estimated using the AGB accumulation model derived from the results of non-destructive plot inventories in Chapter 3; Model P1 (Section 3.3.3), hereafter the model will be referred to as Accumulation Model P1 (AMP1). Oil palm age is assumed to to be the difference between the time of block establishment and the time of scene observation. A Type II Reduced Major Axis Regression (RMA) was then used to fit a regression line between the *in-situ* mean plot RCS and AGB (Ryan *et al.* 2012). An RMA regression was used to minimise the sum of associated errors in both the X (RCS) and Y (AGB (Mg C ha^{-1})) component (Friedman *et al.* 2013, Harper, 2014). The regression was fit using the MATLAB script 'gmregress' published by Trujillo-Ortiz and Hernandez-Walls (2010).

4.4.6) Validation of AGBD timeseries maps

Comparison to non-destructive OP AGB inventories and accumulation models

The mean block AGB for each scene was extracted from each of the digitised blocks retained for AGB map validation, this was compared to the estimated block AGB (AMP1) corresponding to the map timestamp (Model P1, Section 3.3.3).

Non-destructive OP AGB survey plot locations were digitised, plot GPS co-ordinates were used to place a polygon of ~4 ha at the plot location (Chapter 3, Supplementary Table S3.5). The mean plot AGB was then extracted from the AGBD map corresponding to 07th Sep 2017 (non-destructive AGB inventories were conducted between February and March 2019).

Comparison to existing AGBD maps

All aboveground biomass density maps recorded in Table 4.1 were downloaded from supplementary databases (Saatchi *et al.* 2011, Baccini *et al.* 2012, Avitabile *et al.* 2016) and transformed to a consistent geographic coordinate system (GCS WGS 1984). AGBD maps were resampled to a resolution and spatial extent matching that of the Avitabile *et al* (2016) map product (Resolution: 1km, Esri, 2019). A net matching this pixel resolution and extent was produced, and the mean AGB was extracted for each grid square for all AGBD maps.

Comparison to PSF plot inventory data

Census data from a permanent 1 ha plot on the Sabaju estate was used to determine PSF AGB stocks (Koh 2019, pers. comm, 25 February). The plot is located on the Sabaju estate in a secondary peat swamp forest fragment. The plot is logged with the majority of large trees removed (3.162˚N, 113.429˚E). For the purposes of this study the plot is

considered representative of the AGB stocks and vegetation cover present at the plantation sites prior to conversion (Kho 2019, pers. comm, 25 February).

All standing trees with a diameter at breast height (DBH, 1.3 m) > 10 cm were included, tree height and DBH measured for each of these trees, and the family and species names recorded. Wood densities accurate to the family level, or species where possible, were used (Supplementary Table 4.4) together with the allometric equations of Chave *et al.* (2005) for tropical moist forests to estimate the AGB of the 1 ha plot.

4.3) Results

4.3.1) Radar cross section change across the timeseries in the OP blocks

Oil palm planting blocking maps were digitised and the date of conversion from PSF to OP was recorded. The mean radar cross section from each block was then extracted from each SAR scene. When the mean block RCS was pooled for each of the ALOS PALSAR-1/2 satellites the reduction in mean block RCS following OP plantation establishment is clear. The bimodal distribution of pooled block RCS when considering blocks observed using ALOS-1 (684 blocks), reflects the RCS of both pre-conversion PSF and post conversion OP land covers (Figure 4.4). By 2015 the majority of blocks have been converted to OP, and the distribution of the mean block RCS across the scenes observed by ALOS-2 (533 blocks) mirrors the low RCS of OP blocks observed using ALOS-1. However, oil palm blocks with a higher RCS within this range appear more frequently in the later scenes (Figure 4.4).

When considered as a chronosequence, there is a clear reduction in RCS accompanying forest clearance. The block RCS remains consistent before conversion (-10 to 0 YAP) before reducing significantly following deforestation at the time of plantation establishment (YAP > 0) (Figure 4.5). The RCS of OP planting blocks increases gradually between 4 to 10 years after planting (Figure 4.5, ALOS-2). The RCS at YAP = 0 is variable with overlap between PSF, cleared and newly planted OP blocks all grouped into the same age class (Figure 4.5). The planting blocking maps used to inform block digitisation were accurate to the nearest planting year and hence determining the exact land cover status in each block at the time of block SAR scene observation was difficult. However, the RCS of peat swamp forests, which are assumed to have a constant RCS, is higher when observed using ALOS-2. Peat swamp forest had a mean RCS of 0.091 ± 0.001 when observed using ALOS-2 compared to an RCS of 0.067 ± 0.006 in ALOS-1 scenes, this is likely due to differences in satellite specifications (Figure 4.5).

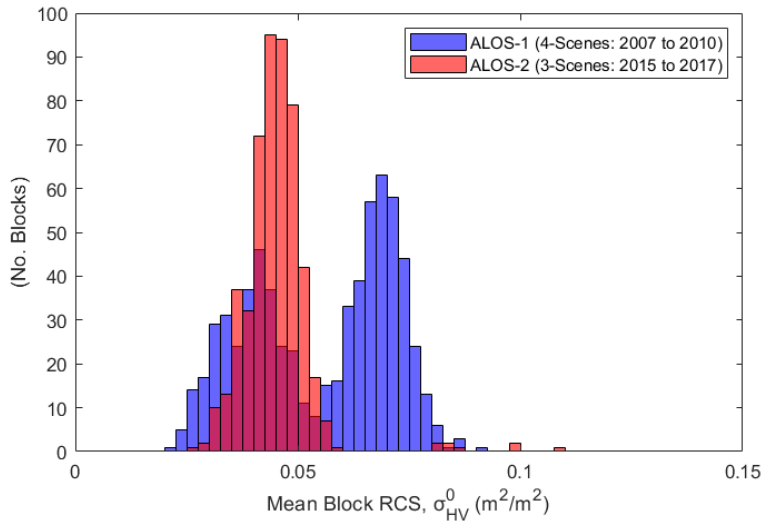

Figure 4.4: Distribution of the mean block radar cross section (RCS), *the RCS of each block in each scene is pooled for the ALOS-1 and ALOS-2 satellites. ALOS-1 scenes span plantation establishment (2007 to early 2011) whereas ALOS-2 scenes observe the plantation post-establishment (4 OP plots are converted in late 2016). Points at which the distributions overlap indicated in purple.*

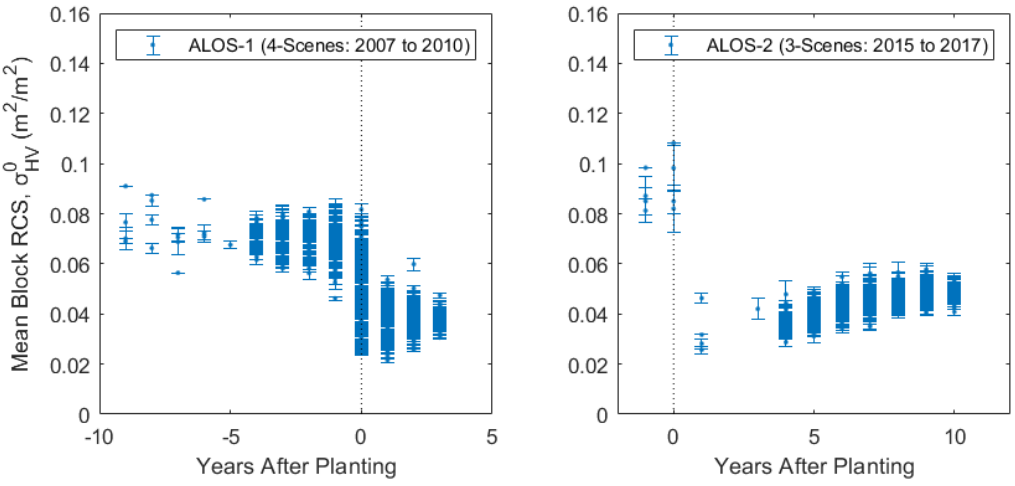

Figure 4.5: Mean block RCS (σ^0_{HV}) prior to and after oil palm plantation establishment *(0 years after planting – indicated as a dashed line). A chronosequence approach is used, mean block RCS is plotted against the years before/after planting at the time of observation (standard error indicated). All blocks as observed in all scenes for each satellite are pooled (ALOS-1 left, ALOS-2 right).*

4.3.2) Calibration of the initial RCS/AGB relationship

The 'biomass matching' approach requires the relationship between the *in-situ* RCS and AGB to be fixed for an initial SAR scene (S_1) (where 167 blocks had been converted to OP at the time of observation aged between 6 to 10 YAP). In order to establish this relationship for the OP blocks in S_1 the mean RCS of calibration blocks was plotted against block AGB as estimated using AMP1. The estimated AGB of oil palms using AMP1 is positive for palms > 2.75 years after planting (Chapter 3, Figure 3.6). The RCS

of calibration and validation blocks before 'biomass matching' was consistent (Supplementary Figure S4.2). A reduced major axis regression was fitted to establish the gain and offset coefficients for scene S_1 (g = 1949.22, o = -60.86) (Figure 4.6). For indicative purposes a least squares regression resulted in an adjusted R^2 of 0.43.

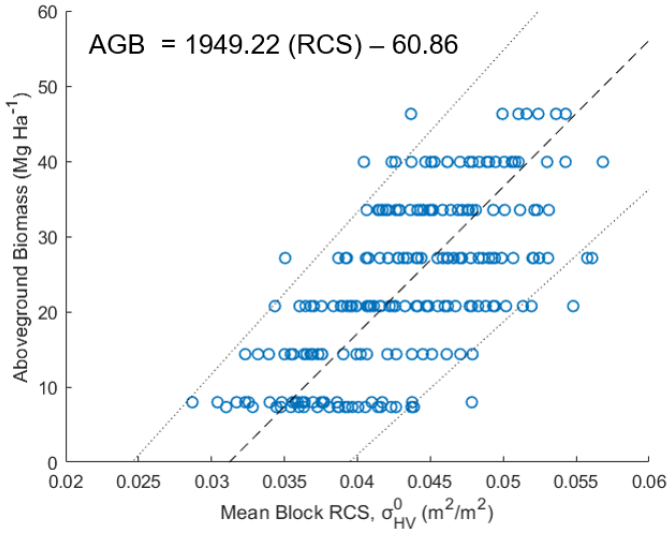

Figure 4.6: RMA Regression of ALOS PALSAR-2 radar cross section and estimated AGB for oil palm 'calibration blocks' *(black dashed line), AGB is estimated using AMP1. The 95% confidence interval of the fit indicated is indicated (black dotted lines).*

4.3.3) 'Biomass Matching' and SAR scene calibration coefficients

Biomass matching routine

The 'biomass matching' optimisation routine was performed with lower and upper quantiles set to 0.21 and 0.79 respectively (step 5 and 6, Section 4.2.4). All pixels within the scene were used in the optimisation (subsampling step = 1). When using a difference threshold of 0.002 (0.02%), iterative convergence was reached after 5 iterations (Figure 4.7).

By the final iteration, the area of the scene where no statistically significant change had been detected covered 264,167 ha (~61.4 %). Statistically significant gains and losses in AGB had been detected across 83,935 ha (~19.5%) and 81,804 ha (19.0%) of the scene (pixel resolution of 1 ha) (Figure 4.8).

The final uncertainty of estimated pixel AGB ranged from ±11.3 to ±21.7 Mg ha^{-1} for estimated AGB pixels of less than 100 Mg ha^{-1}, but this rises to ± 34.0 Mg ha^{-1} for AGB estimates of 200 Mg ha^{-1} (Supplementary Figure S4.3). This uncertainty increases to ± 46.7 Mg ha^{-1} for estimated AGBs of less than 200 Mg ha^{-1} when areas with a slope > 20˚ are included in the SAR scenes.

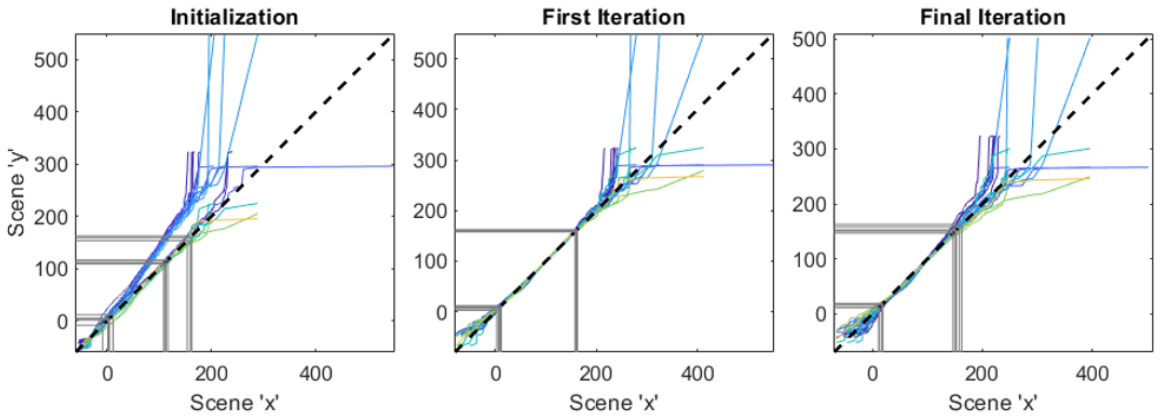

Figure 4.7: 'Biomass matching' plots for the Initialization step (step 3, left), after the first iteration (middle) and after the final iteration (right). *Scene combinations are indicated (a total of 21 combinations), the sorted ascending pixel AGB of scene 'x' (first listed in legend, Mg ha^{-1}) is plotted against the sorted ascending pixel AGB of scene 'y' (second listed in legend, Mg ha^{-1}). To indicate pixel AGB distribution the 5 and 95% quantiles are indicated in grey for each combination.*

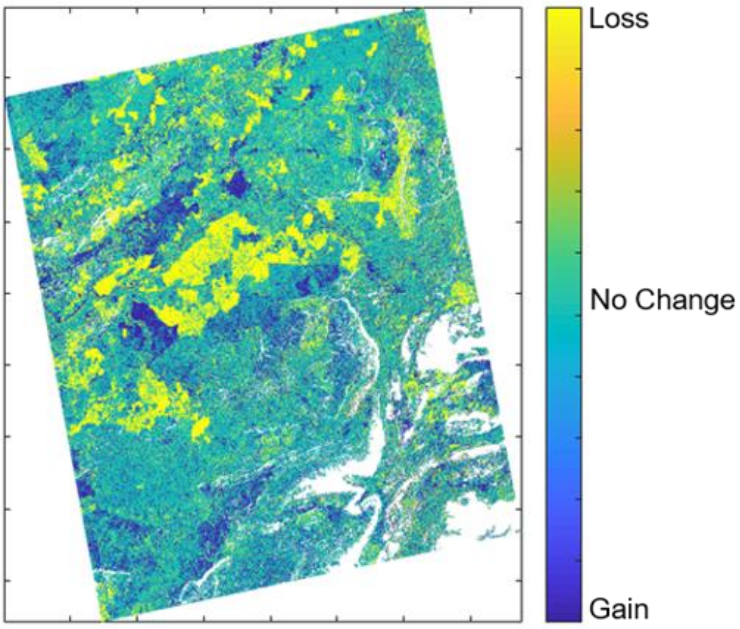

Figure 4.8: Pixel condition after final 'biomass matching' iteration. *Pixels that have not undergone a statistically significant change in AGB across the timeseries (May 2008 to Sept 2017) are indicated ('No-change').*

Scene specific calibration coefficients

Calibration coefficients are optimised for each SAR scene (Table 4.3). For the 7 SAR scenes the offset coefficients ranged from -91.3 to -48.2 Mg ha^{-1} while gain coefficients ranged from 1849.6 to 2808.5 Mg ha^{-1}. Despite similar offsets (*o*), the gain (*g*) is ~41% lower for scenes observed using the ALOS-2 satellite, when compared to ALOS-1 (Figure 4.9).

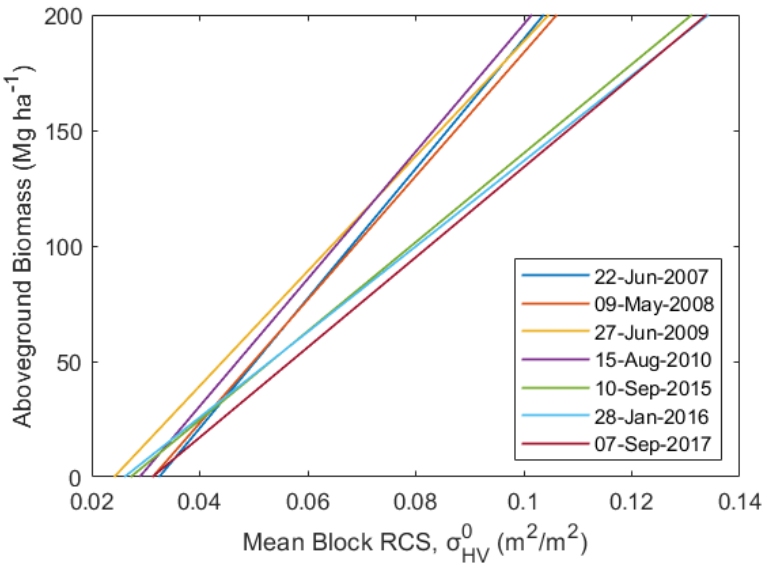

Figure 4.9: Final models fit to define the in-situ relationship between pixel RCS and pixel AGB for each SAR scene. *Scene data and observation satellite indicated, ALOS-1: scenes between 2007 – 2010, ALOS-2: scenes between 2015 and 2017.*

Observation Date	Gain (*g*)	Offset (*o*)
07-Sep-2017	1949.22 *	-60.86 *
28-Jan-2016	1849.60	-48.20
10-Sep-2015	1925.32	-52.41
15-Aug-2010	2754.95	-79.59
27-Jun-2009	2485.61	-60.06
09-May-2008	2672.70	-83.60
22-Jun-2007	2808.53	-91.25

Table 4.3: Final gain and offset coefficients to define the in-situ linear relationship between pixel RCS and pixel AGB for each SAR scene. *Scene data and observation satellite indicated, ALOS-1: scenes between 2007 – 2010, ALOS-2: scenes between 2015 and 2017.*

4.3.4) Aboveground biomass maps and timeseries monitoring

A timeseries of AGB maps was produced using the specific calibration coefficients derived for each SAR scene (Figure 4.10). A significant reduction in AGB can be seen following plantation establishment, with the plantation outline clearly observable in the AGBD maps (Figure 4.10). The maps are grainy, with variation in AGB observed with similar land uses potentially due to SAR speckle noise.

Using the timeseries of AGBD maps; the total AGB of the Sebungan oil palm plantation has reduced by ~99,188 Mg between 2007 and 2017, whilst the Sabaju Estate total AGB has reduced by ~524,517 Mg over the same period. The mean pixel AGB reduced by ~46.6 Mg ha^{-1} in Sebungan and 58.0 Mg ha^{-1} in Sabaju. This suggests that considering both the clearance of peat swamp forest AGB and accumulation of oil palm AGB across

the plantations this LUC has resulted in a total AGB stock reduction of ~623,705 Mg ha^{-1} between 2007 and 2017.

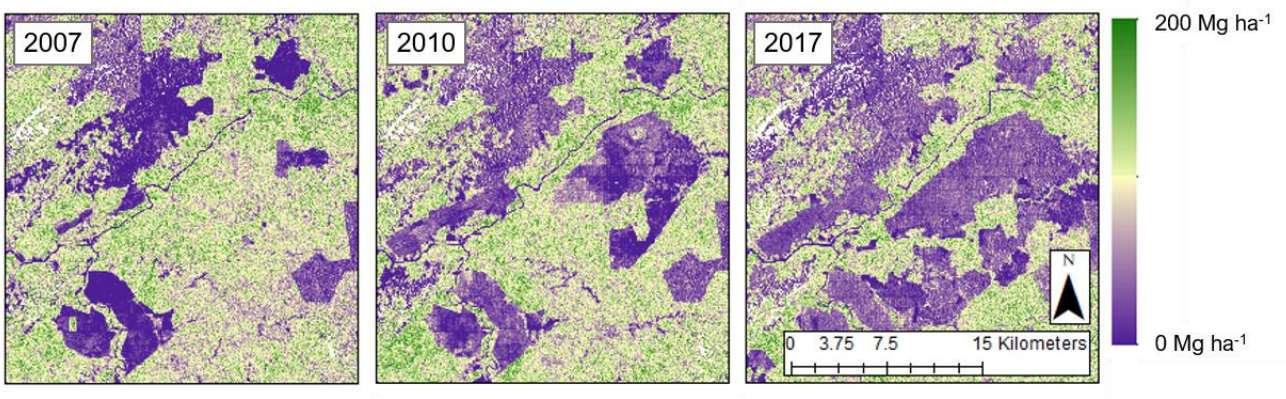

Figure 4.10: A timeseries of AGBD maps at the study site derived from SAR scenes using the 'biomass matching' approach. *All panels have the same geographic situation showing the Sebungan and Sabaju OP plantations. The observation year is indicated (a further 4 scenes have been produced), maps have a resolution of 1-ha.*

The mean AGB was then extracted for each planting block. Example blocks were then randomly selected where complete block conversion had occurred between two SAR observations, and then monitored across the timeseries (Figure 4.11). Randomly selected blocks converted between June-2007 and May-2008 show a reduction in AGB following conversion (Sebungan and Sabaju). However, block AGB does not approach zero for any of the sample blocks immediately following conversion and block AGB remains constant for the remainder of the timeseries. In comparison, the estimated aboveground biomass of blocks converted between June-2009 and August-2010 reaches or approaches zero, with perhaps some AGB accumulation observable (Sabaju only) (Figure 4.11). Considering the AGB estimates before and after conversion and taking into account the uncertainties associated with the estimated pixel AGB values, the results suggest deforestation has taken place. Estimated pixel AGB uncertainties are less than 22 Mg ha^{-1} for all AGB estimates < 150 Mg ha-1, see Supplementary Figure S4.3. Our study suggests the variation of estimated AGB within a single block 3 years prior to conversion, despite AGB likely remaining relatively constant, or potentially reducing as a result of logging (Figure 4.11 (lower panel)).

The chronosequence of mean block AGB plotted against block age (Figure 4.12) reveals the overestimation of AGB for young oil palm blocks in addition to a large variation in AGB estimates for blocks of similar ages (0 to 3 YAP). The range of estimated AGB values within an age class reduces later in the chronosequence when monitoring young mature and mature OP using the second satellite (ALOS-2). The AGB of OP between 4 and 10 YAP does appear to increase with age in agreement with AMP1, however this

agreement is not observed after 10 YAP when AGB appears underestimated (Figure 4.12).

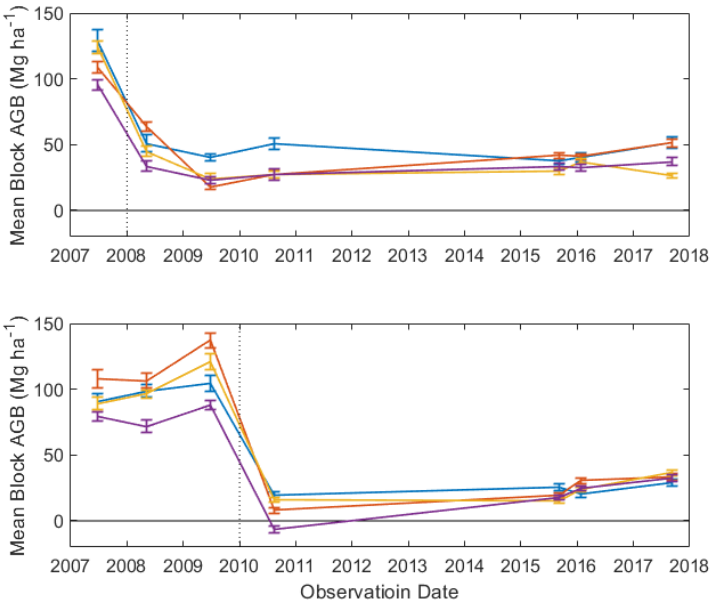

Figure 4.11: Example timeseries for an OP planting block prior to conversion and after oil palm establishment. *Mean block AGB at the time of observation for blocks completely cleared between SAR scenes, standard error indicated. The approximate time of block establishment is indicated as dotted line*.

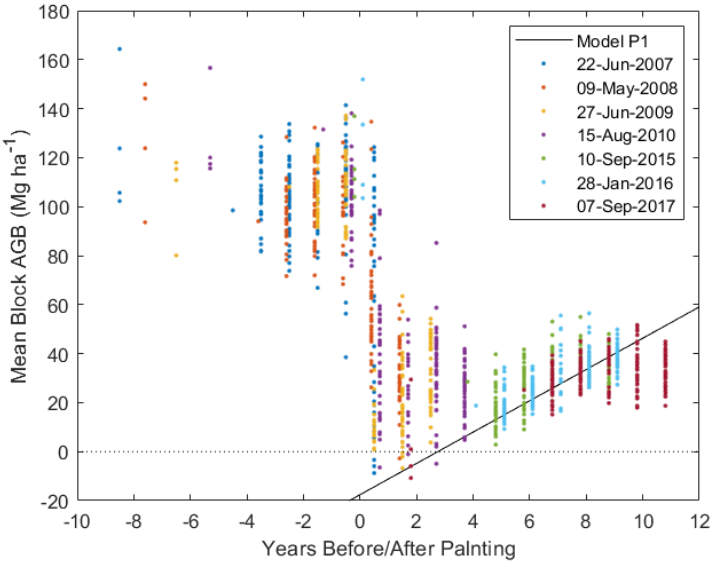

Figure 4.12: Mean block AGB prior to and after oil palm plantation establishment*. A chronosequence approach is used, mean block AGB is plotted against the years before/after planting at the time of observation (AGB = 0 Mg ha^{-1} indicated as a dashed line). All blocks as observed in all scenes for each satellite are pooled (ALOS-1: 2007-2010, ALOS-2: 2015-2017). The aboveground biomass accumulation model AMP1, derived using plot inventories (chapter 3), is plotted as a black line for illustrative purposes.*

4.3.5) Aboveground biomass density map validation

Oil palm AGB: Comparison to OP AGB accumulation models and non-destructive plot inventories

The expected AGB of each 'validation block' based on the age of the block at the time of observation using AMP1 was compared to the estimated block AGB using the 'biomass matching' approach (Figure 4.13) in order to assess the success of using the 'biomass matching'. In general, the 'biomass matching' routine overestimated the plot AGB (Figure 4.13). This overestimation was again most evident in low AGB estimates (younger age classes). The estimated AGB (biomass matching) typically mirrors the AMP1 for blocks with an average AGB of between ~15 and 40 Mg ha^{-1}. However, the predicted AGB of older blocks is underestimated using the 'biomass matching' approach and all age classes have a large range of predicted AGB values (±15 Mg ha^{-1}) (Figure 4.13).

Calibration of the initial RCS/AGB relationship for scene S_1 and much of the analysis of the resulting AGBD timeseries map success has been done by using AMP1 to estimate the AGB of multiple OP planting blocks. This is largely due to the relatively small sample size of non-destructive/semi-destructive surveys conducted in OP inventory plots across the plantations (22 plots), in addition to the lack of *in-situ* AGB structural surveys for any other scene observation date. However, the mean estimated AGB of a 4-ha plot co-located with each inventory plot was extracted from the most recent SAR scene (07-Sep-2017) and compared to the results of the structural surveys (conducted between February and March 2019) (Chapter 3, Table S3.5). However, it must be noted that ~1.5 years of OP growth has occurred between the time of SAR observation and completion of the non-destructive surveys. The AGB accumulation model (AMP1) used to calibrate the SAR data is also derived from the results of these *in-situ* inventories. In addition to this, the 07-Sep-2017 scene had fixed gain and offset coefficients throughout the biomass matching routine and hence has not been optimised by the approach.

Again, the estimated AGB of inventory plots appears close to that quantified using non-destructive inventories for plots with an AGB < 60 Mg ha^{-1} (Figure 4.14). When only young mature and mature plots (YAP > 3, within the calibration range) with an AGB less than 60 Mg ha^{-1} are considered (14 plots) the 'biomass matching' approach over/underestimates the observed plot AGB by an average of 22.7%. When plots with an observed AGB > 60 Mg ha^{-1} are considered this error increases to an average over/under estimation of 34.2%, with a mean underestimation of 62.9% in these higher biomass plots. The young plots < 3 YAP have a mean observed AGB of 3.5 Mg ha^{-1} and

are on greatly over/underestimated by an average of 352.0%. The variation in aboveground biomass stocks observed in the older plots, 11 and 12 years after planting, is not reflected in the aboveground biomass density maps, despite the observed AGB variation within these age classes their estimated AGB remains consistent (see section 3.4.4, Chapter 3, Figure 3.7, Figure 4.14).

Initially SAR RCS appears sensitive to increases in *in-situ* AGB, however this sensitivity is lost at high AGB values > ~60 Mg ha^{-1} after which RCS appears to remain constant (or even reduce) (Figure 4.14). In most instances the mean RCS of the OP planting block is similar to the mean RCS of the 4-ha plot located within that block at the non-destructive inventory site. As expected, the S.E. of the mean block RCS is reduced when compared to the 4-ha plot (Figure 4.14).

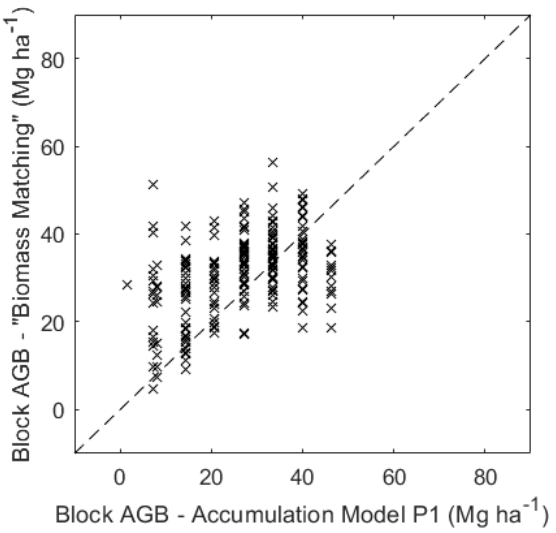

Figure 4.13: Success of AGB estimation in 'Validation Blocks'. *Oil palm AGB estimated using AMP1 against the AGB of 'validation blocks' after the final 'biomass matching iteration' (85 blocks). 1:1 line indicated.*

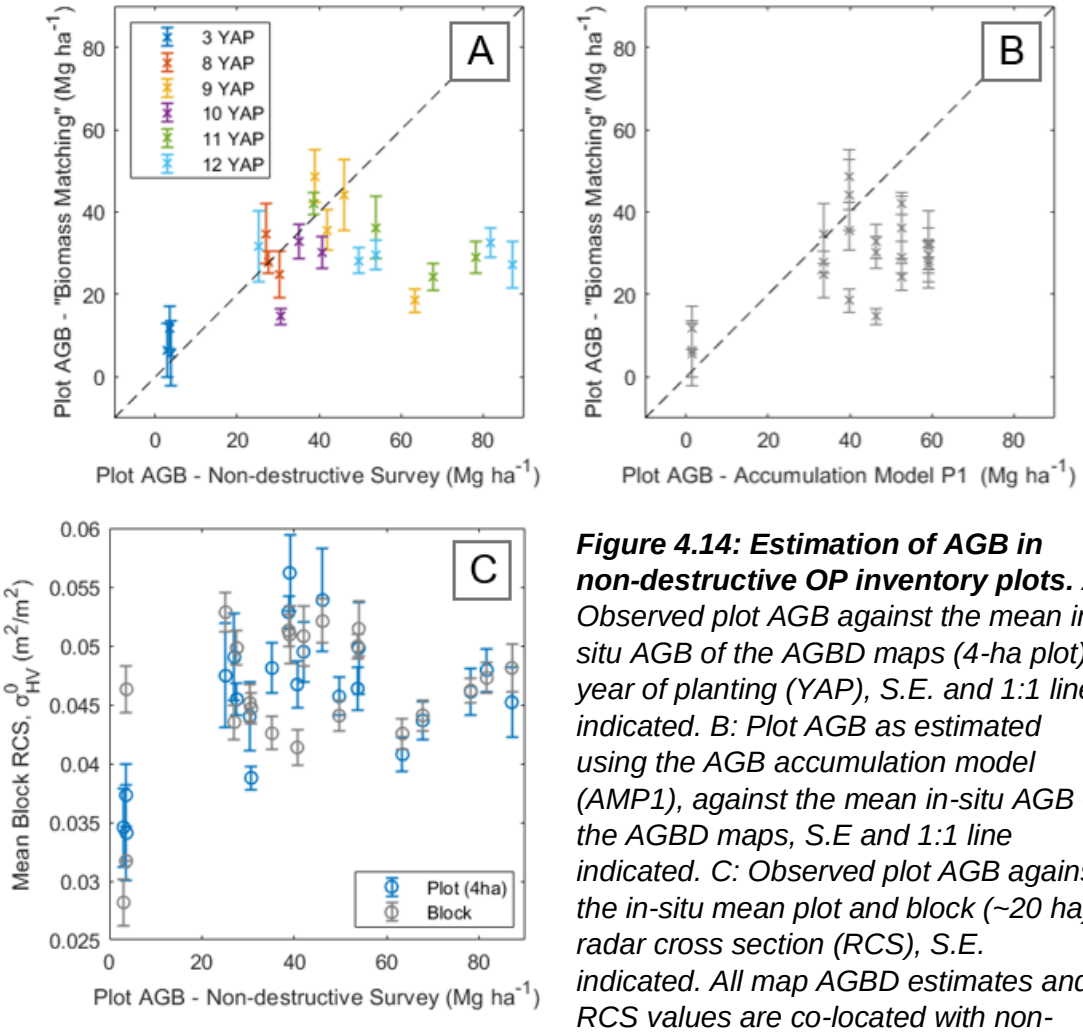

Figure 4.14: Estimation of AGB in non-destructive OP inventory plots. *A: Observed plot AGB against the mean in-situ AGB of the AGBD maps (4-ha plot), year of planting (YAP), S.E. and 1:1 line indicated. B: Plot AGB as estimated using the AGB accumulation model (AMP1), against the mean in-situ AGB of the AGBD maps, S.E and 1:1 line indicated. C: Observed plot AGB against the in-situ mean plot and block (~20 ha) radar cross section (RCS), S.E. indicated. All map AGBD estimates and RCS values are co-located with non-destructive inventory plots using GPS coordinates and are taken from the 07-Sep-2017 SAR scene and corresponding AGB map.*

Peat swamp forest AGB: Comparison to PSF inventories and existing AGBD maps

The relationship between the aboveground biomass of peat swamp forest and the *in-situ* radar cross section in the SAR scenes was not defined at the study site. Despite this, a single AGB inventory estimate representative of the site, AGB estimates from other Malaysian PSFs and the AGBD maps of Avitabile et al (2016) are compared to AGB estimates of PSF biomass in the maps produced here.

The 1-ha plot in a fragment of logged peat swamp forest at the Sabaju Estate site had an AGB of 92.5 Mg ha^{-1}. This was lower than the mean AGB of logged Malaysian PSFs reported in Kho and Jepsen (2015) (117.4 ± 21.4 Mg ha^{-1}), however the majority of the large trees have been removed from the site (Table 4.4, Koh 2019, pers. comm, 25 February).

The mean AGB was extracted from all OP planting blocks that remained completely covered by PSF in the first SAR observation (22-Jun-2007), and the corresponding mean AGB was also extracted from the Avitabile et el (2016) AGBD map (Figure 4.15). A mean aboveground biomass of 203.3 ± 39.3 Mg ha^{-1} was estimated across the plantation prior to conversion in the Avitabile map. The AGB of planting blocks prior to conversion as a result of the biomass matching is more consistent with both the AGB of the inventory plot at the study site and values for logged PSF reported in the literature (Figure 4.15, Table 4.4)

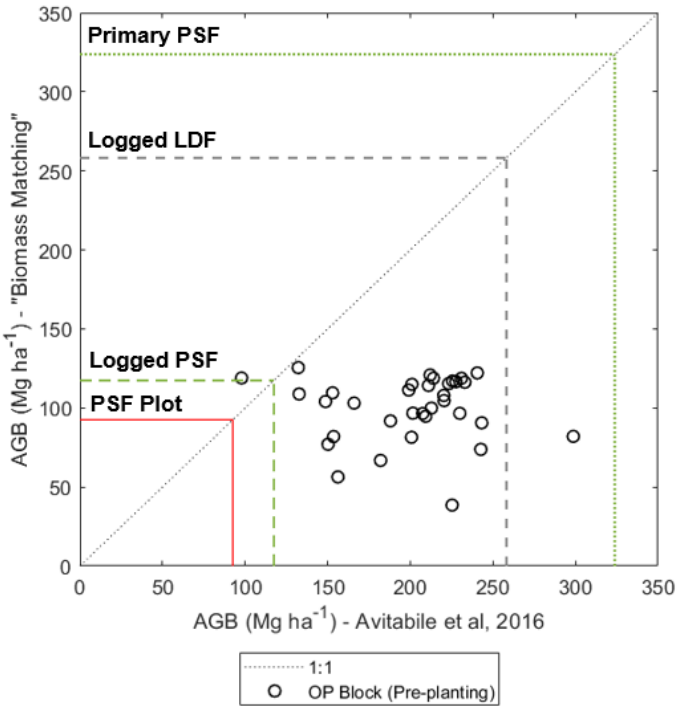

Figure 4.15: Comparison of estimated aboveground biomass stocks in logged/secondary peat swamp forest at the study site. *AGBD estimates of Avitabile et al (2016) are compared with the 2007 AGBD map produced using the 'biomass matching' approach (black open circle), 1:1 line indicated. The AGB of logged and primary peat swamp forest (PSF) and logged lowland Dipterocarp forest (LDF) taken from Kho and Jepsen (2015) are included for comparison. The AGB stock of the inventory plot at the Sabaju Estate is indicated as a red line.*

	Mean AGB (Mg ha^{-1})	**Standard Error**
Peat Swamp Forest		
Primary Forest	323.8	± 25.8
Logged/Secondary Forest	117.4	± 21.4
Lowland Dipterocarp Forest		
Primary Forest	503.8	± 35.0
Logged/Secondary Forest	258.2	± 20.6

Table 4.4: Review of aboveground biomass stocks of Malaysian peat swamp and lowland Dipterocarp forests *(primary and logged/secondary) as reported in Kho and Jepsen, 2015.*

Scene AGB: Comparison to existing AGBD maps

The mean estimated aboveground biomass was extracted for each 1km x 1km grid cell within the 2007 SAR scene (~418,000 ha). This was then compared to the *in-situ* AGB estimated from existing AGBD maps matching this spatial extent (Table 4.1, resolution aggregated to 1km).

There were few AGB estimates greater than 150 Mg ha^{-1} across the AGB map derived from the 2007 SAR scene at a 1 km resolution. Despite this, AGB estimates as high as 500 Mg ha^{-1} are observable in the AGBD map produced by Avitabile et al (2016), suggesting forest cover including primary peat swamp and lowland Dipterocarp forests across the scene (Figure 4.16). The AGB of pixels in the 2007 map produced using the 'matching' routine again shows a distribution of biomass estimates grouped into distinct high and low AGB groups (Figure 4.16).

The Avitabile et al (2016) map is produced by fusing the pantropical AGBD maps of Baccini et al (2012) and Saatchi et al (2011). These map products combine data from inventory plots and satellite LiDAR samples of forest structure upscaled using optical datasets and are multi-date products with input layers ranging from 2000 to 2008 (Section 4.1, Table 4.1). When these AGBD maps are compared across the study scene extent there is broad disagreement between AGB estimates (Figure 4.17). When histograms of predicted biomass distribution are compared, the Saatchi *et al*. (2011) map appears to estimate a much higher AGB than the Baccini *et al*. (2012) map across the scene, with the majority of pixels estimated to be between 300 and 350 Mg AGB ha^{-1} by Saatchi *et al*. (2011). In contrast the Baccini map has a high distribution of pixels with a predicted aboveground biomass between approximately 150 and 300 Mg ha^{-1} (Supplementary Figure S4.4). There are very few pixels with low estimated AGB (<100 Mg ha^{-1}) in any of the AGBD maps either suggesting a lack of large scale deforestation, degradation or logging or the poor prediction of low AGB values in the map products (Figure 4.17, Supplementary Figure S4.4).

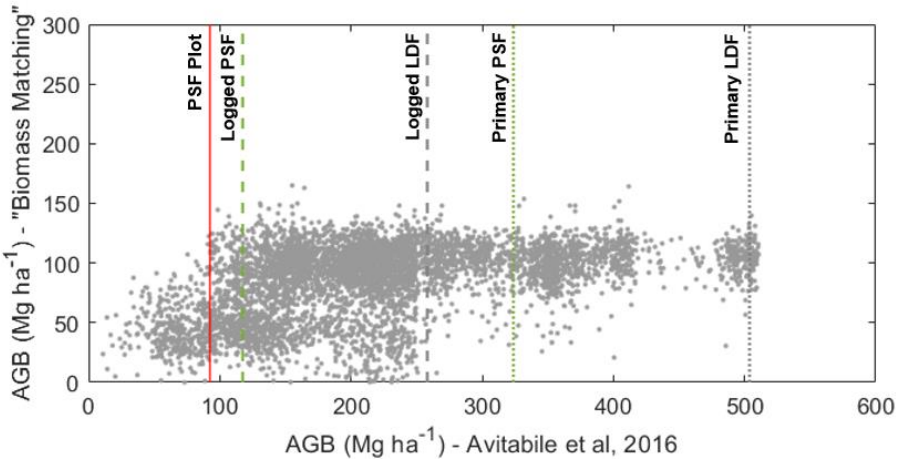

Figure 4.16: Comparison of estimated aboveground biomass stocks across the study scene extent. *AGBD estimates of Avitabile et al (2016) are compared with the 2007 AGBD map produced using the 'biomass matching' approach at a 1-km resolution. The AGB of logged and primary peat swamp forest (PSF) and lowland Dipterocarp forest (LDF) taken from Kho and Jepsen (2015) are included for comparison. The AGB stock of the inventory plot at the Sabaju Estate is indicated as a red line.*

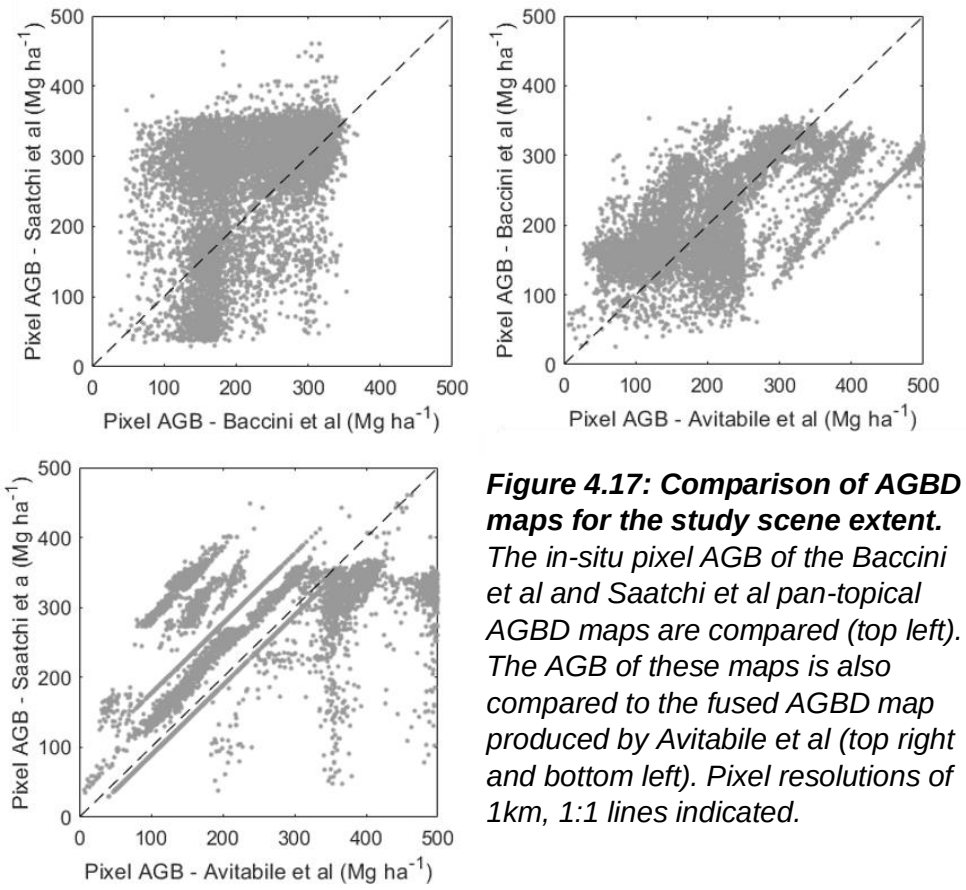

Figure 4.17: Comparison of AGBD maps for the study scene extent. *The in-situ pixel AGB of the Baccini et al and Saatchi et al pan-topical AGBD maps are compared (top left). The AGB of these maps is also compared to the fused AGBD map produced by Avitabile et al (top right and bottom left). Pixel resolutions of 1km, 1:1 lines indicated.*

4.4) Discussion

An initial relationship between the L-band SAR radar cross section and AGB was calibrated, the 'biomass matching' approach was then used to calibrate this relationship for multiple SAR scenes and detect statistically significant deforestation at the time of plantation establishment. Degraded PSF AGB was easily distinguishable from mature OP plantations. The accumulation of OP AGB was well predicted for young mature palms between 4 and 9 YAP, however the relationship between increasing AGB and the RCS saturated at ~45 - 60 Mg ha^{-1}. Existing maps of AGBD were highly divergent across the study area and none captured OP establishment. In the following section the these results will be discussed with regard to the research questions outlined in Section 4.1.

4.4.1) How effective is the 'biomass matching' approach for detecting and mapping the losses and gains in AGB that accompany OP establishment on peat across a timeseries of SAR scenes?

The availability of the ALOS PALSAR-1/2 global mosaic product temporally matches the establishment of the oil palm plantations at the study site and more broadly the expansion of industrial oil palm plantations (IOPP) across tropical peat swamp forests in Malaysian Borneo and Insular South East Asia (Miettinen *et al.* 2017, Kho *et al.* 2011, Gaveau *et al.* 2016). In addition to this, the consistently flat topography at the study site, typical of lowland tropical peatlands is advantageous when using SAR datasets to monitor aboveground biomass stocks (Page *et al.* 2006, Atwood *et al.* 2014). Here, the 'biomass matching' approach has used the freely available Global Mosaic SAR product to detect statistically significant deforestation at a high resolution (1ha) and annual frequency (Figure 4.8, Figure 4.11, Supplementary Figure S4.3).

As peat oil palm plantations mature, the AGB stocks of these plantations approaches the AGB stock of degraded peat swamp forests. However, it should be kept in mind that this OP biomass is temporary and will be removed at the end of the OP planting cycle and that ecosystem services and biodiversity are greatly diminished (Lim *et al*. 2012, Koh and Wilcove. 2008). Logged or secondary Malaysian peat swamp forests have an AGB of 117.4 ± 21.4 Mg ha^{-1} whilst old growth/primary Malaysian peat swamp forests are reported to have AGB stocks of 323.8 ± 25.8 Mg ha^{-1} (Morel *et al.* 2011, Brunig and Klinge, 1977, Ipor *et al.* 2006, Verwer and van der Meer, 2010, Miettinen and Liew, 2009). However, historically logged over or degraded forests are more likely to be converted to industrial oil palm plantations (IOPPs) in the region (Gaveau *et al.* 2014). AGB stocks in oil palm plantations on mineral soils can reach ~94.8 Mg ha^{-1} 25 years after planting (Germer and Sauerborn, 2008). The peat OP AGB accumulation model established here (Chapter 3, AMP1) only extends to 12 years after planting, however, successful plots reached high AGB stocks of up to 87.8 Mg ha^{-1}. Despite this, the radar cross section of

both land cover types remains distinctly different throughout the timeseries, allowing OP plantation establishment to be detected and highlighting the potential to identify even mature oil palm plantations using the 'biomass matching' technique.

Synthetic aperture radar datasets are not a direct measure of aboveground biomass but are sensitive to the volume of woody vegetation structures (Woodhouse *et al.* 2012). In multiple studies oil palm plantations have been distinguished from forests and various other types of woody plantation species using the ALOS PALSAR global mosaic product, with some issues encountered when attempting to distinguish between oil palms and other palm plantation species (coconut*, Cocos nucifera* and oil palm) (Miettinen and Liew, 2011, Miettinen *et al.* 2016, Cheng *et al.* 2016). However, the analysis of optical remotely sensed datasets in conjunction with the automated 'biomass matching' technique is still likely to be necessary in order to reliably distinguish oil palm plantations from other land cover types if the technique were to be used for land over change detection (Miettinen *et al.* 2019). In addition to this, the approach would need to be combined with a mechanism to detect peat soils, or combined with existing peatland maps if it is to be applied specifically to detect and monitor oil palm on peat (Miettinen *et al.* 2016, Gumbricht *et al.*2017, Dargie *et al.* 2017, Draper *et al.* 2014).

4.4.2) When validated using plot inventories and an oil palm AGB accumulation model, how successful is this approach when attempting to accurately quantify AGB stock accumulation?

Validation of oil palm AGB accumulation estimates

L-band radar datasets at the HV polarisation are sensitive to increases in aboveground biomass stocks up to an average of approximately 100 Mg ha^{-1} dependent on surface and vegetation structural characteristics (Supplementary Table S4.1, Yu and Saatchi, 2016). The AGB of the OP plantations at the study site accumulated at ~6.39 ± 1.12 Mg ha^{-1} per year in the first 12 years after planting (Chapter 3). However, this accumulation was highly variable within age classes as a result of palm leaning and eventual palm mortality, a serious limiting factor for oil palm performance on peat (Lim *et al.* 2012).

An initial RMA regression was fitted to relate the estimated OP block AGB (based on block age using AMP1) to the *in-situ* block RCS. Several studies attempt to define the relationship between OP age and *in-situ* RCS. Tan *et al*. (2013) find this relationship to be stronger, although still weak, using the HH polarisation (R^2 = 0.49) when compared to the HV (R^2 = 0.27) using ALOS PALSAR-1 RCS for palms 1 to 25 years after planting on a mineral soil. Again, Darmawan et al (2016) find a stronger relationship when using the HH polarisation (R^2 = 0.63, 2 to 21 years after planting (see Appendices 4). Here, horizontal transmit/vertical receive (HV) is used as the RCS is typically most sensitive to increases in AGB in this polarisation (Yu and Saatchi, 2016, CEOS, 2018). After the

biomass matching routine, AGB accumulation is detected for young mature and mature age classes (YAP 4 to 10) relatively successfully (Figure 4.13). However, the AGB of successful mature plots; with minimal palm leaning and replacement, appears underestimated due to a reduced sensitivity of the radar cross section to increases in AGB at the high end of the aboveground biomass range (Figure 4.12, Figure 4.13, Figure 4.14). It must also be noted that the routine appears to successfully adjust gain and offset coefficients to take into account differences between the ALOS-1 and ALOS-2 satellites when estimating AGB, which exist despite efforts to minimise these differences in the image pre-processing steps (JAXA, 2019b, Mitchard *et al.* 2011).

The AGB of oil palms less than 3 YAP is poorly predicted (Figure 4.12). The 'biomass matching' routine is not calibrated to the AGB of palms less than 3 YAP, this is in part due to AMP1 yielding negative biomass values for palms less than 3 YAP but also due to the low woody biomass volume of the palms within this age range (Chapter 3, Corley and Tinker, 2016, Corley *et al.* 1971, Thenkabail *et al.* 2004). As a result, the young oil palms are likely not the dominant feature contributing to scattering at this point in the timeseries as double-bounce and volume scattering from newly planted young OPs is potentially low (Alemohammad *et al.* 2019). Scattering of the L-band SAR could be dominated by SAR interactions with the ground surface with particular sensitivity to soil moisture in the recently drained peatlands (Izumi *et al.* 2019, Ponnurangam and Rao, 2011, Morel *et al.* 2011, Dargie *et al.* 2017). Across the drained peatland water table depth is likely to fluctuate spatially and temporally (Hooijer *et al.* 2012). SAR Interactions with large piles of coarse woody debris remaining on the site floor following forest clearance may also contribute to the return signal.

Here, the relationship between AGB and the radar cross section was calibrated using AMP1 to increase the number of observations across the plantation. However, the variability in AGB stocks and OP structural characteristics observed within age classes at the site was high, as is typical for oil palms on peat (Othman *et al.* 2009, Dolmat *et al.* 1995). This suggests that calibrating the AGB/RCS relationship using direct *in-situ* observations, as observed in the majority of studies that attempt to map AGB stocks using L-band SAR, may be a more robust approach (Mitchard *et al.* 2011, Morel *et al.* 2011, Ryan *et al.* 2012, Hamdan *et al.* 2015). However, using an accumulation model may be more appropriate for a more structurally consistent plantation monoculture, for example oil palm on mineral soils. The advantage of using an accumulation model to calibrate this relationship is that the model can then be used to validate the results of the 'biomass matching' output (Figure 4.13). The biomass matching approach reduces the dependency of calibration on field plots across the timeseries with obvious advantages (Picard *et al.* 2012, Chave *et al.* 2005, Kho and Jepsen, 2015). However, the true *in-situ*

aboveground biomass of pixels or blocks is not known and hence output accuracy cannot be determined (Hill *et al.* 2013). Comparing the AGBD output map for each scene to the expected AGB as estimated by the accumulation model provides some indication of the success of the routine (assuming the model is a good representation of oil palm AGB accumulation).

Validation of peat swamp forest AGB estimates

The AGB stocks of the peat swamp forest fragment were similar to those reported in the literature for degraded or logged PSFs (Morel *et al.* 2011). The AGB of 92.5 Mg ha^{-1} in the 1-ha plot is low, however the majority of the large trees, which typically constitute around 50% of primary forest AGB (largest 1% DBH within a plot), had been removed (Lutz *et al.* 2018). The AGBD maps produced in this study appear to accurately quantify this AGB stock, with pre-conversion AGB estimated to be ~104.2 ± 19.2 Mg ha^{-1}, however, the AGB/RCS relationship for peat swamp forest land cover was not defined. Generic relationships should not be applied across forest biomes owing to their structural differences, so perceived success when predicting PSF AGB stocks here should be considered with great caution (Woodhouse *et al.* 2012, Brolly and Woodhouse, 2012, Brolly and Woodhouse, 2014, Dobson *et al.* 1996).

4.4.3) In this study, when does the relationship between increasing AGB and increasing RCS saturate?

The 'saturation' or loss of sensitivity to increases in AGB in high biomass plantations and forests remains poorly understood and is commonly attributed to increasing forest canopy opacity (Woodhouse, 2006). However, radar backscatter is increasingly being thought of as a measure of structural trends in forest volume that are correlated with biomass in different ways and further research into the dependency of the aboveground volume/RCS relationship on forest and plantation structure is recommended in a number of studies (Brolly and Woodhouse, 2011, Joshi *et al.* 2017).

Saturation in oil palm plantations

In 'successful' plots where AGB stocks are high, OP stems were typically upright and consistent (Chapter 3), and in these blocks the sensitivity of RCS and AGB seems to have saturated at ~AGB > 45 Mg ha^{-1}. Oil palms have a single growing apex; lateral growth occurs until ~4 years after planting after which the trunk grows vertically with no change in trunk diameter until frond bases are shed approximately 12 YAP (Rees and Tinker, 1963, Henson *et al.* 2012). Oil palm fronds are produced at a rate of ~18-24 per palm per year from 4 YAP onwards and are pruned according to pruning and harvesting cycles. Frond length is limited by the OP planting density, and as a result the volume of the palm crown remains constant (de Berchoux *et al.* 1986, Henson and Dolmat, 2003).

Several empirical and theoretical studies have linked increasing basal area to an increased RSC with eventual saturation as stems and branches become larger when using low frequency radar sensors (L-band and P-band) (Joshi *et al*., 2017, Brolly and Woodhouse, 2012, Brolly and Woodhouse, 2014). However, in successful plots, basal area remains constant in monoculture OP plantations from 4 YAP onwards, with increases in trunk height associated with trunk biomass gain (Rees and Tinker, 1963). Multiple studies report a reduction in RCS with increasing stand height for various woody land cover types including oil palm plantations (Joshi *et al.* 2017, Joshi *et al.* 2015, Mermoz *et al.* 2015, Dobson *et al.* 1992, Rosenvist *et al.* 1996). The crown of forest and plantation species is typically associated with radar volume scattering (Woodhouse, 2006). Increases in crown related parameters such as LAI and frond length were found to correlate more strongly with RCS for oil palm than trunk height or biomass (Rosenvist *et al.* 1996). However, the crown canopy remains constant in volume once the canopy has closed (Rosenvist *et al.* 1996). The dense canopy of oil palm fronds in mature plantations may prevent signal penetration below the top of the canopy even at the L-band (CEOS, 2018). Multiple interacting factors may therefore contribute to this saturation, with further complication added for oil palms on peat in plots where palm leaning and falling is high. Studies have applied airborne LiDAR to predict AGB increases with more success, however this is a more costly route (Nunes *et al.* 2017). Further testing of the relationship between the RCS and OP structure across the planting cycle would be valuable.

Saturation in peat swamp forests

The *in-situ* relationship between peat swamp forest RCS and AGB was not defined and hence the true point of saturation cannot be determined. Both Englhart et al (2011) and Morel et al (2011) attempt to define the relationship between tropical peat swamp forest AGB and RCS (ALOS PALSAR-1 and TerraSAR-X, X-band radar), however both studies define a single relationship that includes PSF alongside multiple regional land cover and types. By exploring the relationship between GLAS LiDAR derived AGB estimates and the ALOS PALSAR global mosaic product, sensitivity of ALOS PALSAR to swamp forest biomass saturated at ~40 Mg ha^{-1} (Yu and Saatchi, 2016). Swamp forests and other partially or fully waterlogged forest types showed a strong scattering component from the vegetation-surface specular reflection due to inundation (Yu and Saatchi, 2016, Dargie *et al.* 2017, Draper *et al.* 2014).

4.4.4) How accurate are existing maps of aboveground biomass density at the study sites and how do these maps compare to each other?

AGB Benchmark maps

Existing aboveground biomass density maps are highly divergent across the study scene extent despite using largely the same input datasets and similar processing chains (Baccini *et al.* 2012, Saatchi *et al.* 2011). This divergence has been attributed to a number of differences, including parameters used in allometric equations, GLAS LiDAR processing methodologies and the datasets used to extrapolate estimates of AGBD (Mitchard *et al.* 2013, Avitabile *et al.* 2016). Neither map is truly a single date product due to mixed input layers, so these maps are potentially capturing the area at different stages of forest degradation (Mitchard *et al.* 2013). Avitabile et al (2016) fuse the AGBD maps and although the product date cannot be defined, the map appears to capture the scene extent pre-oil palm expansion with very few pixels in the OP AGB range at the study site or across the scene extent (Chapter 3, Henson *et al.* 2005). The map could therefore feasibly be used as a benchmark map from which to monitor the changes in AGB associated with OP establishment on peat and mineral soil in the study area and associated emissions from AGB stock changes. However, the divergence observed between two input maps suggest care would be required when interpreting results and associated uncertainties (Mitchard *et al.* 2013, Hill *et al.* 2013).

AGB Change maps

Baccini et al (2017) attempted to quantify biomass losses and gains at annual increments across the pan-tropics between 2003 and 2014 by using the Baccini et al (2012) benchmark map and extending the timeseries of optical datasets used. The resultant losses and gains in AGB across the study scene extent appear to match the spatial extent of changes detected through the biomass matching routine in some locations, however the magnitude of AGB stock change cannot be compared (Supplementary Figure S4.5). Despite this, Hansen et al (2019) found that 43% of estimated carbon losses detected for Southeast Asia were not co-located with Landsat-derived maps of tree cover loss and 72% of the loss-dominant cells in these tree cover maps were not associated with AGB carbon losses in the Baccini maps. In addition to other issues, Hansen et al (2019) attribute this to the tenuous relationship between passive optical reflectance and changes in forest carbon. Given the current rate and scale of oil palm expansion in addition to other land cover changes in the region, current maps of AGB stocks are required at a fine (at least annual) temporal resolution (Gaveau *et al.* 2016, Miettinen *et al.* 2019).

4.4.5) Applications and further research

In line with critiques of existing pantropical AGBD benchmark maps, this study found existing AGBD maps to be highly divergent in the study region (Mitchard *et al.* 2013). With an increased focus on reliable land cover classification the 'biomass matching' approach and ALOS PALSAR-1/2 GMP could inform ongoing efforts to accurately map plantation extent and establishment at a high spatial and temporal resolution (annual), supporting efforts to monitor the success of OP plantations certified as sustainable and track illegal plantation establishment and expansion (Carlson *et al.* 2018, Ivancic and Koh, 2016, Miettinen *et al.* 2019). The temporal resolution of change detection could also be improved by using the ALOS PALSAR-1/2 Level 1.1/1.5 product which features ~3 annual observations (JAXA, 2009, JAXA, 2019). Despite a more demanding pre-processing chain for the user and the reduced accessibility of ALOS PALSAR-2 scenes this would also potentially further improve the reliability of detected changes (Hill *et al.* in prep, ESA, 2016, JAXA, 2009). The accurate prediction of young mature oil palm AGB on peat is promising, however the mechanism causing the saturation of the RCS/AGB relationship as oil palms mature needs to be further explored. This would potentially include extending the timeseries of SAR scenes used here to confirm the saturation of the AGB/RCS relationship and the inclusion of older oil palm blocks. Further evaluation of the relationship between palm stand structural metrics (such as LAI and frond length) and *in-situ* RCS would also be very valuable (Rosenvist *et al.* 1996, Joshi *et al.* 2015). Establishing the relationship between peat swamp forest AGB stocks and the RCS (σ_{HV}^{0}) and incorporating this into 'biomass matching' calibration steps would potentially improve and update current AGBD timeseries maps and supporting efforts to reduce emissions from deforestation and degradation.

4.5 Conclusion

Prior to plantation establishment, the aboveground biomass stocks of the degraded peat swamp forest at our study site were felled and left to decompose. The deforestation that precedes OP plantation establishment is easily detectable when using the ALOS PALSAR-1/2 GMP in the HV polarisation and the 'biomass matching' approach. This is most likely due to the structural differences between peat swamp forest and oil palm wood biomass and the land cover types remain distinguishable across the timeseries of OP growth. ALOS PALSAR-1/2 SAR data should increasingly be used to inform efforts to monitor plantation establishment. 'Biomass matching' is an automated approach that can detect this specific land cover change using an accessible remotely sensed dataset.

However, in order to accurately predict peat OP AGB accumulation, further research into the saturation of RCS sensitivity to increases in AGB in high AGB ranges is needed. This would involve assessing the relationship between OP structural traits and the radar cross

section, research that could initially be conducted in OP plantations on mineral soils. Further investigation using the ‘biomass matching’ approach and the ALOS PALSAR-1/2 GMP in the HH polarisation and ALOS PALSAR-1/2 Level 1.1 product as input datasets may also be valuable. For OP on peat increasing our understanding of the relationship between water table depth and the SAR return immediately following conversion is also advised.

In this study, the success of prediction of PSF biomass cannot be determined, further work to determine the PSF aboveground biomass/RCS relationship is needed. However, the biomass maps produced here offer some improvements on existing AGBD maps in the study area as they more accurately capture low AGB densities which show stark disagreement and pre-date OP expansion and degradation in the region.

Chapter 5: Synthesis and Conclusions

The recent rapid expansion of OP plantations across tropical peatlands has resulted in net ecosystem emissions. In contrast to plantations on mineral soils, the AGB stocks of oil palm plantations on peat and their accumulation over time is rarely addressed in the literature. Here, the accumulation of above ground biomass stocks in a peat OP plantation is quantified and methods to improve AGB stock monitoring at various scales are developed.

In this study, the temporary AGB stocks of successful plantation plots 12 years after planting is similar to the AGB stocks of the highly degraded peat swamp forest the plantations replaced. However, as expected, the annual increases in carbon stocks stored in oil palm AGB (3.07 ± 0.54 Mg C ha^{-1} yr^{-1}) far from offset emissions from peat oxidation even when considering the current conservative IPCC emission factors (15 Mg C ha^{-1} yr^{-1}, [95% CI, 10 to 21]).

The ALOS PALSAR-1/2 global mosaic dataset is free with scenes available from 2007 to present. This allows the observation of the recent OP expansion across tropical peatlands in the study region, unhindered by tropical cloud cover. Testing a novel 'biomass matching' approach, this study aimed to use this L-band SAR product, combined with information derived from plot inventories, to monitor AGB stocks at the study sites. Reliably quantifying annual increases in peat OP AGB stocks across the plantations in is not yet possible using this approach. However, the automated detection of statistically significant increases and decreases in AGB observed here is extremely promising.

Limitations and further research

The aboveground biomass estimates in this study focus on a single oil palm plantation on peat. The representativeness of this plantation compared to other OP plantations on peat across Insular South East Asia (ISEA) must therefore be investigated. The planting density at the site is typical of peat OP plantations. The Sebungan Oil Palm Estate is well managed and high yielding, however, this varies across the Sebungan and Sabaju Estates (see section 2.2). Differences in plantation management, planting density and peat characteristics across ISEA will result in variations in AGB stocks, future studies would ideally compare multiple sites.

The allometric relationships defined here focus on a small sample at a single plantation. Further research is needed to test these allometric relationships and extend the timeseries further to incorporate palms between 12 and 20 years after planting. Following this study, the next steps to improve our understanding of these relationships should

include a variety of peat OP AGB stocks across the region in addition to eventually assessing the AGB stocks of second rotation plantations.

Using the 'biomass matching' approach involves making some potentially unrealistic assumptions about areas of unchanging AGB. Other factors aside from changes in living vegetation structure cause intra-scene variation in the RCS. For instance, changes in precipitation, standing water, soil and vegetation moisture characteristics. In addition to this, the AGB of all living vegetated systems changes over time, even if these changes are small relative to rapid growth or intense degradation.

Further investigation into relationship between OP structure and the in-situ RCS is required. Increasing our current understanding of the interactions between changes in OP structure over time and transitions between dominant scattering mechanisms in the L-band in both the HV and HH polarisation would be beneficial. These studies could be empirical or theoretical and could potentially explain the saturation of the AGB/RCS relationship for oil palm structures compared to surrounding forest systems.

Wider implications for stakeholders

This study presents methodologies for assessing oil palm and frond biomass stocks specifically developed for oil palm on peat, this will hopefully allow plantation managers to accurately quantify and monitor the AGB stocks of oil palms and plantation residues. This may encourage the utilization of a proportion of biomass residues (for instance pruned fronds) in bioenergy production on site and for neighbouring oil mills and communities. Empty fresh fruit bunches are often already utilized for this purpose.

Oil palm mortality as a result of poor palm anchorage and leaning limits plantation fresh fruit bunch production in addition to impacts on biomass stocks. The impact of palm leaning on peat is acknowledged but rarely quantified, this study begins to evaluate the impact of palm leaning and failure on biomass stocks and carbon storage in mature plantations. Hopefully, this will support existing and prompt further efforts to improve our understanding of the mechanisms behind the peat oil palm leaning issue and the development of preventative strategies in existing and second cycle plantations. This will be beneficial not for carbon stocks but also for FFB yield in existing peat OP plantations. For the RSPO the insights into mapping peat OP expansion and growth gained here may inform attempts to detect current and historical deforestation in certified plantations. The enforcement of the sustainable practices will hopefully improve consumer faith in existing OP products certified as sustainable.

The quantifications of AGB stocks presented here, when coupled with extensive ongoing research focused on micro and ecosystem scale fluxes of carbon at the same site will

eventually provide a full lifecycle assessment of the carbon emissions from oil palm on peat. This will inform IPCC land use change emission factors. In addition, the accurate quantification of emissions from this land use change will help to inform the valuing of carbon credit schemes like REDD+ with implications for landowners.

With some development the biomass mapping approaches presented here will improve our ability to detect changes in OP plantation extent and provide an indication of plantation age and planting cycle over a large area. This study highlights the potentially large carbon stock stored in successful mature OP plantations on peat, many of which are nearing the end of their planting cycle. Estimates of future emissions from LUC must consider the eventual clearance of mature peat OP plantations when determining our ability to meet UNFCCC emissions targets.

For the scientific community, this study highlights the potential of new techniques for quantifying changes in biomass stocks using L-band radar. Despite limitations in this ecological context, the 'Biomass Matching' approach may allow the quantification of small-scale increases and decreases in AGB stocks over time in other woody land cover types. Despite the obvious value of course resolution tropical maps of AGBD, this study highlights the limitations of these map products and it is suggested that for some applications they are used with caution.

Appendices 1:

Chapter 2 - Supplementary Material

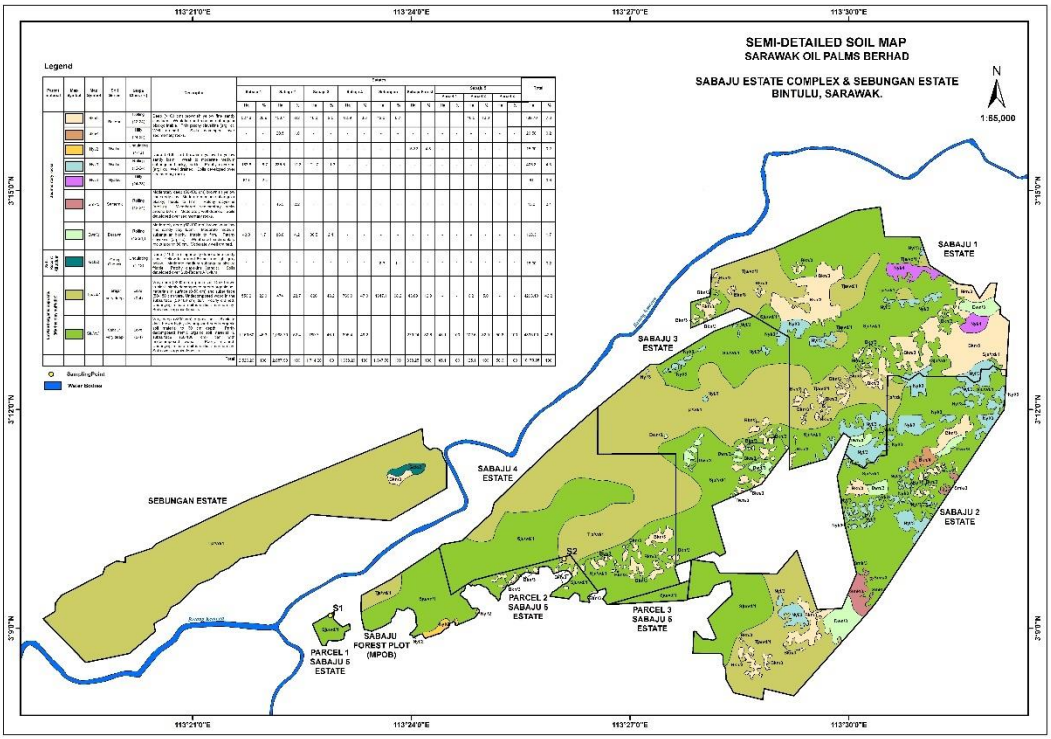

Figure S2.1: *Semi-detailed soil map for the Sabaju Estate Complex and Sebungan Estate, Sarawak Oil Palms Berhard (SOP) (SOP, personal communication, 2017).*

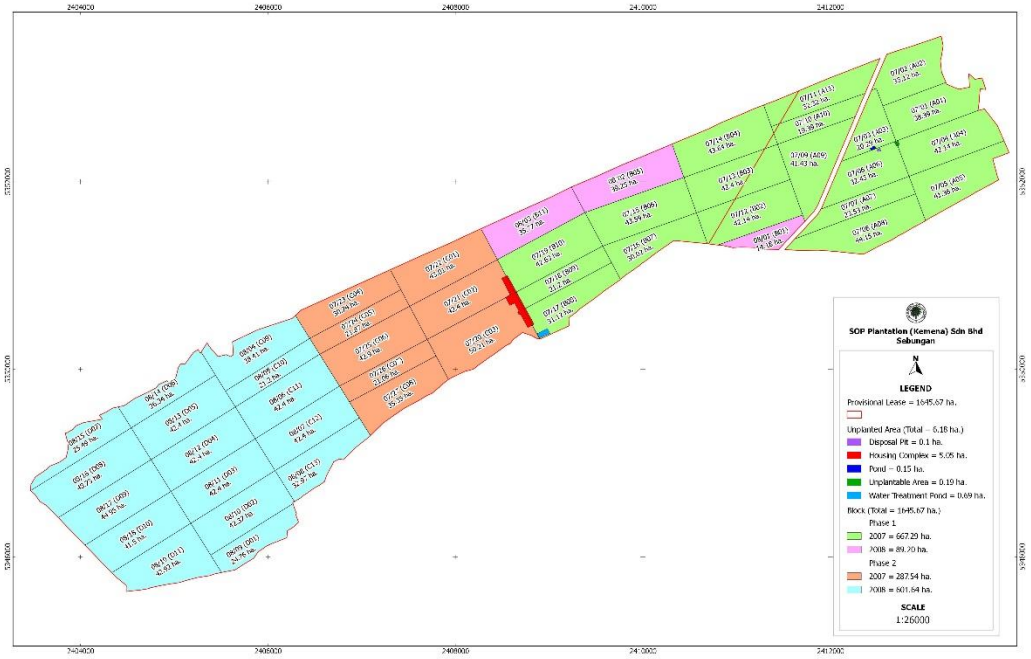

Figure S2.2: *Sarawak Oil Palms Berhard (SOP) planting blocking map for the Sebungan Oil Palm Plantation (SOP, personal communication, 2017).*

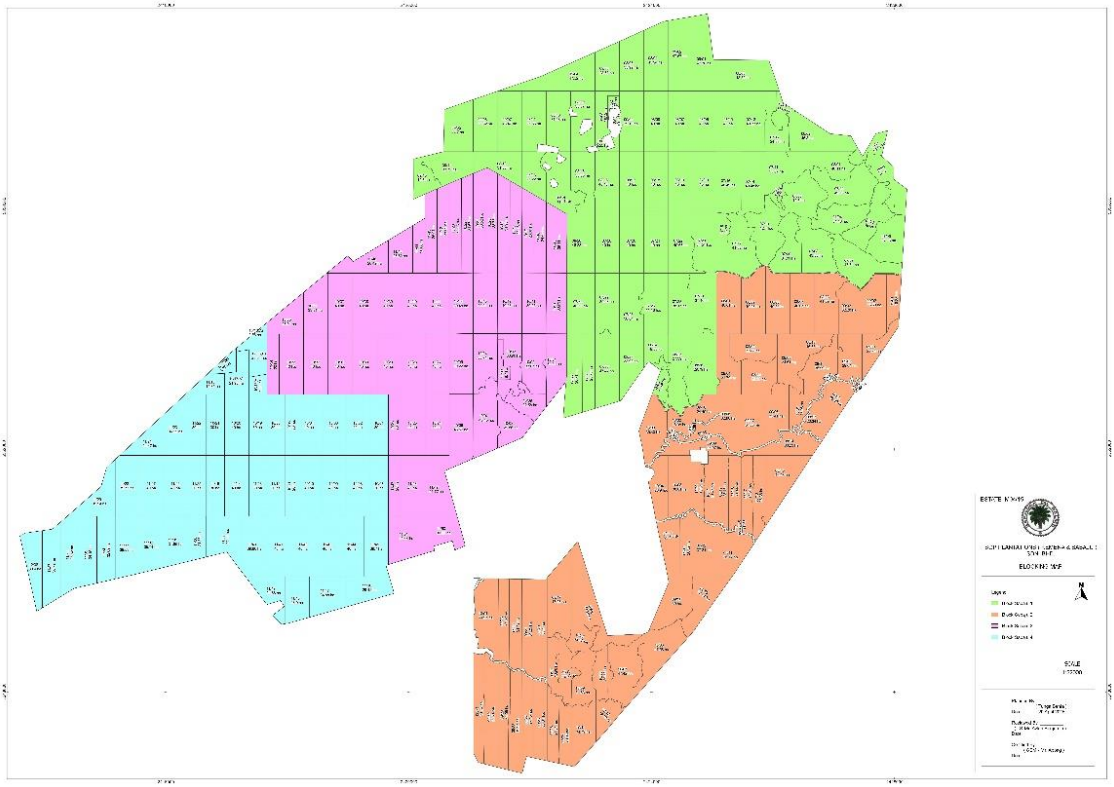

Figure S2.3: *Sarawak Oil Palms Berhard (SOP) planting blocking map for the Sabaju Oil Palm Estate (SOP, personal communication, 2017).*

Appendices 2:

Chapter 3 - Supplementary Material

Table S3.1: Oil palm plot AGB per hectare.

Source	Method	Location/Region	Planting Density	Soil	Note
Henson and Dolmat (2003)[10]	ND	Peninsular Malaysia	160	Peat	
Melling et al (2007)[57]	ND	Sarawak, Malaysia	-	Peat	
Breure (1982)[58]	ND	Papua New Guinea	-	Mineral	
Breure (1988)[59]	ND	Papua New Guinea	-	Mineral	
Dufrene (1989)[60]	ND	Ivory Coast	-	Mineral	
Henson (unpublished, 1993-95)[40]	ND	Selangor, Malaysia	-	Mineral	
Kwan (1994)[41]	ND	Sabah, Malaysia	143	Mineral	
Henson (1995)[61]	ND	Selangor, Malaysia	-	Mineral	
Lamade and Setiyo (1996)[62]	ND	Sumatra, Indonesia	-	Mineral	
Henson (1998)[63]	ND	Selangor, Malaysia	-	Mineral	
Palm et al (1999)[64]	ND	Cameroon	-	Mineral	
Tjitrosemito and Mawardi (2000)[65]	ND	Indonesia			
Banabas (2002)[66]	ND	Papua New Guinea	130	Mineral	
Henson (2007)[67]	ND	Kedah, Malaysia	-	Mineral	
Morel et al (2011)[44]	ND	Sabah, Malaysia	-	Mineral	
Rees and Tinker (1963)[26]	D	Nigeria	-		Destructive harvest: 7 to 22 YAP, 3 repetitions per age class
Ng et al. (1968)[68]	D	Peninsular Malaysia	-	Mineral	
Corley et al (1971)[11]	D	Peninsular Malaysia	148	Mineral	Destructive harvest: 1.5 to 27.5 YAP, 38repetitions per age class
Khalid et al. (1999)[12,13]	D	Peninsular Malaysia	-	Mineral	Destructive harvest: 23 YAP, 10 repetitions
Thenkabail et al. (2004)[46]	D	Benin	-	Mineral	Destructive harvest: Trunk heights of 0.28 to

					1.95 m, 7 palms samples (YAP unknown)
Syahrinudin (2005)[30]	D	Sumatra, Indonesia	-	Mineral	Destructive harvest: 3 to 33 YAP, 3 repetitions per age class
Legros et al. (2006)[69]	D	East Kalimantan, Indonesia	-	Mineral	
Koh et al. (2019)[70]	D, ND	Sarawak, Malaysia	-	Mineral	Destructive harvest: 21 YAP, 10 repetitions

Source material for Figure 6. Outline of studies assessing OP aboveground biomass stocks on mineral soils and peat soils using destructive (D) and non-destructive (ND) methods, planting densities included where possible.

Table S3.2: Characteristics oil palms destructively harvested

Sample No	YAP	No of Fronds	Trunk DBH (m) *	Trunk Length (m)**	Lean Category***
1	12	49	0.50	4.53	M
2	12	40	0.48	3.60	U
3	12	35	0.50	3.70	U
4	8	40	0.69	1.62	U
5	8	34	0.63	1.13	U
6	8	40	0.64	1.45	U
7	3	35	0.45	0.23	-
8	3	38	0.27	0.22	-
9	3	41	0.37	0.18	-

** Trunk DBH measured at breast height (1.30m) using callipers to exclude frond bases, trunk diameter was measured at the trunk midpoint where trunk heights were < 1.3m.*

*** Trunk length was measured to the frond ranked 33 (L33). Where palms were leaning, the trunk length along the inner curve of the palm trunk was recorded.*

**** Leaning categories: M = Mildly leaning, U = Upright.*

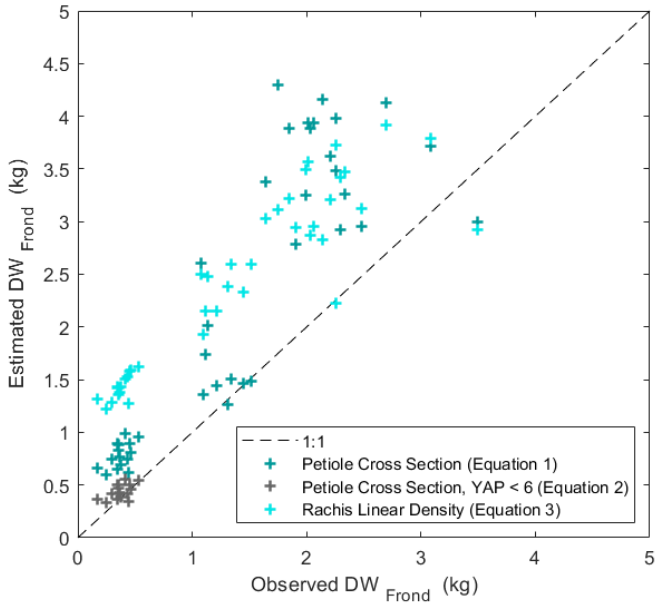

Figure S3.1: Frond DW predicted using existing equations vs observed *frond DW (1:1 line indicated). The equations tested use the petiole cross section (Equation1, Corley et al, 1971[11] and Equation 2, Henson, 1993[10]) and the rachis linear density (Equation 3, Aholoukpè et al, 2013[43]) to estimate the DW of a single frond.*

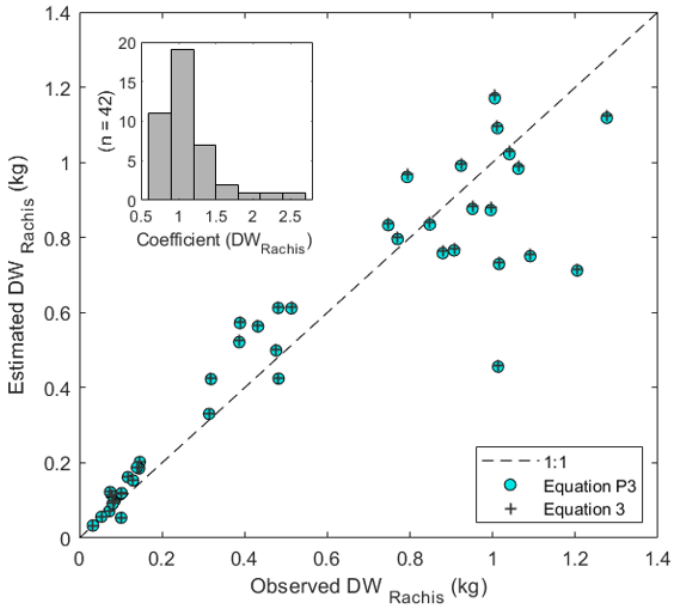

Figure S3.2: Rachis dry weight (DW_{Rachis}) is estimated from the dry linear density of a rachis fragment. *Rachis DW predicted using an existing equation (Equation 3) and an equation derived for peat (Equation P3) are plotted against the observed rachis DW (1:1 line indicated). The distribution of coefficients accounting for the non-constant sectional area of the rachis for each frond are shown (Equation P3, top left).*

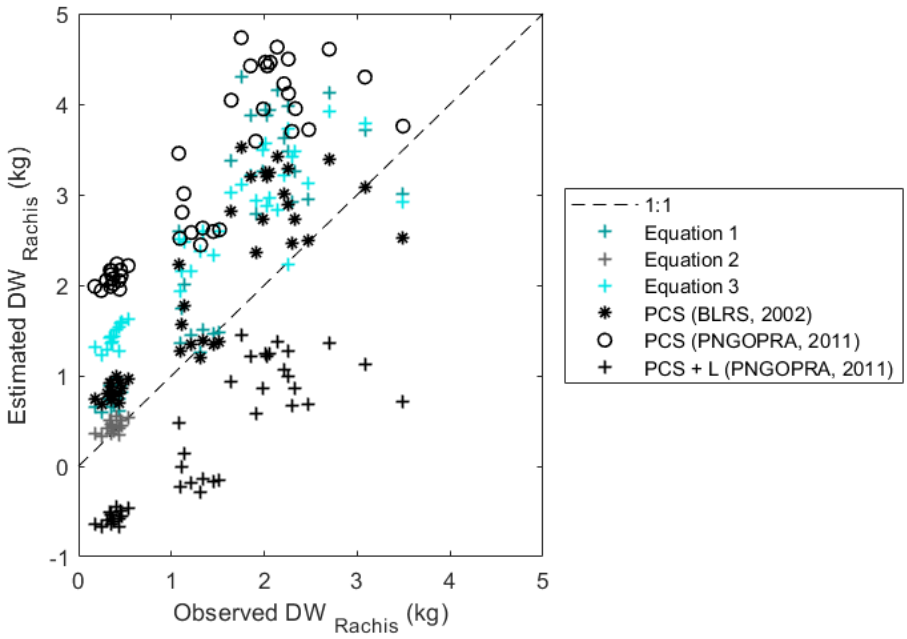

Figure S3.3: Frond DW predicted using existing equations vs the observed frond DW (1:1 line indicated). *Equations tested use the petiole cross section (PCS) and the petiole cross section when combined with frond length (PCS + L) to estimate the DW of a single frond. Allometries recorded in Corley and Tinker, 2016[71,72].*

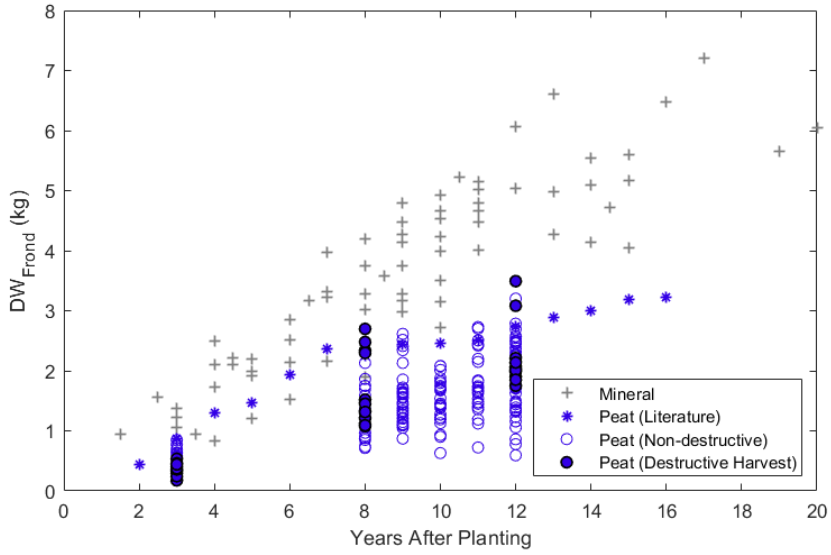

Figure S3.4: Single frond dry weights on mineral and peat soils. *Dry weight of fronds sampled in the non-destructive plot survey (Peat (Non-destructive)) are calculated using Equation P1, destructively harvested fronds are also included. Adapted from Henson 2005[29], including fronds on peat soils (Henson and Dolmat, 2003).*

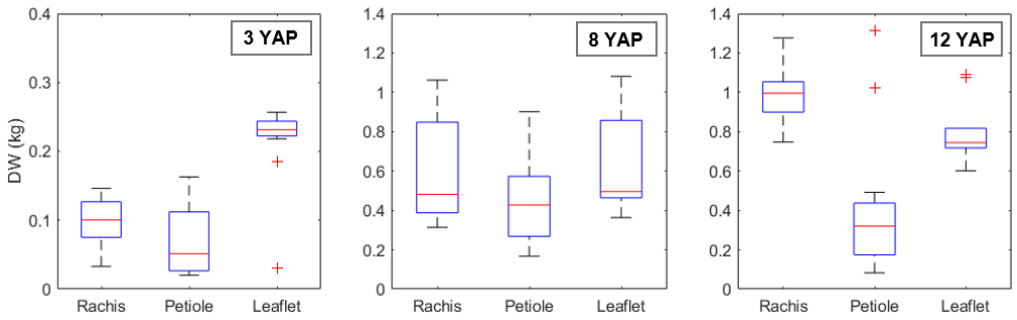

Figure S3.5: Frond component dry weight distribution in immature, young-mature and mature palms. Frond component dry with distribution of single fronds ranked 1, 9,17, 25 and 33 (rachis, petiole and leaflet) in immature (3 YAP), young-mature (8 YAP) and mature (12 YAP) palms. Outliers indicated in red.

No	Component	Equation	Reference	Note
S1	Palm DW	$DW_{Palm} = (0.0976 \times T_{Height} + 0.0706) \times 1000$	Dewi et al, 2009[47]	~0.5 > T_{height} > 9 (m) Derived from semi-destructive methods (R^2 = 0.7342) Location: Indonesia
S2	Palm DW	$DW_{Palm} = 37.47T_{Height} + 3.6334$	Thenkabail et al, 2004[46]	N = 8 0.28 > T_{height} > 1.95 (m) Location: Benin

Table S3.3: Existing allometric equations for estimating total oil palm dry weight (kg). *Where DW_{Palm} is palm dry weight and T_{Height} is trunk height to frond 33 (m).*

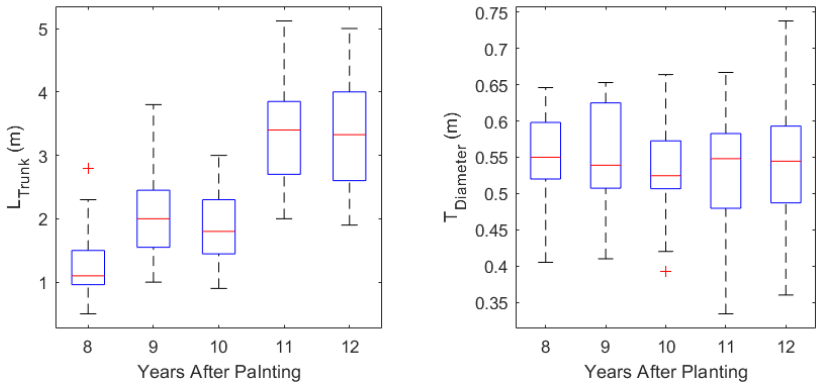

Figure S3.6: Trunk length (left) and DBH (right) (m) as measured in non-destructive surveys. *Data pooled for all plots of the same age. Outliers indicated in red.*

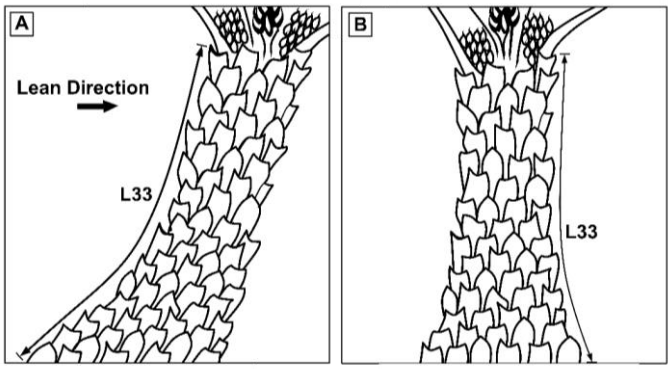

Figure S3.7: Oil palm leaning and length measurement*. Diagram A shows a mildly leaning palm mature palm, Diagram B an upright palm. Trunk length (L33) is measured along the inner curve of the trunk parallel to the lean direction in mildly leaning palms.*

Table S3.4: Categorisation of Oil Palm Leaning on Tropical Peats

Leaning Category	
Upright	Upright
Mild	Leaning at < 45^{o} from the vertical
Severe	Leaning at > 45^{o} from the vertical
Recovered	Leaning palms returning upright state
Fallen (Alive)	Fallen live palm (parallel to the peat), partially rooted
Fallen (Dead)	Fallen dead palm (parallel to the peat), uprooted
Replanted	Immature palm, notably younger than the block age (refill palm following palm mortality)
Missing	Missing palm in planting grid

Table S3.5: Plot locations, Sarawak, Malaysia.

Plot Id	Lat (N)	Long (E)	YAP	Measurement
1	3.1773	113.3729	12	D, ND
2	3.1744	113.3697	12	D, ND
3	3.1705	113.3711	12	D, ND
4	3.1640	113.4187	8	D, ND
5	3.1622	113.4180	8	D, ND
6	3.1628	113.4162	8	D, ND
7	3.1609	113.4207	3	D, ND
8	3.1594	113.4207	3	D, ND
9	3.1604	113.4179	3	D, ND
10	3.1658	113.3524	9	ND
11	3.1884	113.4631	9	ND
12	3.1879	113.4612	9	ND
13	3.1846	113.4593	9	ND
14	3.2333	113.4792	10	ND
15	3.2328	113.4803	10	ND
16	3.2267	113.4723	10	ND
17	3.2267	113.5069	11	ND
18	3.2121	113.5007	11	ND
19	3.2142	113.5035	12	ND
20	3.1559	113.3360	11	ND
21	3.1524	113.3277	11	ND
22	3.1661	113.3467	12	ND

Table S3.5: Plot locations, Sarawak, Malaysia. *Coordinates of OPs destructively harvested (D) and non-destructive plot surveys (ND), decimal degrees. Years after planting (YAP) at the time of measurement recorded (February 2019).*

Supplementary References

57) Melling L., Goh K.J., Beauvais C. & Hatano R. Carbon flow and budget in a young mature oil palm agroecosystem on deep tropical peat. In: Proc. Conf. International Symposium and Workshop on Tropical Peatland. International Peat Society, Yogyakarta, Indonesia, (2007).
58) Breure, C.J. Factors affecting yield and growth of oil palm tenera in West New Britain. *Oleagineux*, **37**, 213-227 (1982).
59) Breure, C.J. The effect of palm age and planting density on the partitioning of assimilates in oil palm (Elaeis guineensis). Exp. Agric. **24**, 53-66 (1988).
60) Dufrene E. (1989). Photosynthese, consommation en eau et modelisation de la production chez le palmier a huile (Elaeis guineensis Jacq.). (Universite Paris-Sud Orsay, 1989).
61) Henson, I.E. Carbon assimilation, water use and energy balance of an oil palm plantation assessed using micrometeorological techniques. In: Proc. Conf. 1993 PORIM International Palm Oil Congress. Palm Oil Research Institute of Malaysia, Kuala Lumpur (1995).
62) Lamade E and Setiyo I E. (1996). Test of Dufrene's production model on two contrasting families of oil palm in North Sumatra In: Proc. Conf. 1996 PORIM International Palm Oil Congress, Agricultural Conference. Palm Oil Research Institute of Malaysia, Kuala Lumpur (1996).
63) Henson I. E. Notes on oil palm productivity. I. Productivity at two contrasting sites. *J. Oil Palm Res.* **10**, 57-67 (1998).
64) Palm, C.A. et al. Carbon sequestration and trace gas emissions in slash-and-burn and alternative land uses in the Humid Tropics. (ACB Climate Change Working Group, Final Report Phase II, 1999).
65) Tjitrosemito, S. & Mawardi, I. Terrestrial carbon stock of oil palm plantation. In: Proc. Conf. Science and Policy Workshop on Terrestrial Carbon and Possible Trading under the CDM. IC-SEA, BIOTROP, Bogor, Indonesia, 2000.
66) Banabas, M. Agronomy Field Trial 305, Final Report. PNGOPRA, Papua New Guinea, 2002.
67) Henson I.E., Zuraidah, Y., Mohd Roslan, M.N., Mohd Haniff, H. & Tarmizi, A.M. Predicting soil water status, evapotranspiration, growth and yield of oil palm in a seasonally dry region of Malaysia. *J. Oil. Palm. Res.* **19**, 398-415 (2007).
68) Ng S. K., Thamboo, S. & de Souza, P. Nutrient contents of oil palms in Malaya. II. Nutrients in vegetative tissues. Malay. Agric. **46**, 332-390 (1968).
69) Legros, S. et al. (2006). Carbohydrate reserves in 9 years old oil palm: nature, distribution and seasonal changes. In: Proc. Conf. 2006 International Oil Palm Conference, Bali, 2006.
70) Koh, L.K., Rumpang, E., Kamarudin, N. and Haryn. M.H. Quantifying total carbon stock of mature oil palm. *J. Oil. Palm. Res.* **31**, 521-527 (2019).
71) PNGOPRA. *2011 Annual Research Report.* (Papua New Guinea Oil Palm Research Association, Kimbe, Papua New Guinea, 2011).
72) BLRS. *Annual Research report, 2001*. (Bah Lias Research Station, North Sumatra, 2002).

Appendices 3:

Chapter 4 - Supplementary Material

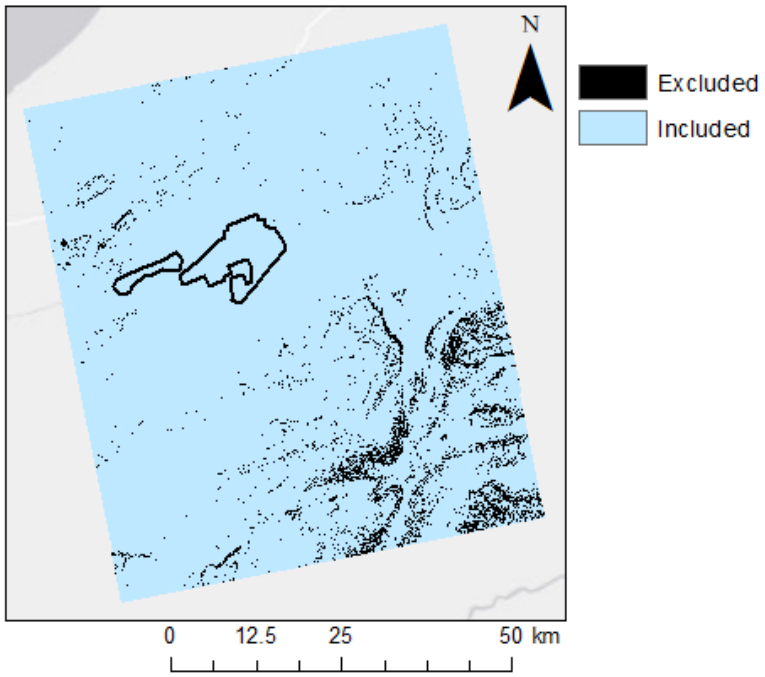

Figure S4.1: Areas included an excluded from 'biomass matching' and AGB estimation. *Exclusion based on a slope > 20˚ calculated using the SRTM DEM (30m resolution). Sebungan and Sabaju oil palm plantations indicated in black.*

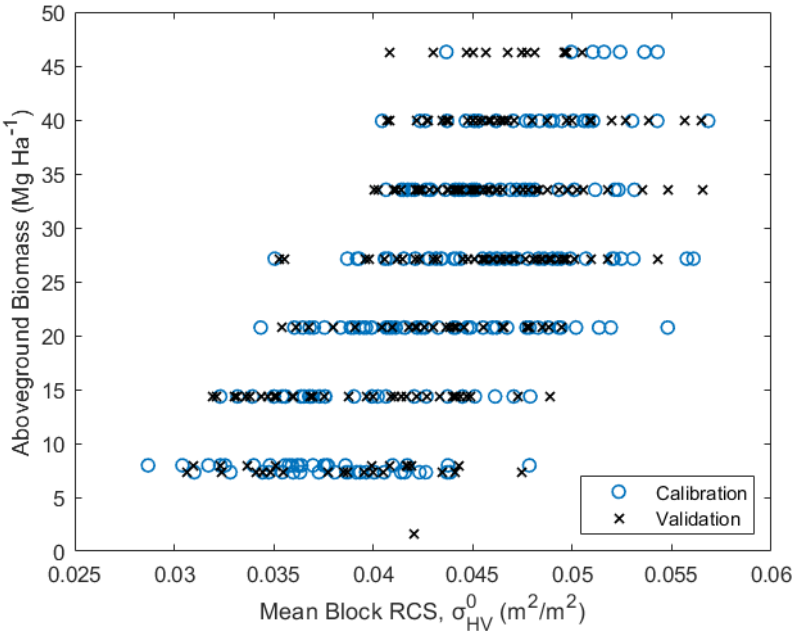

Figure S4.2: RMA Regression of ALOS PALSAR-2 radar cross section and modelled AGB for oil palm 'calibration blocks' and 'validation blocks'.

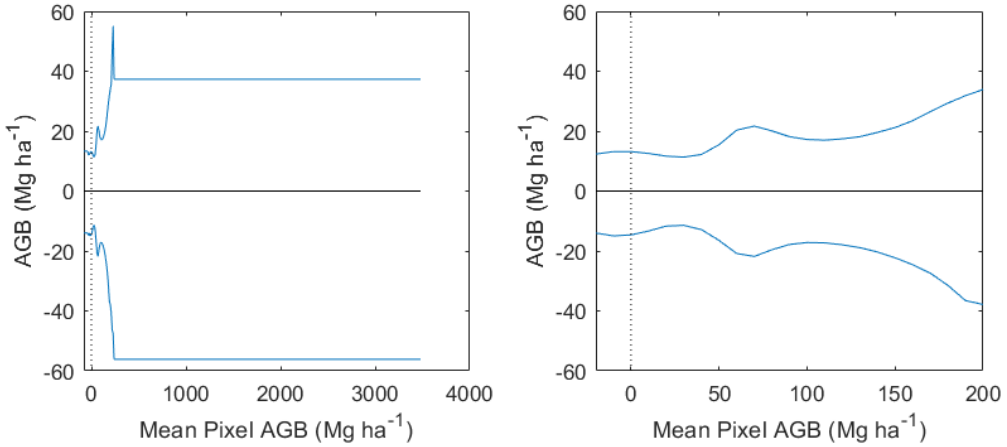

Figure S4.3: Final pixel AGB uncertainty. *Mean pixel AGB of all pixels (left) and pixels with an AGB < 200 Mg ha-1 (right) against estimated pixel AGB uncertainty after the final iteration*

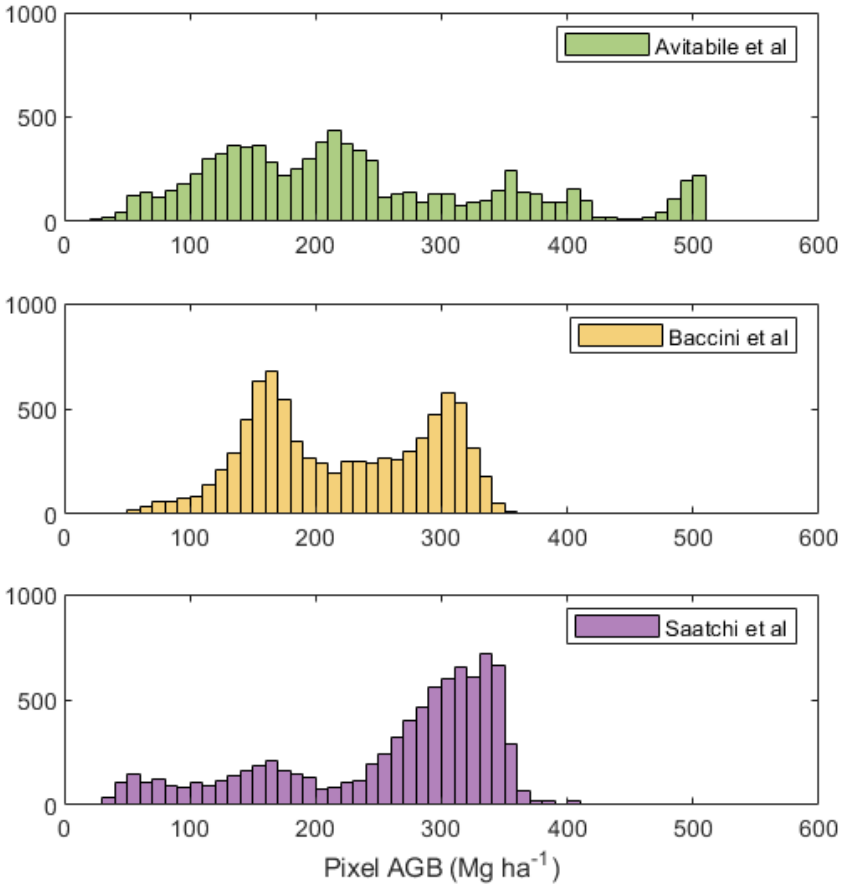

Figure S4.4: Distribution of pixel AGB estimates across the study scene *for the Avitabile (top), Baccini (middle) and Saatchi (bottom) Pantropical AGBD maps (1 km resolution).*

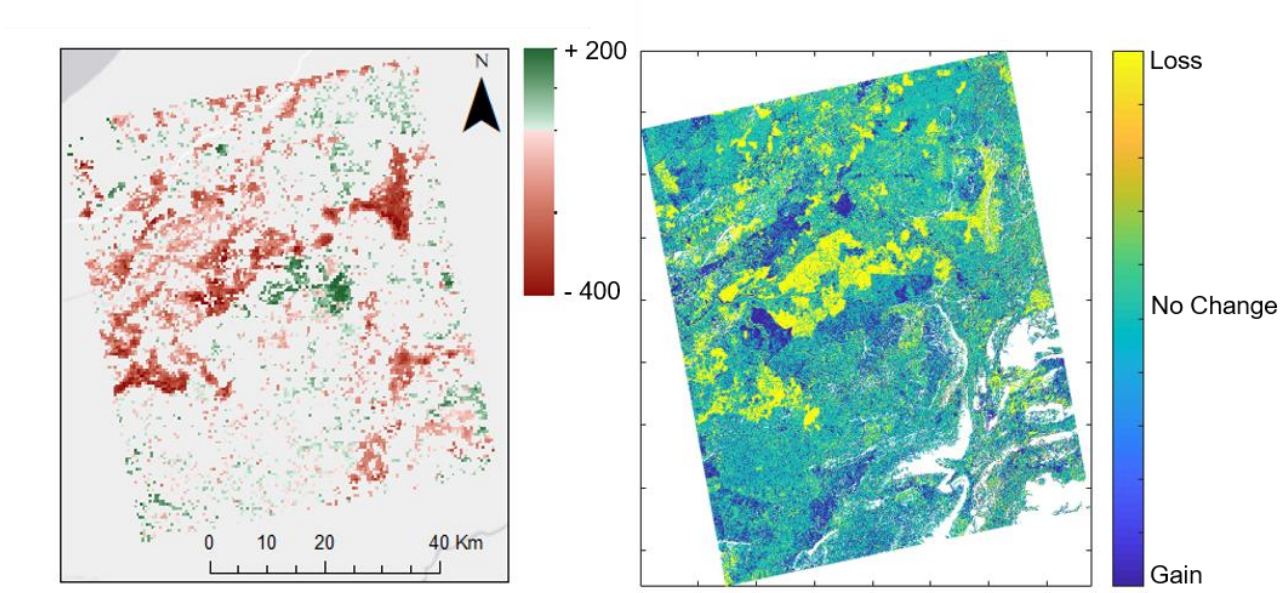

Figure S4.5: Aboveground biomass loss and gain (MgC ha-1) between 2003 and 2014 at the study site, *taken from Baccini et al, 2017 (Left). Detected AGB losses and gains, final 'Biomass Matching' iteration – this study (Right).*

Supplementary Table S4.1: Aboveground biomass estimation using radar datasets (spaceborne SAR products only)

Source	Location	Vegetation Type	Condition	Annual rainfall	Extent	Period (Single*) (Timeseries**)	Product	Band (Polarisation)	Calibration dataset	Model Saturtion
Englhart et al, 2011	Central Kalimantan, Indonesian Borneo	Tropical Peat swamp forest, Heath, Riparian forest and seasonally flooded wetlands	Heavily degraded following recurrent fire episodes	~2000 to 3000 mm	280,062 ha	May 2007 to October 2008 (Dry season only)*	ALOS PALSAR-1	L-Band	140 forest plots in various forest types and disturbance levels LiDAR measurement producing a continual spatial dataset (3970 points)	126 Mg Ha^{-1}
						2008 and 2009 (Dry season only)*	TerraSAR-X	X-Band (VV)		80 Mg Ha^{-1}
								Combined L- and X-Bands		307 Mg Ha^{-1}
Mitchard et al, 2011	Central Africa	Tropical forest – Savanah transition	Protected national park and settlement	~1720 mm	1,500,000 ha	July – August 2007 (Dry season only)	ALOS PALSAR-1	L-band (HH and HV)	4 1-ha Savanna plots, 4 1-ha forest plots, a 0.4-ha transitional plot ha and 8 20 × 200 m transects	150–200 Mg Ha^{-1}
						November – March 1996 (Dry season only)**	JERS-1	L-Band (HH)		-
Morel et al, 2011	Sabah, Malaysian Borneo	Tropical Lowland Forest, Peat swamp	Secondary tropical lowland forest types	~2000 to 3000 mm	330,000 ha	September – October 2008 (Dry season only)*	ALOS PALSAR-1	L-Band (HV)	127 ha of plot inventories distributed throughout	100 Mg Ha^{-1}

		forest, Oil Plantation and Timber Plantation	and Plantations						Sabah in various forest types and disturbance levels	
Ryan et al, 2012	Central Mozambique	Miombo woodland, Scattered Savanah	Deforested and degraded (Small scale agriculture and charcoal production)	~900 mm year	116,000 ha	June 2007 – October 2010**	ALOS PALSAR-1	L-Band (HV)	96 Inventory plots (0.1 to 2.2 ha)	-
Atwood et al, 2014	Tanana Valley, Alaska	Boreal Forest	Stand structure and composition largely determined by past wildfires – majority burned in the past 25 years			January 2006 and May 2011* (Dry season – post snowmelt)	ALOS PALSAR	L-band (HV)	79 field plots have been measured and 27 coincident lidar flight lines	-
Baghdadi et al, 2015	São Paulo, Brazil	Eucalyptus plantation	0 to 7 years after planting (planting to harvest)	-	-	August 2009*	ALOS PALSAR-1	L-Band (HV)	695 Eucalyptus stands	50 Mg Ha^{-1}
Hamdan, 2015	Peninsular Malaysia	Tropical Hill Dipterocarp Forest and Lowland Dipterocarp Forest (Well drained)	Reserve Forest and National Parks		5,257,395 ha	May to December 2010*	ALOS PALSAR-1	L-Band (HV)	352 30*30m sample plots (2011 and 2012)	200 Mg Ha^{-1}
Joshi et al, 2015	Denmark,	Species trial plots (even age), Conifer	Species trial plots (even age), Conifer		-	October/November 2007 *	ALOS PALSAR-1	L-Band (HV)	113 plots of an area of 0.07 ha to 0.23 ha	130 Mg Ha^{-1}

		and Broadleaf	and Broadleaf						Airborne LiDAR scans	
Omar et al, 2017	Peninsular Malaysia	Tropical Hill Dipterocarp Forest and Lowland Dipterocarp Forest (Well drained)	Reserve Forest and National Parks	-	5,257,395 ha	March to June 2016*	ALOS PALSAR-2	L-Band (HV)	332 Sample Nests (20m Radius)	200 Mg Ha^{-1}
						November 2016*	Sentinel-1A	C-Band (VV, VH)		100 Mg Ha^{-1}

Table S4.2: **Global 25m Resolution PALSAR-2/PALSAR Mosaic product tiles acquired**

Tile ID	Satellite	Scene Date	Incidence Angle	Polarisation	Orbit (pass)
N03E113_07	ALOS-1	22-Jun-2007	34.3˚	HV	Ascending
N04E113_07	ALOS-1	22-Jun-2007	34.3˚	HV	Ascending
N03E113_08	ALOS-1	09-May-2008	34.3˚	HV	Ascending
N04E113_08	ALOS-1	09-May-2008	34.3˚	HV	Ascending
N03E113_09	ALOS-1	27-Jun-2009	34.3˚	HV	Ascending
N04E113_09	ALOS-1	27-Jun-2009	34.3˚	HV	Ascending
N03E113_10	ALOS-1	15-Aug-2010	34.3˚	HV	Ascending
N04E113_10	ALOS-1	15-Aug-2010	34.3˚	HV	Ascending
N03E113_15	ALOS-2	10-Sep-2015	36.7˚	HV	Ascending
N04E113_15	ALOS-2	10-Sep-2015	36.7˚	HV	Ascending
N03E113_16	ALOS-2	28-Jan-2016	36.6˚	HV	Ascending
N04E113_16	ALOS-2	28-Jan-2016	36.6˚	HV	Ascending
N03E113_17	ALOS-2	07-Sep-2017	36.6˚	HV	Ascending
N04E113_17	ALOS-2	07-Sep-2017	36.6˚	HV	Ascending

ALOS GMP tile ID and observation characteristics, scene dates correspond the observation date of the track matching the study site scene extent, tiles with the same observation dates are merged. The SRTM3 (2007-2010) and SRTM1 (2015-) DEMs are used by JAXA to terrain correct scenes (JAXA, 2017).

Table S4.3: Landsat-5 scenes used to inform OP planting block digitisation

Tile ID	Satellite	Scene Date
LT05_L1TP_119058_20060614_20161121_01_T1	Landsat-5 (TM)	14-Jun-2006
LT05_L1TP_119058_20070329_20161116_01_T1	Landsat-5 (TM)	29-Mar-2007
LT05_L1TP_119058_20070703_20161113_01_T1	Landsat-5 (TM)	03-Jul-2007
LT05_L1TP_119058_20070804_20161111_01_T1	Landsat-5 (TM)	04-Aug-2007
LT05_L1TP_119058_20080502_20161101_01_T1	Landsat-5 (TM)	02-May-2008
LT05_L1TP_119058_20081228_20170111_01_T1	Landsat-5 (TM)	28-Dec-2008
LT05_L1TP_119058_20090318_20161027_01_T1	Landsat-5 (TM)	18-Mar-2009
LT05_L1TP_119058_20090419_20161026_01_T1	Landsat-5 (TM)	19-Apr-2009
LT05_L1TP_119058_20090809_20161022_01_T1	Landsat-5 (TM)	09-Aug-2009
LT05_L1TP_119058_20100812_20161014_01_T1	Landsat-5 (TM)	12-Aug-2010
LT05_L1TP_119058_20110815_20161007_01_T1	Landsat-5 (TM)	15-Aug-2011

The majority of the visual analysis of Landsat images was undertaken using visible and near infrared bands (RGB composite: Band 3: Visible (0.63 - 0.69 µm), Band 4: Near-Infrared (0.76 - 0.90 µm), Band 5: Near-Infrared (1.55 - 1.75 µm)).

Table S4.4: Wood density sources (Peat Swamp Forest)

Source No	Reference
1	Oey Djoen Seng. 1951. in Soewarsono, P.H. (1990) Specific gravity of Indonesian Woods and Its Significance for Practical Use FRPDC Forestry Department, Bogor, Indonesia.
2	Ginoga, B., Hadjib, N. and Karnasudirdja, S. (1980) Sifat Fisis dan Mekanis beberapa Jenis Kayu. Indonesia Bagian, Laporan BPHH No. 153.
4	Lemmens, R.H.M.J., Soerjanegara, I. and Wong, W.C. (1995) PROSEA 5: Timber trees: Minor commercial timbers, Backhuys Publishers, The Netherlands
5	Desch, H.E. 1996. Timber: structure, properties, conversion and use. 7th Edition. Palgrave Macmillan, New York.
7	Desch, H.E. 1996. Timber: structure, properties, conversion and use. 7th Edition. Palgrave Macmillan, New York.
8	World Agroforestry, 'Tree functional attributes and ecological database – wood density'. Website Accessed: 9th December 2019: http://db.worldagroforestry.org//wd

Sources for wood densities used to estimate the AGB of logged peat swamp forest (PSF) at the Sabaju Estate. Census data from a 1 ha permanent plot in the logged secondary PSF identified all trees with a DBH > 10 cm (20 families, 33 species) (Koh 2019, pers. comm, 25 February). Wood density data was obtained from various sources (1-8) and allometric equations (Chave et al, 2005) where used to estimate AGB.

Appendices 4:

Chapter 4 - Oil Palm age/RCS (σ^0_{HH})

ALOS PALSAR-2 GMP scenes in the HH horizontal transmit/horizontal receive (HH) polarisation where also acquired for 2015, 2016 and 2017 (10-Sep-2015, 28-Jan-2016, 07-Sep-2017). Following acquisition, the pre-processing steps in outlined Section 4.2.1. were undertaken to convert the DN to the RCS (σ^0_{HH}). The mean RCS of each oil palm block was then extracted for both the HV and HH polarisation and compared to the block age at the time of observation (Appendix Figure S4.6). The relationship between block age and the in-situ mean RCS was stronger in the HH polarisation (R^2 = 0.514) when compared to the HV (R^2 = 0.345).

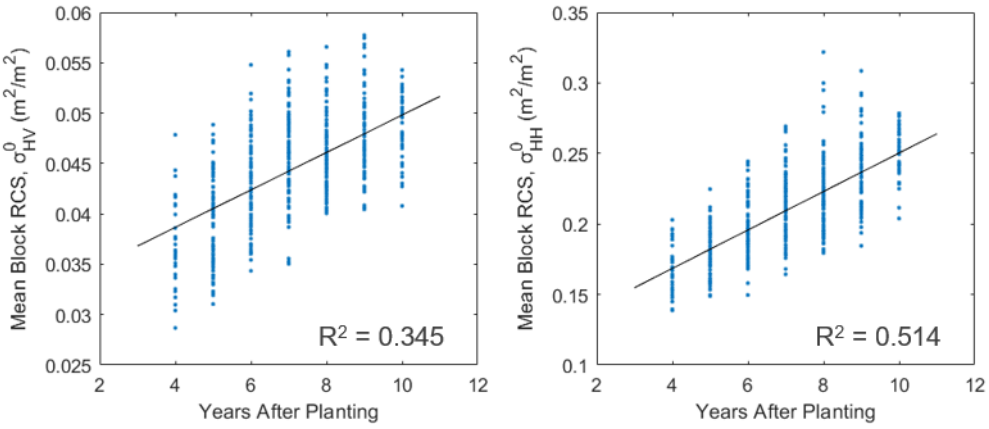

Figure S4.6: Mean block RCS σ^0 in the HV (left) and HH (right) polarisations between 4 to 10 years after planting (ALOS-2). *A chronosequence approach is used, mean block RCS is plotted against the years before/after planting at the time of observation. Linear regression models and R^2 values indicated.*

Bibliography

Abnisa, F., Arami-Niya, A., Daud, W.W., Sahu, J.N. and Noor, I.M. (2013) Utilization of oil palm tree residues to produce bio-oil and bio-char via pyrolysis. *Energy conversion and management*, *76*: 1073-1082.

Abram, N.K., MacMillan, D.C., Xofis, P., Ancrenaz, M., Tzanopoulos, J., Ong, R., Goossens, B., Koh, L.P., Del Valle, C., Peter, L. and Morel, A.C. (2016) Identifying where REDD+ financially out-competes oil palm in floodplain landscapes using a fine-scale approach. *PloS one*, *11*(6): 156481.

Aholoukpe, H., Dubos, B., Flori, A., Deleporte, P., Amadji, G., Chotte, J.L. and Blavet, D. (2013) Estimating aboveground biomass of oil palm: allometric equations for estimating frond biomass. *Forest Ecology and Management*, *292*: 122-129.

Alemohammad, S.H., Jagdhuber, T., Moghaddam, M. and Entekhabi, D., 2019. Soil and Vegetation Scattering Contributions in L-Band and P-Band Polarimetric SAR Observations. *IEEE Transactions on Geoscience and Remote Sensing*, *57*(11): 8417-8429.

Anaya, J.A., Chuvieco, E. and Palacios-Orueta, A. (2009) Aboveground biomass assessment in Colombia: A remote sensing approach. *Forest Ecology and Management*, *257*: 1237-1246.

Angelsen, A., Brown, S. and Loisel, C., (2009). *Reducing emissions from deforestation and forest degradation (REDD): an options assessment report*. Meridian Institute, Washington.

Arneth, A., Sitch, S., Pongratz, J., Stocker, B.D., Ciais, P., Poulter, B., Bayer, A.D., Bondeau, A., Calle, L., Chini, L.P. and Gasser, T. (2017) Historical carbon dioxide emissions caused by land-use changes are possibly larger than assumed. *Nature Geoscience*, *10*(2): 79-84.

ASF (2019). MapReady User Manual, Alaska Satellite Facility, Fairbanks, Alaska.

Atwood, D.K., Andersen, H.E., Matthiss, B. and Holecz, F. (2014). Impact of topographic correction on estimation of aboveground boreal biomass using multi-temporal, L-band backscatter. *IEEE Journal of Selected Topics in Applied Earth Observations and Remote Sensing*, *7*: 3262-3273.

Austin, K.G., Mosnier, A., Pirker, J., McCallum, I., Fritz, S. and Kasibhatla, P.S. (2017) Shifting patterns of oil palm driven deforestation in Indonesia and implications for zero-deforestation commitments. *Land use policy*, *69*: 41-48.

Avitabile, V., Herold, M., Heuvelink, G.B., Lewis, S.L., Phillips, O.L., Asner, G.P., Armston, J., Ashton, P.S., Banin, L., Bayol, N. and Berry, N.J. (2016) An integrated pan-tropical biomass map using multiple reference datasets. *Global change biology*, *22*(4): 1406-1420.

Baccini, A., Walker, W., Carvalho, L., Farina, M., Sulla-Menashe, D. and Houghton, R.A. (2017). Tropical forests are a net carbon source based on aboveground measurements of gain and loss. *Science*, *358*: 230-234.

Baccini, A.G.S.J., Goetz, S.J., Walker, W.S., Laporte, N.T., Sun, M., Sulla-Menashe, D., Hackler, J., Beck, P.S.A., Dubayah, R., Friedl, M.A. and Samanta, S. (2012) Estimated carbon dioxide emissions from tropical deforestation improved by carbon-density maps. *Nature climate change*, *2*(3): 182.

Baghdadi, N., Le Maire, G., Bailly, J.S., Osé, K., Nouvellon, Y., Zribi, M., Lemos, C. and Hakamada, R. (2014) Evaluation of ALOS/PALSAR L-Band Data for the Estimation of Eucalyptus Plantations Aboveground Biomass in Brazil. *IEEE Journal of Selected Topics in Applied Earth Observations and Remote Sensing*, *8*(8): 3802-3811.

Balenzano, A., Mattia, F., Satalino, G. and Davidson, M.W. (2010) Dense temporal series of C- and L-band SAR data for soil moisture retrieval over agricultural crops. *IEEE Journal of Selected Topics in Applied Earth Observations and Remote Sensing*, *4*: 439-450.

Ballhorn, U., Siegert, F., Mason, M. and Limin, S. (2009) Derivation of burn scar depths and estimation of carbon emissions with LIDAR in Indonesian peatlands. *Proceedings of the National Academy of Sciences*, *106*(50): 21213-21218.

Bereiter, B., Eggleston, S., Schmitt, J., Nehrbass-Ahles, C., Stocker, T.F., Fischer, H., Kipfstuhl, S. and Chappellaz, J. (2015) Revision of the EPICA Dome C CO2 record from 800 to 600 kyr before present. *Geophysical Research Letters*, *42*(2), pp.542-549.

Birdsey, R., Angeles-Perez, G., Kurz, W.A., Lister, A., Olguin, M., Pan, Y., Wayson, C., Wilson, B. and Johnson, K., 2013. Approaches to monitoring changes in carbon stocks for REDD+. *Carbon Management*, *4*(5): 519-537.

Brienen, R.J., Phillips, O.L., Feldpausch, T.R., Gloor, E., Baker, T.R., Lloyd, J., Lopez-Gonzalez, G., Monteagudo-Mendoza, A., Malhi, Y., Lewis, S.L. and Martinez, R.V. (2015) Long-term decline of the Amazon carbon sink. *Nature*, *519*: 344.

Brolly, M. & Woodhouse, I. (2014) Long wavelength SAR backscatter modelling trends as a consequence of the emergent properties of tree populations. *Remote Sensing*, *6*(8):7081-7109.

Brolly, M. and Woodhouse, I.H. (2012) A "Matchstick Model" of microwave backscatter from a forest. *Ecological modelling*, *237*: 74-87.

Brunig, E.F. & Klinge H. (1977) Comparison of the phytomass structure of equatorial 'rain-forest' in central Amazonas, Brazil, and in Sarawak, Borneo. *The Gardens' Bulletin Singapore* 29: 81–101.

Burrough, P. A., and McDonell, R. A., 1998. Principles of Geographical Information Systems (Oxford University Press, New York), 190 pp.

Busch, J., Ferretti-Gallon, K., Engelmann, J., Wright, M., Austin, K.G., Stolle, F., Turubanova, S., Potapov, P.V., Margono, B., Hansen, M.C. and Baccini, A., 2015. Reductions in emissions from deforestation from Indonesia's moratorium on new oil palm, timber, and logging concessions. *Proceedings of the National Academy of Sciences*, *112*(5): 1328-1333.

Butler, R.A., Koh, L.P. and Ghazoul, J. (2009) REDD in the red: palm oil could undermine carbon payment schemes. *Conservation letters*, *2*(2): 67-73.

Byerlee, D., Falcon, W.P. and Naylor, R., 2017. *The tropical oil crop revolution: food, feed, fuel, and forests*. Oxford University Press.

Carlson, K.M., Curran, L.M., Asner, G.P., Pittman, A.M., Trigg, S.N. and Adeney, J.M. (2013) Carbon emissions from forest conversion by Kalimantan oil palm plantations. *Nature Climate Change*, *3*(3): 283.

Carlson, K.M., Curran, L.M., Ratnasari, D., Pittman, A.M., Soares-Filho, B.S., Asner, G.P., Trigg, S.N., Gaveau, D.A., Lawrence, D. and Rodrigues, H.O. (2012) Committed carbon emissions, deforestation, and community land conversion from oil palm plantation expansion in West Kalimantan, Indonesia. *Proceedings of the National Academy of Sciences*, *109*(19): 7559-7564.

Carlson, K.M., Goodman, L.K. and May-Tobin, C.C. (2015) Modeling relationships between water table depth and peat soil carbon loss in Southeast Asian plantations. *Environmental Research Letters*, *10*(7): 074006.

Carlson, K.M., Heilmayr, R., Gibbs, H.K., Noojipady, P., Burns, D.N., Morton, D.C., Walker, N.F., Paoli, G.D. and Kremen, C. (2018). Effect of oil palm sustainability certification on deforestation and fire in Indonesia. *Proceedings of the National Academy of Sciences*, *115*: 121-126.

CEOS. (2018) *A Layman's Interpretation Guide to L-band and C-band Synthetic Aperture Radar data*, Committee on Earth Observation Satellites, California Institute of Technology, USA

Chave, J., Andalo, C., Brown, S., Cairns, M.A., Chambers, J.Q., Eamus, D., Fölster, H., Fromard, F., Higuchi, N., Kira, T. and Lescure, J.P. (2005) Tree allometry and

improved estimation of carbon stocks and balance in tropical forests. *Oecologia*, *145*: 87-99.

Cheng, Y., Yu, L., Cracknell, A.P. and Gong, P. (2016) Oil palm mapping using Landsat and PALSAR: A case study in Malaysia. *International journal of remote sensing*, *37*: 5431-5442.

Cheng, Y., Yu, L., Xu, Y., Lu, H., Cracknell, A.P., Kanniah, K. and Gong, P., (2018). Mapping oil palm extent in Malaysia using ALOS-2 PALSAR-2 data. *International Journal of Remote Sensing*, 39(2): 432-452

Cook, S., Whelan, M.J., Evans, C.D., Gauci, V., Peacock, M., Garnett, M.H., Kho, L.K., Teh, Y.A. and Page, S.E. (2018) Fluvial organic carbon fluxes from oil palm plantations on tropical peatland. *Biogeosciences*, *15*(24): 7435-7450.

Corley R H V, Gray, B. S. and Ng, S. K. (1971). Productivity of the oil palm (Elaeis guineensis Jacq.) in Malaysia. Experimental Agriculture, 7, 129-136.

Corley R.H.V. & Gray B.S. (1976) Yield and yield components in Oil palm research (ed. R.H.V. Corley, R.H.V, Hardon, J.J. & Wood, B.J.), pp. 77-86, Elsevier.

Corley, R.H.V. and Tinker, P.B., 2016. *The oil palm*. John Wiley & Sons.

Couwenberg, J., Dommain, R. and Joosten, H. (2010) Greenhouse gas fluxes from tropical peatlands in south-east Asia. *Global Change Biology*, *16*(6): 1715-1732.

Dabboor, M. and Brisco, B., 2018. Wetland monitoring and mapping using synthetic aperture radar. *Wetlands management: Assessing risk and sustainable solutions*, *IntechOpen* 13.

Dargie, G.C., Lewis, S.L., Lawson, I.T., Mitchard, E.T., Page, S.E., Bocko, Y.E. and Ifo, S.A. (2017) Age, extent and carbon storage of the central Congo Basin peatland complex. *Nature*, *542*: 86.

Darmawan, S., Takeuchi, W., Haryati, A., AM, R.N. and Na'aim, M., 2016, June. An investigation of age and yield of fresh fruit bunches of oil palm based on ALOS PALSAR 2. In *IOP Conference Series: Earth and Environmental Science* 37: 12037

de Berchoux, Ch., Jacquemard, J.C., Kouamé, M.B., Lecoustre, R., 1986. Morphologiede la croissance et du développement des différents organes du palmier à huileen plantation. In: Croissance et développement du palmier à huile. Institut deRecherche pour les Huiles et Oléagineux (IRHO), station principale de La Mé,Bingerville, pp. 226–366.

de Vries, S.C., van de Ven, G.W., van Ittersum, M.K. and Giller, K.E. (2010). Resource use efficiency and environmental performance of nine major biofuel crops, processed by first-generation conversion techniques. *Biomass and Bioenergy*, *34*(5): 588-601.

Den Besten, J.W., Arts, B. and Verkooijen, P. (2014) The evolution of REDD+: An analysis of discursive-institutional dynamics. *Environmental Science & Policy*, *35*: 40-48.

Dobson, M.C., Ulaby, F.T., LeToan, T., Beaudoin, A., Kasischke, E.S. and Christensen, N., (1992) Dependence of radar backscatter on coniferous forest biomass. *IEEE Transactions on Geoscience and remote Sensing*, *30*(2): 412-415.

Dolmat M., Hamdan A.B., Zulkifli H. & Ahmad Tarmizi M. (1996) Fertiliser requirement of oil palm on peat – an update. In: Proc. 1996 PORIM Int. Palm Oil Congr. Competitiveness for the 21st century (Ed. by D. Ariffin et al.), pp. 131-142, Palm Oil Research Institute of Malaysia, Kuala Lumpur

Draper, F.C., Roucoux, K.H., Lawson, I.T., Mitchard, E.T., Coronado, E.N.H., Lähteenoja, O., Montenegro, L.T., Sandoval, E.V., Zaráte, R. and Baker, T.R., 2014. The distribution and amount of carbon in the largest peatland complex in Amazonia. *Environmental Research Letters*, *9*(12): 124017.

Englhart, S., Keuck, V. and Siegert, F. (2011) Aboveground biomass retrieval in tropical forests—The potential of combined X-and L-band SAR data use. *Remote sensing of environment*, *115*(5): 1260-1271.

ESA. (2009), Synthetic Aperture Radar Synthetic Aperture Radar Land Applications Land Applications Tutorial, European Space Agency, Paris, France.
ESA. (2016), *ALOS PALSAR Orthorectification*, European Space Agency, Paris, France.
ESRI (2019) Aggregate, Accessed 06th December 2019, http://desktop.arcgis.com/en/arcmap/10.3/tools/spatial-analyst-toolbox/aggregate.htm.
FAO, (2019) FAOSTAT Food and Agriculture Data, Website Accessed 20th January 2019, http://www.fao.org/faostat/en/#home.
FAO, 2006, *Forests and Climate Change Working Paper 5: Definitional issues related to reducing emissions from deforestation in developing countries*, Food and Agriculture Organization of the United Nations, Rome.
Fisher, B., Edwards, D.P., Giam, X. and Wilcove, D.S., (2011) The high costs of conserving Southeast Asia's lowland rainforests. *Frontiers in Ecology and the Environment*, *9*(6): 329-334.
Friedman, J., Bohonak, A.J. and Levine, R.A., (2013). When are two pieces better than one: fitting and testing OLS and RMA regressions. Environmetrics, 24(5): 306-316.
Garrett, R.D., Carlson, K.M., Rueda, X. and Noojipady, P. (2016). Assessing the potential additionality of certification by the round table on responsible soybeans and the roundtable on sustainable palm oil. *Environmental Research Letters*, *11*(4): 045003.
Gatto, M., Wollni, M., Asnawi, R. and Qaim, M., 2017. Oil palm boom, contract farming, and rural economic development: Village-level evidence from Indonesia. *World Development*, *95*: 127-140.
Gaveau, D.L., Sheil, D., Salim, M.A., Arjasakusuma, S., Ancrenaz, M., Pacheco, P. and Meijaard, E., 2016. Rapid conversions and avoided deforestation: examining four decades of industrial plantation expansion in Borneo. *Scientific reports*, *6*: 32017.
Gaveau, D.L., Sloan, S., Molidena, E., Yaen, H., Sheil, D., Abram, N.K., Ancrenaz, M., Nasi, R., Quinones, M., Wielaard, N. and Meijaard, E. (2014). Four decades of forest persistence, clearance and logging on Borneo. *PloS one*, *9*(7), p.e101654.
Germer, J. & Sauerborn, J. (2008) Estimation of the impact of oil palm plantation establishment on greenhouse gas balance. *Environment, Development and Sustainability*, 10(6): 697-716.
GFW, 2019a, *Indonesian Peatlands*, Website accessed 24th December 2019, http://data.globalforestwatch.org/datasets/d52e0e67ad21401cbf3a2c002599cf58_10/data
GFW, 2019b, *Malaysian Peatlands*, Website accessed 24th December 2019, http://data.globalforestwatch.org/datasets/d52e0e67ad21401cbf3a2c002599cf58_10/data
Ghazoul, J., Burivalova, Z., Garcia-Ulloa, J. and King, L.A., (2015). Conceptualizing forest degradation. *Trends in ecology & evolution*, *30*(10): 622-632.
Gibbs, H.K., Brown, S., Niles, J.O. and Foley, J.A. (2007). Monitoring and estimating tropical forest carbon stocks: making REDD a reality. *Environmental Research Letters*, *2*(4), 45023.
Griscom, B.W., Adams, J., Ellis, P.W., Houghton, R.A., Lomax, G., Miteva, D.A., Schlesinger, W.H., Shoch, D., Siikamäki, J.V., Smith, P. and Woodbury, P., 2017. Natural climate solutions. *Proceedings of the National Academy of Sciences*, *114*: 11645-11650.
Gumbricht, T., Roman-Cuesta, R.M., Verchot, L., Herold, M., Wittmann, F., Householder, E., Herold, N. and Murdiyarso, D. (2017) An expert system model for mapping tropical wetlands and peatlands reveals South America as the largest contributor. *Global Change Biology*, *23*(9): 3581-3599.
Hamdan, O., Hasmadi, I.M., Aziz, H.K., Norizah, K. and Zulhaidi, M.H., 2015. L-band saturation level for aboveground biomass of dipterocarp forests in peninsular Malaysia. *Journal of Tropical Forest Science*: 388-399.

Hamzah, N., Tokimatsu, K. and Yoshikawa, K. (2019) Solid fuel from oil palm biomass residues and municipal solid waste by hydrothermal treatment for electrical power generation in Malaysia: a review. *Sustainability*, *11*(4): 1060.

Hansen, M.C. and Loveland, T.R. (2012) A review of large area monitoring of land cover change using Landsat data. *Remote sensing of Environment*, *122*: 66-74.

Hansen, M.C., Potapov, P. and Tyukavina, A. (2019). Comment on “Tropical forests are a net carbon source based on aboveground measurements of gain and loss”. *Science*, *363*(6423): 3629.

Hansen, M.C., Potapov, P.V., Moore, R., Hancher, M., Turubanova, S.A.A., Tyukavina, A., Thau, D., Stehman, S.V., Goetz, S.J., Loveland, T.R. and Kommareddy, A. (2013) High-resolution global maps of 21st-century forest cover change. *science*, *342*: 850-853.

Harper, A.B., Powell, T., Cox, P.M., House, J., Huntingford, C., Lenton, T.M., Sitch, S., Burke, E., Chadburn, S.E., Collins, W.J. and Comyn-Platt, E. (2018) Land-use emissions play a critical role in land-based mitigation for Paris climate targets. *Nature communications*, *9*: 2938.

Harper, W. V.(2014) Reduced major axis regression: Teaching alternatives to least squares. ICOTS9 Contributed Paper, Ohio, USA.

Hasnol, O., Darus, F. M. and Mohammed, A. T. (2009) Experiences in Peat Devalopment of Oil Palm Planting in the MPOB Research Station at Sessang, Sarawak. Oil Palm Bulletin 58: 1-13.

Henson, I.E. & Dolmat, M.T. (2003) Physiological analysis of an oil palm density trial on a peat soil. *Journal of Oil Palm Research*, 15

Henson, I.E., 2005, September. OPRODSIM, a versatile, mechanistic simulation model of oil palm dry matter production and yield. In Proceedings of PIPOC 2005 International Palm Oil Congress, Agriculture, Biotechnology and Sustainability Conference (pp. 801-832). Malaysian Palm Oil Board Kuala Lumpur.

Henson, I.E., Betitis, T., Tomda, Y. and Chase, L.D. (2012) The estimation of frond base biomass (FBB) of oil palm. *Journal of oil palm research*, *24*: 1473-1479.

Hergoualc'h, K. and Verchot, L.V., (2011). Stocks and fluxes of carbon associated with land use change in Southeast Asian tropical peatlands: A review. *Global Biogeochemical Cycles*, *25*(2).

Hess, L.L., Melack, J.M. and Simonett, D.S. (1990) Radar detection of flooding beneath the forest canopy: a review. *International Journal of Remote Sensing*, *11*(7): 1313-1325.

Hill, T.C., Williams, M., Bloom, A.A., Mitchard, E.T. and Ryan, C.M. (2013). Are inventory based and remotely sensed above-ground biomass estimates consistent?. *PLoS One*, *8*(9), p.e74170.

Hooijer, A., Page, S., Canadell, J.G., Silvius, M., Kwadijk, J., Wosten, H. and Jauhiainen, J. (2010). Current and future CO_2 emissions from drained peatlands in Southeast Asia. *Biogeosciences*.

Hooijer, A., Page, S., Jauhiainen, J., Lee, W.A., Lu, X.X., Idris, A. and Anshari, G. (2012) Subsidence and carbon loss in drained tropical peatlands. *Biogeosciences*, *9*(3): 1053-1071.

Houghton, R.A. (2005) Aboveground forest biomass and the global carbon balance. *Global Change Biology*, *11*(6): 945-958.

IPCC (2013) Climate Change 2013: The Physical Science Basis. Contribution of Working Group I to the Fifth Assessment Report of the Intergovernmental Panel on Climate Change [Stocker, T.F., D. Qin, G.-K. Plattner, M. Tignor, S.K. Allen, J. Boschung, A. Nauels, Y. Xia, V. Bex and P.M. Midgley (eds.)]. Cambridge University Press, Cambridge, United Kingdom and New York, NY, USA, 1535

IPCC (2014) 2013 Supplement to the 2006 IPCC Guidelines for National Greenhouse Gas Inventories: Wetlands ed T Hiraishi, T Krug, K Tanabe, N Srivastava, J Baasansuren, M Fukuda and T G Troxler. Intergovernmental Panel on Climate Change (IPCC), Switzerland.

IPCC (2018) Global Warming of 1.5°C. An IPCC Special Report on the impacts of global warming of 1.5°C above pre-industrial levels and related global greenhouse gas emission pathways, in the context of strengthening the global response to the threat of climate change, sustainable development, and efforts to eradicate poverty [Masson-Delmotte, V., P. Zhai, H.-O. Pörtner, D. Roberts, J. Skea, P.R. Shukla, A. Pirani, W. Moufouma-Okia, C. Péan, R. Pidcock, S. Connors, J.B.R. Matthews, Y. Chen, X. Zhou, M.I. Gomis, E. Lonnoy, T. Maycock, M. Tignor, and T. Waterfield (eds.)]. In Press.

Ipor, I.B., Tawan, C.S., Mustafa, H.F. (2006) Floristic structure and tree species composition. In Abang F, Das I (eds) *The Biodiversity of a Peat Swamp Forest in Sarawak*, 61–86. Institute of Biodiversity and Environmental Conservation, Sarawak.

Ivancic, H. and Koh, L.P. (2016). Evolution of sustainable palm oil policy in Southeast Asia. *Cogent Environmental Science*, *2*: 1195032.

Izumi, Y., Widodo, J., Kausarian, H., Demirci, S., Takahashi, A., Razi, P., Nasucha, M., Yang, H. and Tetuko SS, J. (2019) Potential of soil moisture retrieval for tropical peatlands in Indonesia using ALOS-2 L-band full-polarimetric SAR data. *International Journal of Remote Sensing*, *40*(15): 5938-5956.

Jauhiainen, J. and Silvennoinen, H. (2012) Diffusion GHG fluxes at tropical peatland drainage canal water surfaces. *Suo*, *63*(3-4): 93-105.

JAXA (1997) Polarimetric observation by PALSAR, Website accessed 04nd April 2020, https://www.eorc.jaxa.jp/ALOS/en/img_up/pal_polarization.htm

JAXA (2009) *ALOS/PALSAR Level 1.1/1.5 product Format description,* Japan Aerospace Exploration Agency, Tokyo.

JAXA (2017) *Global 25m Resolution PALSAR-2/PALSAR Mosaic and Forest/Non-Forest Map (FNF) Dataset Description,* Japan Aerospace Exploration Agency (JAXA), Tokyo.

JAXA (2019a) *ALOS Systematic Observation Strategy – PALSAR*, Website accessed 22nd December 2019, https://www.eorc.jaxa.jp/ALOS/en/obs/palsar_strat.htm

JAXA 2(019b) *Global PALSAR-2/PALSAR/JERS-1 Mosaic and Forest/Non-Forest map*, Website accessed 22nd December 2019, https://www.eorc.jaxa.jp/ALOS/en/palsar_fnf/fnf_index.htm

Joosten, H., Couwenberg.C., von Unger, M. & Emmer., I. (2016) *Peatlands, Forests and the Climate Architecture: Setting Incentives through Markets and Enhanced Accounting.* German Environment Agency, Greifswald, Germany.

Joshi, N., Mitchard, E., Schumacher, J., Johannsen, V., Saatchi, S. and Fensholt, R. (2015) L-band SAR backscatter related to forest cover, height and aboveground biomass at multiple spatial scales across Denmark. *Remote Sensing*, *7*(4): 4442-4472.

Joshi, N., Mitchard, E.T., Brolly, M., Schumacher, J., Fernández-Landa, A., Johannsen, V.K., Marchamalo, M. and Fensholt, R. (2017) Understanding 'saturation'of radar signals over forests. *Scientific reports*, *7*(1): 3505.

Joshi, N., Mitchard, E.T., Woo, N., Torres, J., Moll-Rocek, J., Ehammer, A., Collins, M., Jepsen, M.R. and Fensholt, R. (2015) Mapping dynamics of deforestation and forest degradation in tropical forests using radar satellite data. *Environmental Research Letters*, *10*(3): 034014.

Kho, L.K. and Jepsen, M.R. (2015). Carbon stock of oil palm plantations and tropical forests in M alaysia: A review. *Singapore Journal of Tropical Geography*, *36*(2): 249-266.

Koh, L.P. and Wilcove, D.S. (2008) Is oil palm agriculture really destroying tropical biodiversity?. *Conservation letters*, *1*(2): 60-64.

Koh, L.P., Miettinen, J., Liew, S.C. and Ghazoul, J. (2011). Remotely sensed evidence of tropical peatland conversion to oil palm. *Proceedings of the National Academy of Sciences*, *108*(12): 5127-5132.

Lauknes, T.R. (2011) Rockslide mapping in Norway by means of interferometric SAR time series analysis. PhD Thesis. University of Tromoso.

Lawson, I.T., Kelly, T.J., Aplin, P., Boom, A., Dargie, G., Draper, F.C.H., Hassan, P.N.Z.B.P., Hoyos-Santillan, J., Kaduk, J., Large, D. and Murphy, W. (2015) Improving estimates of tropical peatland area, carbon storage, and greenhouse gas fluxes. *Wetlands ecology and management*, *23*(3): 327-346.

Le Quéré, C., Andrew, R.M., Friedlingstein, P., Sitch, S., Pongratz, J., Manning, A.C., Korsbakken, J.I., Peters, G.P., Canadell, J.G., Jackson, R.B. and Boden, T.A. (2018) Global carbon budget 2017. *Earth System Science Data Discussions*, pp.1-79.

Lee, J.S., Grunes, M.R. and De Grandi, G. (1999) Polarimetric SAR speckle filtering and its implication for classification. *IEEE Transactions on Geoscience and remote sensing*, *37*(5): 2363-2373.

Leifeld, J. and Menichetti, L. (2018) The underappreciated potential of peatlands in global climate change mitigation strategies. *Nature communications*, *9*(1): 1071.

Liew, R.K., Nam, W.L., Chong, M.Y., Phang, X.Y., Su, M.H., Yek, P.N.Y., Ma, N.L., Cheng, C.K., Chong, C.T. and Lam, S.S. (2018) Oil palm waste: an abundant and promising feedstock for microwave pyrolysis conversion into good quality biochar with potential multi-applications. *Process Safety and Environmental Protection*, *115*: 57-69.

Lim, K.H., Lim, S.S, Parish. F. and Suharto, r. (eds) 2012. RSPO Manual on Best Management Practices (BMPs) for Existing Oil Palm Cultivation on Peat. RSPO, Kuala Lumpur.

Liu, J., Bowman, K.W., Schimel, D.S., Parazoo, N.C., Jiang, Z., Lee, M., Bloom, A.A., Wunch, D., Frankenberg, C., Sun, Y. and O'Dell, C.W., 2017. Contrasting carbon cycle responses of the tropical continents to the 2015–2016 El Niño. *Science*, *358*(6360): 5690.

Lüthi, D., Le Floch, M., Bereiter, B., Blunier, T., Barnola, J.M., Siegenthaler, U., Raynaud, D., Jouzel, J., Fischer, H., Kawamura, K. and Stocker, T.F. (2008) High-resolution carbon dioxide concentration record 650,000–800,000 years before present. *Nature*, *453*(7193): 379-382.

Lutz, J.A., Furniss, T.J., Johnson, D.J., Davies, S.J., Allen, D., Alonso, A., Anderson-Teixeira, K.J., Andrade, A., Baltzer, J., Becker, K.M. and Blomdahl, E.M. (2018) Global importance of large-diameter trees. *Global Ecology and Biogeography*, *27*(7): 849-864

Manning, F.C., Kho, L.K., Hill, T.C., Cornulier, T. and Teh, Y.A. (2019) Carbon emissions from oil palm plantations on peat soil. *Frontiers in Forests and Global Change*, *2*: 37.

Mermoz, S., Réjou-Méchain, M., Villard, L., Le Toan, T., Rossi, V. and Gourlet-Fleury, S. (2015) Decrease of L-band SAR backscatter with biomass of dense forests. *Remote Sensing of Environment*, *159*: 307-317.

Miettinen, J & Liew, S.C. (2009) Estimation of biomass distribution in Peninsular Malaysia and in the islands of Sumatra, Java and Borneo based on multi-resolution remote sensing land cover analysis. *Mitigation and Adaptation Strategies for Global Change* 14: 357–73.

Miettinen, J. & Liew, S.C. (2011) Separability of insular Southeast Asian woody plantation species in the 50 m resolution ALOS PALSAR mosaic product. *Remote Sensing Letters*, *2*: 299-307.

Miettinen, J., Gaveau, D.L. and Liew, S.C. (2019). Comparison of visual and automated oil palm mapping in Borneo. *International Journal of Remote Sensing*, *40*(21): 8174-8185.

Miettinen, J., Hooijer, A., Vernimmen, R., Liew, S.C. and Page, S.E. (2017). From carbon sink to carbon source: extensive peat oxidation in insular Southeast Asia since 1990. *Environmental Research Letters*, *12*(2): 024014.

Miettinen, J., Shi, C. and Liew, S.C. (2016). Land cover distribution in the peatlands of Peninsular Malaysia, Sumatra and Borneo in 2015 with changes since 1990. *Global Ecology and Conservation*, *6*: 67-78.

Miettinen, J., Shi, C., Tan, W.J. and Liew, S.C. (2012). 2010 land cover map of insular Southeast Asia in 250-m spatial resolution. *Remote Sensing Letters*, *3*: 11-20.

Milder, J.C., Arbuthnot, M., Blackman, A., Brooks, S.E., Giovannucci, D., Gross, L., Kennedy, E.T., Komives, K., Lambin, E.F., Lee, A. and Meyer, D. (2015) An agenda for assessing and improving conservation impacts of sustainability standards in tropical agriculture. *Conservation biology*, *29*: 309-320.

Mitchard, E.T., 2018. The tropical forest carbon cycle and climate change. *Nature*, *559*: 527-534

Mitchard, E.T., Feldpausch, T.R., Brienen, R.J., Lopez-Gonzalez, G., Monteagudo, A., Baker, T.R., Lewis, S.L., Lloyd, J., Quesada, C.A., Gloor, M. and Ter Steege, H. (2014) Markedly divergent estimates of Amazon forest carbon density from ground plots and satellites. *Global Ecology and Biogeography*, *23*(8): 935-946.

Mitchard, E.T., Saatchi, S.S., Baccini, A., Asner, G.P., Goetz, S.J., Harris, N.L. and Brown, S. (2013). Uncertainty in the spatial distribution of tropical forest biomass: a comparison of pan-tropical maps. *Carbon balance and management*, *8*(1): 10.

Mitchard, E.T., Saatchi, S.S., Lewis, S.L., Feldpausch, T.R., Woodhouse, I.H., Sonké, B., Rowland, C. and Meir, P (2011). Measuring biomass changes due to woody encroachment and deforestation/degradation in a forest–savanna boundary region of central Africa using multi-temporal L-band radar backscatter. *Remote Sensing of Environment*, *115*(11): 2861-2873.

Morel, A.C., Fisher, J.B. and Malhi, Y., (2012) Evaluating the potential to monitor aboveground biomass in forest and oil palm in Sabah, Malaysia, for 2000–2008 with Landsat ETM+ and ALOS-PALSAR. *International Journal of Remote Sensing*, *33*(11): 3614-3639.

Morel, A.C., Saatchi, S.S., Malhi, Y., Berry, N.J., Banin, L., Burslem, D., Nilus, R. and Ong, R.C. (2011). Estimating aboveground biomass in forest and oil palm plantation in Sabah, Malaysian Borneo using ALOS PALSAR data. *Forest Ecology and Management*, *262*(9): 1786-1798.

MPOB (2011). *BEST MANAGEMENT PRACTICES OF OIL PALM CULTIVATION ON PEATLAND,* Malaysian Oil Palm Board, Kuala Lumpur.

Murdiyarso, D., Dewi, S., Lawrence, D. and Seymour, F. (2011) *Indonesia's forest moratorium: A stepping stone to better forest governance?*. Cifor.

Murdiyarso, D., Hergoualc'h, K. and Verchot, L.V. (2010) Opportunities for reducing greenhouse gas emissions in tropical peatlands. *Proceedings of the National Academy of Sciences*, *107*(46): 19655-19660.

Murdiyarso, D., Lilleskov, E. and Kolka, R. (2019) Tropical peatlands under siege: the need for evidence-based policies and strategies. *Mitigation and adaptation strategies for global change*, *24*(4), pp.493-505.

Mysiak, J., Surminski, S., Thieken, A., Mechler, R. and Aerts, J.C. (2016) Brief communication: Sendai framework for disaster risk reduction–success or warning sign for Paris?. *Natural Hazards and Earth System Sciences*, *16*(10) 2189-2193.

Nomura, K. and Mitchard, E.T. (2018) More than meets the eye: using Sentinel-2 to map small plantations in complex forest landscapes. *Remote Sensing*, *10*(11): 1693.

Nunes, M., Ewers, R., Turner, E. and Coomes, D. (2017) Mapping aboveground carbon in oil palm plantations using LiDAR: A comparison of tree-centric versus area-based approaches. *Remote Sensing*, *9*(8), p.816.

Omar, H., Misman, M. and Kassim, A. (2017) Synergetic of PALSAR-2 and Sentinel-1A SAR polarimetry for retrieving aboveground biomass in dipterocarp forest of Malaysia. *Applied Sciences*, *7*(7): 675.

Othman, H.A.S.N.O.L., Mohammed, A.T., Harun, M.H., Darus, F.M. and Mos, H. (2010). Best management practices for oil palm planting on peat: Optimum groundwater table. *MPOB Information Series*, *528*: 1-7.

Page S E and Hooijer A 2014 Environmental impacts and consequences of utilizing peatlands Towards Climate Responsible Peatland Management Practices: Part 1 ed R Biancalani and A Avagyan, Food and Agriculture Organization of the United Nations (FAO), Rome.

Page, S.E., Morrison, R., Malins, C., Hooijer, A., Rieley, J.O. and Jauhiainen, J. (2011b). Review of peat surface greenhouse gas emissions from oil palm plantations in Southeast Asia. *White paper*, (15).

Page, S.E., Rieley, J.O. and Banks, C.J. (2011a) Global and regional importance of the tropical peatland carbon pool. *Global Change Biology*, *17*(2): 798-818.

Page, S.E., Rieley, J.O. and Wüst, R. (2006) Lowland tropical peatlands of Southeast Asia. *Developments in Earth Surface Processes*, *9*:145-172.

Page, S.E., Rieley, J.O., Shotyk, Ø.W. and Weiss, D. (1999) Interdependence of peat and vegetation in a tropical peat swamp forest. In *Changes And Disturbance In Tropical Rainforest In South-East Asia*

Page, S.E., Siegert, F., Rieley, J.O., Boehm, H.D.V., Jaya, A. and Limin, S., (2002) The amount of carbon released from peat and forest fires in Indonesia during 1997. *Nature*, *420*: 61.

Page, S.E., Wust, R. and Banks, C., 2010. Past and present carbon accumulation and loss in Southeast Asian peatlands. *Pages News*, *18*(1): 25-26.

Page, S.E., Wűst, R.A.J., Weiss, D., Rieley, J.O., Shotyk, W. and Limin, S.H. (2004) A record of Late Pleistocene and Holocene carbon accumulation and climate change from an equatorial peat bog (Kalimantan, Indonesia): implications for past, present and future carbon dynamics. *Journal of Quaternary Science*, *19*(7): 625-635.

Pan, Y., Birdsey, R.A., Fang, J., Houghton, R., Kauppi, P.E., Kurz, W.A., Phillips, O.L., Shvidenko, A., Lewis, S.L., Canadell, J.G. and Ciais, P. (2011). A large and persistent carbon sink in the world's forests. *Science*, *333*: 988-993.

Patra, P.K., Crisp, D., Kaiser, J.W., Wunch, D., Saeki, T., Ichii, K., Sekiya, T., Wennberg, P.O., Feist, D.G., Pollard, D.F. and Griffith, D.W., 2017. The Orbiting Carbon Observatory (OCO-2) tracks 2–3 peta-gram increase in carbon release to the atmosphere during the 2014–2016 El Niño. *Scientific reports*, *7*: 13567.

Picard, N., Saint-André, L. and Henry, M. (2012) Manual for building tree volume and biomass allometric equations: from field measurement to prediction. *Manual for building tree volume and biomass allometric equations: from field measurement to prediction, FAO; Food and Agricultural Organization of the United Nations.*

Piwowar, J. M. (1997) *Radar Image Characteristics, Complex Scattering Examples*. Geomatics International, RADARSAT Learning Program.

Ponnurangam, G.G. and Rao, Y.S., (2011) Soil moisture mapping using ALOS PALSAR and ENVISAT ASAR data over India. In *2011 3rd International Asia-Pacific Conference on Synthetic Aperture Radar (APSAR)* Institute of Electrical and Electronics Engineers.

PRI (2018), *Penundaan dan evaluasi perizinan perkebunan kelapa sawit serta peningkatan produktivitas perkebunan kelpa sawit, Instruki presiden nomor 8 tahun 2018*, Presiden Republik Indonesia, Jakarta, Indonesia.

Rees, A.R. and Tinker, P.B.H. (1963) Dry-matter production and nutrient content of plantation oil palms in Nigeria. Plant and Soil, 19: 19-32.

Rist, L., Feintrenie, L. and Levang, P., 2010. The livelihood impacts of oil palm: smallholders in Indonesia. *Biodiversity and conservation*, *19*(4): 1009-1024

Rochmyaningsih, D., (2019) Making peace with oil palm. *Science*, *365*:112-115.

Rosenqvist, Å., 1996. Evaluation of JERS-1, ERS-1 and Almaz SAR backscatter for rubber and oil palm stands in West Malaysia. *Remote Sensing*, *17*(16): 3219-3231.
RSPO (2018), *Principles and Criteria: For the Production of Sustainable Palm Oil*. Roundtable on Sustainable Palm Oil, Kuala Lumpur, Malaysia.
Saatchi, S.S., Harris, N.L., Brown, S., Lefsky, M., Mitchard, E.T., Salas, W., Zutta, B.R., Buermann, W., Lewis, S.L., Hagen, S. and Petrova, S. (2011) Benchmark map of forest carbon stocks in tropical regions across three continents. *Proceedings of the national academy of sciences*, *108*(24) 9899-9904.
Sayer, J., Ghazoul, J., Nelson, P. and Boedhihartono, A.K. (2012) Oil palm expansion transforms tropical landscapes and livelihoods. *Global Food Security*, *1*(2):114-119.
Schimel, D., Stephens, B.B. and Fisher, J.B., 2015. Effect of increasing CO2 on the terrestrial carbon cycle. *Proceedings of the National Academy of Sciences*, *112*(2): 436-441.
Sheil, D., Casson, A., Meijaard, E., Van Noordwjik, M., Gaskell, J., SunderlandGroves, J., Wertz, K. and Kanninen, M., (2009). *The impacts and opportunities of oil palm in Southeast Asia: What do we know and what do we need to know?* Center for International Forestry Research (CIFOR), Bogor, Indonesia.
Shimada, M., Isoguchi, O., Tadono, T. and Isono, K., (2009). PALSAR radiometric and geometric calibration. IEEE Transactions on Geoscience and Remote Sensing, 47(12): 39153932.
Silk, J.W.F., Aiba, S.I., Brearley, F.Q., Cannon, C.H., Forshed, O., Kitayama, K., Nagamasu, H., Nilus, R., Payne, J., Paoli, G. and Poulsen, A.D., 2010. Environmental correlates of tree biomass, basal area, wood specific gravity and stem density gradients in Borneo's tropical forests. *Global Ecology and Biogeography*, *19*: 50-60.
Sitch, S., Friedlingstein, P., Gruber, N., Jones, S.D., Murray-Tortarolo, G., Ahlström, A., Doney, S.C., Graven, H., Heinze, C., Huntingford, C. and Levis, S., 2015. Recent trends and drivers of regional sources and sinks of carbon dioxide. *Biogeosciences*, *12*(3): 653-679.
Tan, K.P., Kanniah, K.D. and Cracknell, A.P. (2013) Use of UK-DMC 2 and ALOS PALSAR for studying the age of oil palm trees in southern peninsular Malaysia. *International Journal of Remote Sensing*, *34*(20): 7424-7446.
Thenkabail P S, Stucky N, Griscon B W, Ashton M S, Diels J, van der Meer B and Enclona E. (2004) Biomass estimations and carbon stock calculations in the oil palm plantations of African derived savannas using IKONOS data*. International Journal of Remote Sensing*, 25, 1-27
Trujillo-Ortiz, A. and R. Hernandez-Walls. (2010). gmregress: Geometric Mean Regression (Reduced Major Axis Regression). Website Accessed 06th December 2019, http://www.mathworks.com/matlabcentral/fileexchange/27918-gmregress
Turetsky, M.R., Benscoter, B., Page, S., Rein, G., Van Der Werf, G.R. and Watts, A. (2015). Global vulnerability of peatlands to fire and carbon loss. *Nature Geoscience*, *8*: 11-14.
Tyukavina, A., Baccini, A., Hansen, M.C., Potapov, P.V., Stehman, S.V., Houghton, R.A., Krylov, A.M., Turubanova, S. and Goetz, S.J. (2015) Aboveground carbon loss in natural and managed tropical forests from 2000 to 2012. *Environmental Research Letters*, *10*(7): 74002.
UNFCC, 2015 *Paris Agreement*, United Nations, Paris.
USGS, *EarthExplorer - Home*, Website Accessed: 06th December 2018, https://earthexplorer.usgs.gov/,
Van der Werf, G.R., Morton, D.C., DeFries, R.S., Olivier, J.G., Kasibhatla, P.S., Jackson, R.B., Collatz, G.J. and Randerson, J.T. (2009) CO 2 emissions from forest loss. *Nature geoscience*, *2*: 737.

Verwer, C.C. and van der Meer, P.J. (2010) Carbon Pools in Tropical Peat Forests—Towards a Reference Value of Forest Biomass Carbon in Relatively Undisturbed Peat Swamp Forests in Southeast Asia. Alterra, Wageningen.

Vijay, V., Pimm, S.L., Jenkins, C.N. and Smith, S.J. (2016) The impacts of oil palm on recent deforestation and biodiversity loss. *PloS one*, *11*(7): 0159668.

Wang, W., Ciais, P., Nemani, R.R., Canadell, J.G., Piao, S., Sitch, S., White, M.A., Hashimoto, H., Milesi, C. and Myneni, R.B., 2013. Variations in atmospheric CO2 growth rates coupled with tropical temperature. *Proceedings of the National Academy of Sciences*, *110*(32): 13061-13066.

Whitmore, T.C., 1984. Tropical Rain Forests of the Far East. Clarendon Press, Oxford, UK

Wicke, B., Sikkema, R., Dornburg, V. and Faaij, A. (2011). Exploring land use changes and the role of palm oil production in Indonesia and Malaysia. *Land use policy*, *28*: 193-206.

Woodhouse, I. H., 2006, Introduction to Microwave Remote Sensing, Boca Raton, FL, CRC Press, Taylor & Francis Group

Woodhouse, I.H., Mitchard, E.T., Brolly, M., Maniatis, D. and Ryan, C.M. (2012) Radar backscatter is not a 'direct measure' of forest biomass. *Nature climate change*, *2*(8): 556.

Xie, Y., Sha, Z. and Yu, M. (2008).Remote sensing imagery in vegetation mapping: a review. *Journal of plant ecology*, *1*: 9-23.

Yu, Y. and Saatchi, S. (2016) Sensitivity of L-band SAR backscatter to aboveground biomass of global forests. *Remote Sensing*, *8*(6): 522.